UNIVERSITY OF THE
WITWATERSRAND,
JOHANNESBURG

Modelling the memory of the Free Space Optical Channel for use in the design of Error Correcting Codes

Xongile Nghatsane

Supervisors: Dr. Mitchell Cox and Prof. Ling Cheng

A dissertation submitted to the Faculty of Engineering and the Built Environment, University of the Witwatersrand, Johannesburg, in fulfilment of the requirements for the degree of Master of Science in Engineering.

2021

Declaration

I, the undersigned, hereby declare that the work contained in this dissertation is my own original work and that I have not previously in its entirety or in part submitted it at any university for a degree.

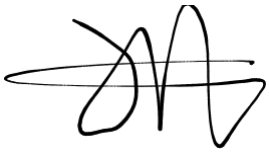

Xongile Nghatsane

Braamfontein, Johannesburg
19 January 2022

Abstract

Free Space Optics based communication links are an attractive potential approach for solving the last mile challenge, which will enable social advancement in more rural areas. Turbulence, however, remains a significant challenge in the use of Free Space Optical (FSO) channels. While models exist to predict how the turbulence affects the signal, these models often do not account for the memory in the channel. Furthermore, typical fading models accurately predict the average effect of the channel on a signal but not the distribution of the errors and the individual length of events such as deep fades. To better model and study the channel, this research demonstrates an alternative approach to modelling the channel: Fritchman Markov modelling. Fritchman Markov models capture the memory of a channel allowing for simulations and designs based thereon to be more accurate. A short-range link has been established and used to train a three state Fritchman Model to allow channel simulation. The models developed have accomplished better approximations of the digital behaviour of the channel when compared to traditional Probability Distribution Function (PDF)-based models. The techniques used to train the models have been demonstrated. The trained models capture the system's memory, allowing for better utilisation of channel capacity, which proves vital for the design of efficient Error Correcting Codes (ECC) for the channel.

FSO channels are packet erasure channels that are best suited by rateless codes. The aforementioned models have been used to simulate the application of ECC for the channel in the form of Luby Transform (LT) codes to show the efficacy of the models. This research has shown that rateless codes are not only suitable for the FSO channel but also that rateless code based transmission methods would be more suited for the channel. It is shown that the use of rateless codes results in similar throughput for a fixed overhead in comparison to a traditional method that would utilise retransmission. The performance of the LT code based system does, however, improve significantly with increased overhead allowing for a predicted better channel utilisation with increased turbulence strengths compared to retransmission based methods. The use of the Fritchman models had also shown that the memory of the channel could be utilised when the models are used to capture this memory. The short-range nature of the link means that the models and the resulting ECC do not fully predict behaviour in very high turbulence situations. Consequently, the work presented is not comprehensive for a full system design for use on real-world links, but it serves as crucial steps towards using and improving FSO links.

Acknowledgements

I would like to thank Mitchell Cox and Ling Cheng for their work as supervisors and friends during this research. Their advice has been invaluable and has allowed me to learn more than I was expecting. I have learnt about myself during this journey and with their help, I have become a better person. Though I step away from Academia for now, I will always value the time I spent with them and the lesson they have imparted upon me. In addition, I would like to thank all the people at the Optical Communications Lab for always being available for advice and help during this time.

I would also like to acknowledge the support of the South African National Research Foundation as well as the Center for Telecommunications Access and Services for their financial support during my MSc.

Contents

List of Figures

List of Tables

List of Acronyms

ARMA	Auto-Regressive Moving-Average
ARQ	Automatic Repeat Request/Query
BER	Bit Error Rate
BP	Belief Propogation
BSC	Binary Symmetric Channel
CRC	Cyclic Redundancy Check
ECC	Error Correcting Codes
EFR	Error Free Run
FEC	Forward Error Correction
FPGA	Field Programmable Gate Array
FSO	Free Space Optical
Gbps	Gigabits per second
GE	Gaussian Elimination
HMM	Hidden Markov Models
IG	Incremental Gaussian Elimination
IID	Independent and Identically Distributed
ISP	Internet Service Provider
LDPC	Low Density Parity Check
LOS	Line Of Sight
LFSR	Linear Feedback Shift Register
LT	Luby Transform
MLSD	Maximum-Likelihood Sequence Detection
NRZ-OOK	Non-Return to Zero On-Off Keying
OFG	On the Fly Gaussian Elimination
PDF	Probability Distribution Function

RF	Radio Frequency
RS	Reed Solomon
SI	Scintillation Index
TCP	Transmission Control Protocol
XOR	Exclusive Or

List of Symbols

Γ	Gamma function	–
λ	Wavelength of laser used for link	m
σ_I^2	Scintillation Index	–
a_{xy}	Probability of transition to state y when in state x	–
d	Degree of LT encoded symbol in	–
D_x	The X^{th} decoded symbol resulting from an LT decoder	–
$G[x]$	The X^{th} row in matrix G	–
G	A matrix corresponding the encoded LT symbols	–
H_b	Binary entropy function	–
I	Optical Intensity of received signal	$\mathrm{W.m^{-2}}$
K	Number of symbols used for encoding LT codes	–
k	Wave number	$\mathrm{m^{-1}}$
L	Length of link	m
LT''_x	An intermediate symbol resulting from two XORs with a row of G.	–
LT'_x	An intermediate resulting from XOR with a row of G.	–
LT_x	The X^{th} encoded symbol produced by an LT encoder	–
LT_{Bx}	An intermediate partially decoded symbol in a BP based LT decoder	–
m	Length of a gap in a binary sequence	–
M_x	The X^{th} message symbol used as input for an LT encoder	–
N_e	Number of errors in a binary sequence	–
N_g	Number of gaps in a binary sequence	–
p	Probability of error being omitted by a Binary Symmetric Channel	–
T	Temperature of air	°C
u	Speed of wind in the channel	$\mathrm{m.s^{-1}}$

Resulting Publications

Journal Papers

1. X. Nghatsane L. Cheng, and M. A. Cox, "Fritchman modeling for correlated turbulence-induced errors in FSO communication," *Applied Optics 60*, 1801–1808 (2021)

Under Review

2. X. Nghatsane L. Cheng, and M. A. Cox, "Improving the resilience of free-space optical links using Luby-Transform codes" submitted to the *OSA Continuum*, 2022.

CHAPTER 1

Introduction

WITH the ever-increasing digital nature of society, telecommunications form a vital part of developed nations. Optical fibre forms the backbone of the modern Internet, and multiple methods of communication are used for short-distance or "last mile" connections. Radio Frequency (RF) is sometimes used, but Free Space Optical (FSO) communication is an attractive alternative because of interference and bandwidth limitations in the heavily used radio frequency spectrum. State of the art experimental FSO systems have been demonstrated at data rates on the order of petabits per second over a lab bench [1], to hundreds of gigabits per second in simulated turbulence [2]. Modern, commercial FSO technology can sustain gigabits per second over several kilometres, making FSO a viable technology for future brownfields installations where fibre is too difficult or too expensive to install [3, 4]. For these reasons, it is expected that FSO will be a significant part of the future 6G era [5, 6]. Still, FSO has also been suggested as a possible technology to help bridge the digital divide [7].

Telecommunications have been identified as a crucial aspect to improving the material conditions in developing nations as information sharing is a key aspect of the modern age. In developed counties, this is primarily achieved using optical fibre backbones. While these backbones are extremely reliable, they suffer from high establishment costs due to requiring the optical fibres themselves and the work to lay said fibres into the ground. This establishes a feedback loop in which the links are too expensive to feasibly yield a good return on investment which causes the nations to develop slowly, meaning they aren't able to pay for the links. A suitable alternative that can also reach the same throughputs as these traditional methods is FSO because this forgoes the cost of the optical fibre, and establishing the links is theoretically as simple as establishing two transceivers with Line Of Sight (LOS).

This theoretical ease assumes that the links can achieve the same reliability as fibre optic based links. Due to transmitting in the air, the channel suffers distortions due to atmospheric turbulence. Thus, this assumption cannot be so easily made, and techniques must be used to mitigate the effect of the distortions. Various "passive" attempts have been made at increasing the range and throughput of FSO channels, including using spatial modes of light for multiplexing and even diversity [8–12]. Unfortunately, these methods cannot be used in isolation, and ultimately, digital techniques must be employed. These techniques require accurate digital channel models, and once they have been developed, they can be used in simulations to allow for more optimal designs for the channel.

The development of accurate channel models will allow for rapid iteration of solutions without the bottleneck of real-time transmissions and alterations of the channel. Using a channel model also allows for testing solutions on modelled states on the channel while the channel is not available in that state. With comprehensive modelling, less frequent states, such as fog and rain, can be tested without relying on uncontrollable weather.

There are a variety of models and associated modelling techniques for communications channels. To identify if an existing model and/or modelling technique can be applied to the FSO channel, a literature review of the work in the field must be conducted. This will allow for the identification of a potential gap in the field and the extent of such a gap that may warrant entirely new models and associated techniques. Choosing the Error Correcting Codes (ECC) to be used requires a similar process. This literature review will form the basis of the research question that will drive this dissertation.

1.1 Literature Review

There are two primary approaches to digital communication channel modelling: signal based techniques and digital channel model-based techniques. The main difference is that signal based techniques rely on simulating the signal as it would be if transmitted in the channel. This includes modulation and demodulation, and the model is typically used to induce signal distortion resulting in bit-level errors. The digital channel-based method forgoes the modulation and demodulation; instead, it produces bitstreams directly. These are typically error streams that can be used with the transmitted bitstream to simulate the effects of signal distortion.

FSO systems are predominantly modelled using signal based techniques, and this is primarily in the form of Probability Distribution Function (PDF)-based models. The models most often used are the Log-Normal and Gamma-Gamma models [13–16]. While the Log-Normal and Gamma-Gamma do see widespread use, the models do not capture the memory of the system due to being PDF-based and the sampling being Independent and Identically Distributed (IID). To solve this, an Auto-Regressive Moving-Average (ARMA) based time series model has been presented to capture the memory of angle-of-arrival fluctuations, which result in focal-spot beam wander and hence fading [8].

Due to not requiring modulation, demodulation and simulation of the signal on the channel, digital techniques typically require less simulation time. These models are predicated on producing a vector of symbols that represent errors. The vectors produced can be within a simulation to be added to a vector of source symbols, reproducing errors that would occur on the channel. Due to capturing channel memory, Markov based models are a potential solution to develop models that capture the memory of the FSO channel. Here, a communications channel is stated to have memory when the outputs of the channel at different times are correlated [17].

Markov based models present as a possible means to model the FSO channel using a digital model that also captures the memory of the channel. Markov chains have been used extensively in hybrid RF/FSO system modelling, which are systems in which RF and FSO systems are used in conjunction to take advantage of both technologies. RF and FSO each suffer from different atmospheric conditions, so a combination of both can be utilised for optimal reliability. Markov chains have been used to model the link selection that would be required for soft switching if one of the links suffered an outage [18]. Expressions for the outage probability given weather parameters were provided, thus aiding the future design of hybrid systems. A demonstration link in Qatar used Markov modelling for a Hybrid FSO/RF link using Raptor codes to facilitate soft switching [19]. Their Markov chain was also used to model the fading and derive a mathematical expression for the outage probability. In a similar vein, Hidden Markov Models (HMM)s have been used to simulate the variation in fading and turbulence due to weather in an FSO/RF hybrid channel. This study was focused on modelling the fade correlation and different propagation states of the hybrid system [20].

Markov chains have also been used to develop models for analysing a pure FSO channel's fading behaviour. These chains have been developed using turbulence state information and verified using a turbulence chamber [21]. An eight and 64-state Markov model of the received signal in a 1.8 km urban FSO link is presented in [22]. Comparisons of the measured data were shown to fit existing distributions for FSO. The proposed Markov model fits the measured data while also capturing the non-stationary nature of the channel. Ray tracing has also been used in conjunction with Markov chains to model the FSO channel [23]. Markov modelling has been used to optimise an Maximum-

Likelihood Sequence Detection (MLSD) algorithm [24], where a single step Markov chain is used to simplify the algorithm used significantly.

Markov models have also proven useful in modelling overall network performance rather than signal-only effects. They have been used to develop models for the channel state of an FSO channel, focusing on cross-layer performance, the effects on the commonly-used Transmission Control Protocol (TCP) and technologies such as Automatic Repeat Request/Query (ARQ) and Adaptive Modulation Coding [25, 26]. A similar study focused on the loss of Ethernet frames in an FSO based system [27]. Here, the Gilbert-Erasure channel is used to model frame loss. The applicability of the model is shown in relation to the training data but not to a simulation-based on "conventional" PDF models. Markov based models have been shown in use on the channel, but none have been used to capture and demonstrate the memory in the channel. This forms a gap that Fritchman Markov models can potentially fill. While Fritchman models can potentially fill this gap in the field, utilising the memory in the channel requires specific ECC. In addition, the applicability of the Fritchman models for the design and simulation of ECC must be shown.

Fountain codes are a potential candidate to show the applicability as they are suited for bursty channels, and existing work will be used to inform if they have potential on the FSO channel. In [28], several different fountain codes on the FSO channel (Luby Transform (LT), Raptor and RaptorQ codes) were demonstrated to show the potential suitability of rateless codes for the FSO channel. FSO based links are considered for use in a hybrid RF/FSO link and a study has been done to optimise this configuration using short length Raptor codes [29]. The Raptor codes were used to facilitate a soft switching mechanism to take advantage of both channels without the need for channel feedback. There has been a demonstration of a Raptor coded system implemented on a Field Programmable Gate Array for real-world use on an existing link [30]. The Raptor coded system proved to be relatively inexpensive to implement on a Hybrid RF/FSO link.

The same link has been used for previous studies for measurements to drive FSO channel models for use in Raptor code simulation [31]. These simulations have shown that Raptor coded systems can perform better than uncoded systems, particularly in harsh weather conditions. Another study directly compared the performance of LT codes to a re-transmit based system on a simulation of an FSO channel [32]. It was demonstrated that the LT codes are not a one size fits all solution as at certain channel conditions, the re-transmit performed better than the LT coded system. The use of LT codes on the FSO channel as an error channel instead of an erasure channel has been shown [33]. The study shows the performance of an LT coded system with various modulation techniques and on various traditional PDF-based models for the FSO channel.

While the aforementioned studies did demonstrate good use of fountain codes on FSO channels, these studies generally either used established PDF-based FSO channel models to simulate the FSO channel or physical experiments. The FSO channel exhibits memory which is inherent in Taylor's frozen turbulence hypothesis, [34–37] but PDF-based models do not accurately capture this memory because PDF-based models are IID. Taking all of the channel characteristics into consideration is critical to designing optimal FEC codes that enable longer distance and more reliable FSO communications.

While real-world testing is a potential solution, it requires the links to be established and test infrastructure, which presents a challenge. A simulation-based method is preferred as this allows rapid testing of multiple conditions and code configurations. Consequently, if Fritchman Markov models can capture the memory of the system as they show potential for, then the suitability of the models and the LT codes when taking memory into account can be demonstrated by simulating LT codes on the Fritchman models developed. This observation forms the basis of the research question that is the focus of this dissertation.

1.2 Research Question

As discussed in the literature review, the pervasiveness of the traditional PDF-based models for the channel has resulted in many studies drawing meaningful conclusions about the FSO channel's digital techniques. However, these studies are inherently limited by the channel models that are being used, leading to suboptimal solutions. This is particularly important for the design of ECC because the memory of the channel makes the design of ECC difficult as burst channels are notoriously difficult to correct [38–42]. The corollary of the effect of memory is that if the memory is accounted for in the design, then the channel's capacity will be better utilised. Increasing the capacity improves the prospects of using the FSO channel for solving the Last Mile Problem. Consequently, a gap has been identified in the field regarding digital models that capture the memory of the FSO channel.

Channel models that capture the system's memory are needed. Still, they must also be confirmed for use in ECC design, and Fritchman Markov models have been identified as a potential solution for the modelling. LT codes have also been identified to have good potential use on the FSO channel. They can potentially work well with the models, demonstrating the suitability of the models and the code. To achieve these ends, the broad question that is the basis for the research conducted is as follows:

How can we harness the memory of the FSO channel to design more optimal ECC?

This is a relatively large question and is approached by breaking it down into two sub-questions. These two sub-questions together form the bulk of the overall contribution of the dissertation.

1. *Can the memory of the FSO channel be modelled using Fritchman Markov modelling within the context of digital communications, and how well can this memory be captured?*

2. *How can we use the Fritchman model of FSO memory to aid the design of fountain code-based error correction to improve the channel's throughput?*

1.3 Research Impact and Motivation

One of the primary factors that slow the adoption of FSO links is the limited range of FSO links with current commercial systems having a low range. Increasing the range of FSO links is an important study area as it can prove crucial to solving the Last Mile Problem by lowering the costs needed to cover a set distance thus making expansion more attractive to Internet providers. Various methods for increasing the effective range of an FSO link exist, but these can be limited by cost due to the hardware required and legal limits to the optical transmission power. Techniques to increase the link range based on changing the physical nature of the laser exist, but this dissertation is focused on digital techniques [43].

This research focuses on improving the digital techniques available for use primarily by proposing models that better capture the channel's memory. To the author's knowledge, there is no existing work for using Fritchman Markov models to capture the memory of the system. The models that are largely used do not capture the memory resulting in unused potential channel capacity. Using the techniques provided in this research, designers can model the channel to a degree that allows increased channel capacity, increasing the throughput and range of FSO links.

This performance improvement will make FSO links a more attractive alternative, thus increasing Internet Service Provider (ISP) adoption rates which will aid in tackling the digital divide. It is noted that the research cannot be directly applied to create an entire physical system. Still, it can improve the efficiency of design iteration of real systems while using a model that more accurately represents the channel. This simulation efficiency is shown in applying LT codes to the channel. It serves to show both the application of LT codes to the channel and the usability of the obtained models.

Should this research be utilised for future development of FSO based systems, it will allow more efficient design and research. This will accelerate the adoption of FSO based systems which are inherently cheaper than existing fibre optics solutions as mentioned above. The focus is not on the

development of a full system that can be implemented on a link. Instead, the intent is to lay the groundwork that can be used to inform and aid the design of such a system. By achieving this goal, steps can be made towards addressing the Last Mile Problem and bridging the digital divide.

1.4 Dissertation Layout

1.4.1 Background

This chapter gives background information required to understand the research that will be presented. The information is split into three main areas detailing atmospheric turbulence, Fritchman Markov model and LT codes. The background on the atmospheric turbulence details how it is measured and its effects on the channel. The use of Fritchman Markov models for bursty channels, including an algorithm for training the models and a method to measure how well the channel has been modelled, is then presented. Finally, the application of LT codes to erasure channels, particularly the FSO channel and the encoding and decoding process, will be discussed.

1.4.2 Fritchman modelling for correlated turbulence-induced errors in FSO communication

The results from the modelling aspect of the research have been submitted and published in the Journal of Applied Optics. This chapter uses the published study as a basis to present the results of the study. The information presented in this chapter serves as an answer to the first research sub-question. Models that capture the channel's memory are shown, while traditional PDF-based models are shown not to capture this memory. Several of the developed models are compared with the channel and PDF-based simulation of the channel in the form of Error Free Run plots. The techniques used for modelling are presented here, and it is noted that the approach will have to be adapted for use on more realistic channels though the results are expected to be similar. While the work presented shows better conformity to the channel's behaviour than traditional PDF-based models, it is noted that the PDF-based models have the advantage that a model can be used without a link being established. Future work is suggested to focus on developing Fritchman models based on similar channel parameters to promote their adoption further.

1.4.3 Optimising free-space optical communication throughput in turbulence with Luby-Transform codes

The techniques from the previous chapter are used to train models to simulate the channel and implement an LT code-based system on it. In addition, the trained models are used for further analysis of the memory in the channel. This aspect of the research has been submitted to the OSA Continuum and serves as an answer to the second research sub-question. To show the effect of LT codes on the channel, the throughput of three schemes is presented: uncoded, Reed Solomon (RS) coded and RS + LT coded. It is noted that at the chosen threshold of 30%, the LT coded system has similar or better throughput than the RS coded system while also having the advantage of scaling extremely well with additional overhead. While the results presented are for a simulation in which a fixed number of packets are sent, a real-world solution would use continuous transmission, which further benefits LT codes compared to the other two schemes that would utilise a form of ARQ. Future work is suggested to implement more advanced Fountain codes in the form of Raptor codes and an adaptive system to minimise the overhead introduced.

1.4.4 Conclusion

In this final chapter,the dissertation is concluded with a summary of the research done and the impact and contributions of the work done. In addition, future work based on this research and potential applications of the work is discussed.

CHAPTER 2

Background

THIS chapter serves to provide a general background need to understand the work done for this research. Due to the work being done in the form of multiple publications, this background will encompass the backgrounds of the publications with greater detail. The chapters corresponding to the publications will consequently have no backgrounds. Background on atmospheric turbulence and its effects on the FSO channel will be discussed first in Sec. 2.1. The efficient design of solutions to tackle these effects requires channel modelling, and the basis for the techniques used in this research are detailed in Sec. 2.2. Following this, LT codes that are ideal for use on erasure channels are detailed in Sec. 2.3 with details regarding the encoding and decoding of these codes.

2.1 Atmospheric Turbulence

In contrast to a more isolated transmission medium like optical fibre, the propagation of laser beams in the air is affected by several physical phenomena, with the most significant being atmospheric turbulence. Aberrations due to turbulence are caused by randomly varying cells of air that have different temperatures and thus different refractive indexes which move around due to physical processes such as wind and convection.

These cells have various sizes. The larger cells cause large-scale turbulence effects such as beam wander, whereas the smaller cells within the larger cells predominantly cause wavefront distortion known as scintillation [44, 45]. The combination of these effects leads to random fluctuations in the received wavefront and, therefore, the received intensity, known as turbulence-induced signal fading.

The Scintillation Index, SI, is an intuitive measure of turbulence strength and is defined as the normalised variance of the irradiance fluctuations given by

$$\sigma_I^2 = \frac{\langle I^2 \rangle}{\langle I \rangle^2} - 1, \tag{2.1}$$

where I is the received optical intensity and $\langle \cdot \rangle$, represents the ensemble average. The wind speed naturally has an impact on the turbulence characteristics and can be used to calculate an important measure of turbulence called the correlation time, which naturally describes how long the turbulence conditions can be assumed to be correlated, given by

$$\tau = \frac{\sqrt{\lambda L}}{u}, \tag{2.2}$$

where u is the perpendicular (to the direction of laser propagation) wind velocity, λ is the wavelength of the laser, and L is the propagation distance. For a typical system that is being used over several

kilometres, the correlation time is typically in the order of milliseconds, barring extreme wind speeds. When considering the high-speed links that FSO is typically used for, milliseconds represent significant amounts of data on the scale of millions of bits at a Gbit speed range.

The correlation time is an indicator of the memory present in the channel as correlated channel conditions will result in correlated bit-level behaviour. Taking advantage of this memory improves channel capacity, but the most notable models for turbulence do not account for this memory.

Not accounting for the memory in the channel can result in under-utilised channel capacity. While memory causes the errors to be distributed in a bursty manner (a challenging but solvable problem with the correct FEC codes), taking advantage of the memory allows for designs that better approach the Shannon capacity of the system.

As mentioned in the introduction, notable models for turbulence-induced intensity fluctuations are based on Gamma-Gamma and Log-Normal distributions. While the Gamma-Gamma model is generally more accurate under a wider range of turbulence conditions from weak to strong, the simpler Log-Normal model is accurate for weak turbulence conditions in shorter FSO links and is the model used in this work.

The Gamma Gamma model seeks to model irradiance fluctuation with a method that more closely relates to the phenomena in the channel compared to a method like Log Normal. This is achieved by the small and large scale irradiance fluctuations can be summarised as two independent processes that are based on Gamma distributions [44, 45]. These are described as follows:

$$p_X(X) = \frac{\alpha(\alpha X)^{\alpha-1}}{\Gamma(\alpha)} exp(-\alpha X), \alpha > 0, X > 0 \tag{2.3}$$

$$p_Y(Y) = \frac{\beta(\beta Y)^{\beta-1}}{\Gamma(\beta)} exp(-\beta Y), \beta > 0, Y > 0 \tag{2.4}$$

$$\tag{2.5}$$

where Γ is the gamma distribution. This has shown good compliance to the phenomena present on the channel. The resultant PDF is as follows:

$$\begin{aligned} p(I) &= \int_0^\infty p_Y(I|X) p_x(X)\, dX \\ p(I) &= \frac{2(\alpha\beta)^{(\alpha+\beta)/2}}{\Gamma(\alpha)\Gamma(\beta)} I^{(\alpha+\beta)/2-1} K_{\alpha-\beta}(2\sqrt{\alpha\beta I}), I > 0 \end{aligned} \tag{2.6}$$

and this is called the Gamma-Gamma distribution. As with the Log-Normal distribution, this is PDF-based and thus contains no memory. Studies have shown that the Gamma-Gamma is more accurate than the Log-Normal in most cases, barring low turbulence scenarios in which the Log-Normal conforms to the channel better[46].

The Log-Normal distribution is based on the so-called Rytov variance, σ_R^2, another measure of irradiance variance. In weak turbulence where $\sigma_R^2 \ll 1$, the Rytov variance is approximately equal to the scintillation index, which is conducive to experimental measurement. The Rytov variance for a plane wave (or collimated Gaussian beam) is given by

$$\sigma_R^2 = 1.23 C_n^2 k^{7/6} L^{11/6}, \tag{2.7}$$

where C_n^2 is the refractive index structure constant and $k = 2\pi/\lambda$ is the wave number. The log intensity variation is given by

$$l = \ln \left| \frac{A(r)}{A_0(r)} \right|^2 \tag{2.8}$$

where l is the log intensity variation, r is the position vector of the signal and $A_0(r)$ is the amplitude of the received signal in a turbulence-free channel, while $A(r)$ is the amplitude of the signal in a turbulent channel. Through manipulation of the above parameters, the PDF for the log-normal distribution is found as given by

$$\mathrm{P}(I) = \frac{1}{\sqrt{2\pi\sigma_R^2}} \frac{1}{I} \exp\left\{ -\frac{(\ln(I/I_0) - E[l])^2}{2\sigma_R^2} \right\} \tag{2.9}$$

for $I \geq 0$, where $E[l]$ is the expectation of the log intensity variation [44]. The PDF produces a distribution of the intensity normalised by $E[l]$.

Using the PDF shown in Eq. 2.9, samples of the received irradiance can be taken. With increased turbulence strength, the likelihood of a deep fade and errors increases. The chance of a deep fade occurring across many samples can be calculated by sampling using the PDF above and setting a threshold such that any sample below that threshold is a deep fade. If the usable threshold is defined as I_u, then the probability of a deep fade occurring based on the PDF defined in Eq. 2.9 can be found by integrating the given PDF over $[-\infty, I_u]$. Since I must be strictly non-negative, this simplifies the integral as follows:

$$\mathrm{P}(I < I_u) = \int_{-\infty}^{I_u} \mathrm{P}(I)\,\mathrm{d}I = \int_{0}^{I_u} \mathrm{P}(I)\,\mathrm{d}I. \tag{2.10}$$

The fades will be randomly distributed because the samples are IID.

In a typical FSO system that uses Non-Return to Zero On-Off Keying (NRZ-OOK) modulation, the choice of the optimal threshold for I_u is typically driven by existing techniques and insight [47]. Factors such as the noise inherent to the equipment should also be taken into consideration. With more sensitive equipment and less noise, the threshold can be lower as the noise is less likely to distort the signal to the degree that it causes errors.

2.2 Fritchman Markov Models for Errors

Early methods of modelling bursty communications channels were based on the Binary Symmetric Channel (BSC) [48, 49]. The BSC works on the assumption that a telecommunications channel can be modelled as having a constant error probability of p, where an error would cause a bit flip. This is described as

$$\begin{aligned} P[Y = 1|X = 1] &= 1 - p \\ P[Y = 0|X = 0] &= 1 - p \\ P[Y = 1|X = 0] &= p \\ P[Y = 0|X = 1] &= p \end{aligned} \tag{2.11}$$

The model is characterised by each output being entirely independent of previous outputs. Due to the simplistic nature of the channel, calculating the capacity of the channel is relatively straightforward: the capacity of the channel is described as

$$C = 1 - H(p) \tag{2.12}$$

where

$$H(p) = -p \log p - (1 - p) \log(1 - p) \tag{2.13}$$

Gilbert-Elliot channels are an extension of the BSC in which the channel is based on a Markov process and is represented by multiple states that are each BSC [49]. The channel has two states: a good one and a bad one, and they can transition to each other. The Gilbert-Elliot channel can be represented as shown in Fig. 2.1.

Due to being based on a Markov process, the Gilbert-Elliot channel can capture the memory of a channel. While in each state, the channel can be described using Eq. 2.11 with the error probabilities substituted for p_g or p_b where p_g and p_b are the error probabilities of the good and bad state, respectively.

Fritchman models are Markov models that were formed as an extension of the Gilbert-Elliot model [50]. Fritchman models are N-state partitioned Markov models that have proven suitable for modelling bursty communication channels. The states are partitioned into two groups with N and $N - k$ states, representing "good" and "error" channel states. This is an important feature for modelling a communication channel as these states, and the distribution of their occurrences are important to a systems designer. Conveniently, the model can be used without knowing the

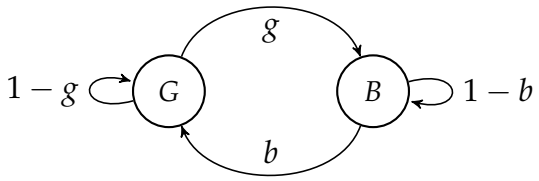

Figure 2.1: Gilbert-Elliot channel model. The two states can each transition to each other, and each represent a different BSC with their own error probabilities. The good state is represented by G and the bad state by B, and g and b are the probabilities to transition to the other state, respectively.

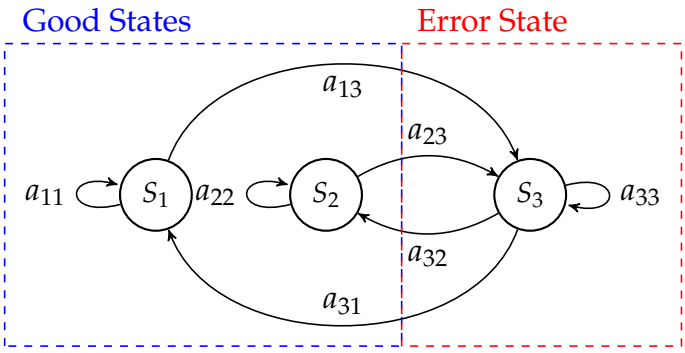

Figure 2.2: Three state Fritchman model that presents the state transition matrix shown in Eq. 2.15. Note that there are no transitions between states S_1 and S_2. The figure's ellipsis represents the possibility of extending the number of good states if needed to better model the system in question.

cause of the states, which can represent turbulence-induced phenomena such as the beam wandering completely off the receiver for a time, causing a burst of errors. An example of a three-state Fritchman model with two good states and one bad state is shown in Fig. 2.2.

The models presented in this study are first-order models and can be described using an $N \times N$ state transition matrix. The entries in the state transition matrix, A, represent the probabilities of transitioning to one state from a specific current state, is expressed as

$$\mathrm{a}_{ij} = \mathrm{P}(s_t = S_j | s_{t-1} = S_i). \tag{2.14}$$

The structure of a Fritchman model is quite particular. It is standard practice to use one error state and $N - 1$ good states to describe bursty communication channels. Errors can only be emitted by the error state. Fritchman models are Semi-Hidden Markov models because the system's state can be discerned when there is an error, but not when there is no error. The states are assumed to only transition to themselves or states in the other partition, as can be seen in Fig. 2.2, which has a state transition matrix given by

$$A = \begin{bmatrix} a_{11} & 0 & a_{13} \\ 0 & a_{22} & a_{23} \\ a_{31} & a_{32} & a_{33} \end{bmatrix}. \tag{2.15}$$

Note that there are zeros in the matrix, indicating that the states cannot transition within their partition. In addition to the state transition matrix, the Fritchman model is also described by an emission matrix. Assuming the model is being used to produce an add-modulo-two error sequence, the emission matrix will be a $2 \times N$ matrix that gives the probability of each state emitting either an error or not. Since the good states do not output errors, the emission matrix for the model shown in Fig 2.2 is given by

$$B = \begin{array}{c} \begin{matrix} S_1 & S_2 & S_3 \end{matrix} \\ \begin{bmatrix} 1 & 1 & 0 \\ 0 & 0 & 1 \end{bmatrix} \end{array} \begin{array}{l} Good \\ Error \end{array}, \tag{2.16}$$

which has been annotated for convenience. Note that the probabilities are either one or zero, indicating that the states only have one possible output corresponding to the partition they are in.

The last element required to describe the model is the initial state probability vector. This provides the probability of being in a specific state when the model is started, given by

$$\Pi = \begin{bmatrix} \pi_1 & \pi_2 & \pi_3 \end{bmatrix}. \tag{2.17}$$

Fritchman models can capture the channel's memory because the models are fully described using a state transition matrix, an initial state probability vector and an emission matrix defined as $F = (A, B, \Pi)$. This causes the states to correspond to channel conditions. The model parameters can be found using the Baum-Welch algorithm.

2.2.1 Baum-Welch Algorithm

The Baum-Welch algorithm is an iterative algorithm that uses an initial estimate for the parameters of the Markov model and a sequence from the system that is being modelled [51–53]. The algorithm finds the possible sequence of states that could have produced the given output sequence. Using these traced sequences, the state transition matrix is modified to produce a sequence that closely matches the predicted sequence, measured using mean squared error. The algorithm is ideal for training Hidden and Semi Hidden Markov Models, which Fritchman Models are a subset of, as previously stated.

Running the algorithm to train an HMM is a tradeoff between model accuracy and run time, with increased run time not having a proportionate effect on the conformity of the trained model and the signal used to train it. Careful effort must be taken when deciding the initial parameters of the model to ensure the model that is produced is a Fritchman model, as not all HMMs are Fritchman models. This is done by using an initial state transition matrix of the form:

$$A_0 = \begin{bmatrix} a_{11} & 0 & a_{13} \\ 0 & a_{22} & a_{23} \\ a_{31} & a_{32} & a_{33} \end{bmatrix}. \tag{2.18}$$

where the a_{xx} is the probability of staying in state x once in state x and the a_{xy} of transitioning to state y while in state x. To ensure the trained model is a Fritchman, the $a_{xx} \geq a_{xy}$. The initial matrix used to train the models presented in this study is as follows:

$$A_0 = \begin{bmatrix} 0.7 & 0 & 0.3 \\ 0 & 0.5 & 0.5 \\ 0.1 & 0.2 & 0.7 \end{bmatrix}. \tag{2.19}$$

The closer the initial state is to a model that captures the channel, the less time will be taken to reach convergence. The state above was chosen to represent a model with one error state, a good state that tends to stay good and a good state that is likely to stay good or transition to an error with similar probabilities. This would allow for capturing both the memory and random errors of the channel

2.2.2 Memory Visualisation

Since the goal is to model the presence and degree of memory in an FSO system, a way to measure and visualise it is required. A useful and intuitive method to show the presence of memory is called an Error Free Run (EFR) distribution.

An error-free run is defined as the interval between two consecutive errors in an error sequence (a sequence of zeros and ones, where the ones represent received errors) as defined by

$$\mathrm{P}(0^m|1) = [1 - \mathrm{P}_g(m-1)]\mathrm{P}(0^1|1), \tag{2.20}$$

where

$$\mathrm{P}(0^1|1) = \frac{N_g}{N_e}, \tag{2.21}$$

and

$$\mathrm{P}_g(m-1) = \frac{N_g(1) + N_g(2) + N_g(3) + \ldots + N_g(m-1)}{N_g}. \tag{2.22}$$

Here, m is the length of the interval between successive errors and $\mathrm{P}(0^m|1)$ is the probability of m error-free outputs given the occurrence of an error. N_g is the total number of gaps, N_e is the total number of errors and $N_g(m)$ is the number of gaps of length m [54]. Here, a gap is defined as the region between two successive errors.

The EFR of a sequence from a channel with no memory would have high probabilities initially, but due to having no memory, there would be a sharp drop off in probability as the interval length grew. The Bit Error Rate (BER) of the sequence would limit the sharpness of this drop. In contrast, the EFR of a channel with memory would naturally also drop, but it would have a significantly longer tail, possibly with additional features depending on the nature of the system.

This is an important feature for modelling a communication channel as these states, and the distribution of their occurrences are important to a systems designer. Conveniently, the model can be used without knowing the cause of the states, which can represent turbulence-induced phenomena such as burst errors caused by the beam wandering completely off the receiver for a time.

2.3 Luby-Transform Codes

Forward error correction uses methods, primarily in the form of added redundancy, to correct errors in data transmission without the need for retransmission of data, provided the errors can be corrected. The most basic form of Forward Error Correction (FEC) is a repetition code in which N copies of the data are transmitted, and the resultant data is obtained using an average of the received data. This results in a code rate of $1/N$, representing how much useful information can be retrieved from a block of received data.

More robust coding methods exist, such as convolutional codes, RS codes, Low Density Parity Check (LDPC) codes, but they all share a common characteristic. The code rate is fixed, so a given amount of source data for a chosen configuration will always result in a specific amount of encoded data. These fixed-rate codes are very well suited to solving random errors but are not suited for erasures. Due to being a fixed rate, each of the encoded symbols must arrive to receive the entire message, and thus symbols being dropped requires retransmission.

Rateless codes are designed to solve this problem and are more suited to symbol erasure channels, such as the FSO channel. In contrast to the aforementioned fixed-rate codes, rateless codes can theoretically produce an infinite number of symbols which is why they are also known as Fountain codes. A suitable number of these symbols can be used to decode and retrieve the source data, but crucially, no symbol is more important than any other, so symbol erasures are recovered by design. One such implementation of rateless codes is LT codes [55].

2.3.1 Encoding

LT codes work by taking the source data and creating encoded data using a series of Exclusive Or (XOR), represented as $\oplus$ in the Equations and Figures, operations. In contrast to fixed-rate codes, the encoded symbols are the same length as the source symbols. Due to using XORs, the encoded symbols form a system of simultaneous equations that can be solved to decode the symbols. Given K source symbols, the system can be solved with K linearly independent symbols. In practice, the number of symbols needed is more than K due to the information contained by some encoded symbols being entirely redundant. The source symbols that are used to encode each symbol are determined with a degree distribution. The degree of an encoded symbol is the number of symbols XORed to

form the encoded symbol. Once a degree, d is obtained by sampling the chosen distribution, d indices are randomly selected. The source symbols corresponding to these indices are XOR-ed to form the encoded LT symbol. This process can be seen for three of the symbols for a system of four source symbols in Figs. 2.4 to 2.6 with the resulting system seen in Fig. 2.3. Based on the degrees and indices chosen, the encoded symbols, as well as the degrees associated, can be written as follows:

$$d = 1, \qquad LT_1 = M_1 \tag{2.23}$$
$$d = 2, \qquad LT_2 = M_2 \oplus M_3 \tag{2.24}$$
$$d = 2, \qquad LT_3 = M_2 \oplus M_4 \tag{2.25}$$
$$d = 2, \qquad LT_4 = M_3 \oplus M_4 \tag{2.26}$$
$$d = 3, \qquad LT_5 = M_1 \oplus M_2 \oplus M_3 \tag{2.27}$$
$$d = 2, \qquad LT_6 = M_1 \oplus M_3 \tag{2.28}$$

where LT_x and M_x are the x^{th} encoded and source symbols, respectively. These encoded symbols as well as the information about which symbols comprise are sent to the transmitter as can be seen in Fig. 2.3. The transmitted symbols essentially form a system of simultaneous equations, thus K independent symbols translate to the K equations needed to solve the equations and thus decode the symbols. The source data and encoded symbols shown produce the following set of equations:

$$\begin{bmatrix} 1 & 0 & 0 & 0 \\ 0 & 1 & 1 & 0 \\ 0 & 1 & 0 & 1 \\ 0 & 0 & 1 & 1 \\ 1 & 0 & 1 & 1 \\ 1 & 0 & 0 & 1 \end{bmatrix} \begin{bmatrix} M_1 \\ M_2 \\ M_3 \\ M_4 \end{bmatrix} = \begin{bmatrix} LT_1 \\ LT_2 \\ LT_3 \\ LT_4 \\ LT_5 \\ LT_6 \end{bmatrix}, \tag{2.29}$$

that can be solved to retrieve the source data, where LT_x and M_x are the x^{th} encoded and source symbols, respectively.

Once decoding is complete, the receiver signals back to the sender that the symbols have been recovered, and transmission of the next set of symbols can begin. If this signal is not received, the transmitter will continue coding and sending LT symbols under the assumption that the previous symbols were insufficient to solve the system and/or that symbols were dropped/erased. Only six symbols are shown for clarity regarding the codes. Still, this system would keep producing newly encoded symbols and inevitably repeat the old ones until it was signalled to stop, whether from a timeout procedure or a signal from the receiver that the message had been decoded or a similar mechanism.

Several decoding algorithms have trade-offs in complexity, computational cost and the number of symbols beyond the theoretical N that the algorithm needs to work i.e. the overhead. The commonly used methods are Belief Propogation (BP) and various improvements on Gaussian Elimination (GE) such as Incremental Gaussian Elimination (IG) and a recently developed method: On the Fly Gaussian Elimination (OFG) [56, 57]. While the latter two are all essentially Gaussian Elimination to various degrees of optimisation, BP is fundamentally different and realises on receiving symbols of degree one, a limitation not present in GE based methods.

2.3.2 Decoding: Belief Propagation

Belief propagation is one of the commonly used methods for decoding LT codes [55]. The algorithm uses symbols of degree one to decode received symbols, and it cannot begin until at least one symbol of degree one is received. A symbol of degree is essentially just a symbol, and so when it is received, it is added to the decoded symbols. When a new symbol is received with a degree greater than 1, the decoded symbols are checked to see if the received symbol contains any of the decoded symbols. If the received symbol contains some decoded symbols, it is XOR-ed with all relevant decoded symbols. This produces a new symbol whose degree has decreased by one for every symbol that was part of

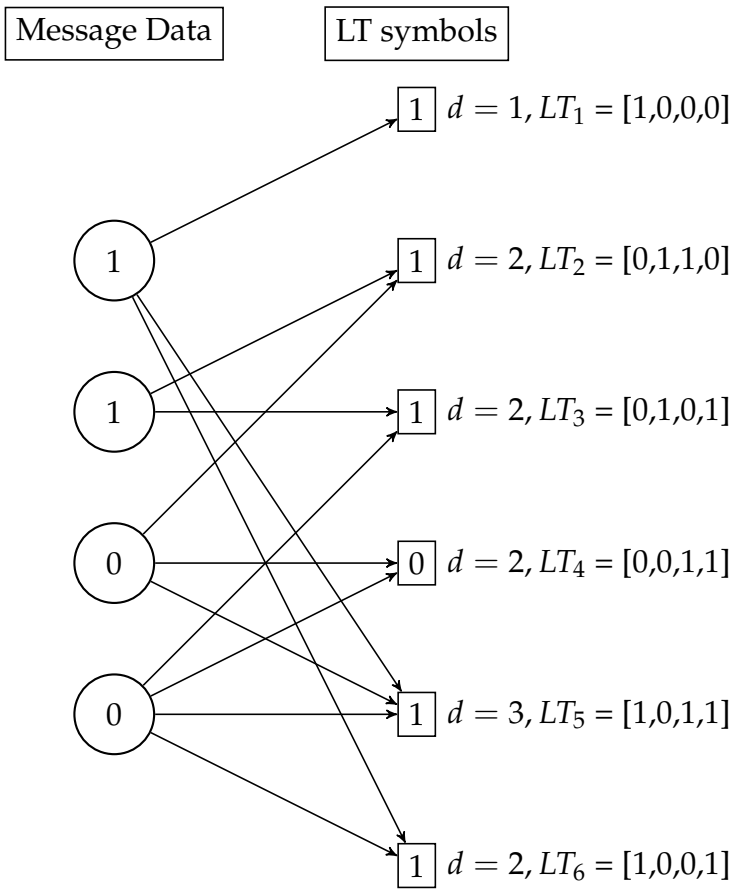

Figure 2.3: An illustration of how LT codes work. The encoded symbols are of varying degrees, indicating the number of symbol symbols XOR-ed to make them, and the symbol symbols used is noted with each LT symbol to enable decoding.

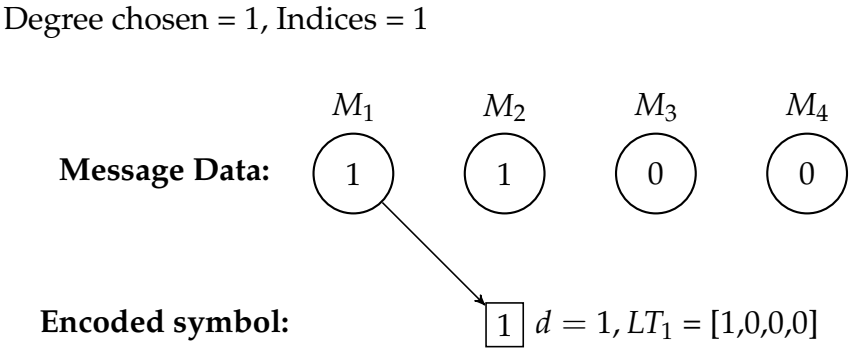

Figure 2.4: The process of encoding the first symbol can be seen. The degree chosen for this symbol is one, and the index randomly chosen for that is 1, and so the first symbol becomes the encoded symbol.

it and the decoded symbols. If the new symbol now has a degree of one is added to the decoded symbols; if the degree is zero, it is discarded as no useful information was gained, and if it still has a degree higher than one, it is kept in a buffer. This process repeats until a new symbol of degree one is found either by simply arriving in that form or by decomposition of higher degree symbols.

This relatively simple process does not involve directly solving a complex system of linear equations and so is computationally cheaper than GE based methods. This does, however, come at the cost of overhead. For Fig. 2.3, GE-based methods would decode at the fourth encoded symbol resulting in no overhead. Like GE, OFG creates a matrix representing simultaneous equations that can be solved

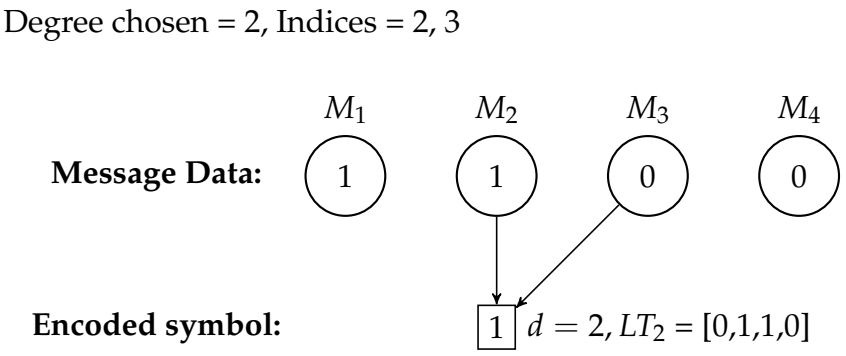

Figure 2.5: The process of encoding the second symbol can be seen. The degree chosen for this symbol is 2, and the indices randomly chosen for that are 2 and 3, and so those two data symbols are XOR-ed, and the result is an encoded symbol.

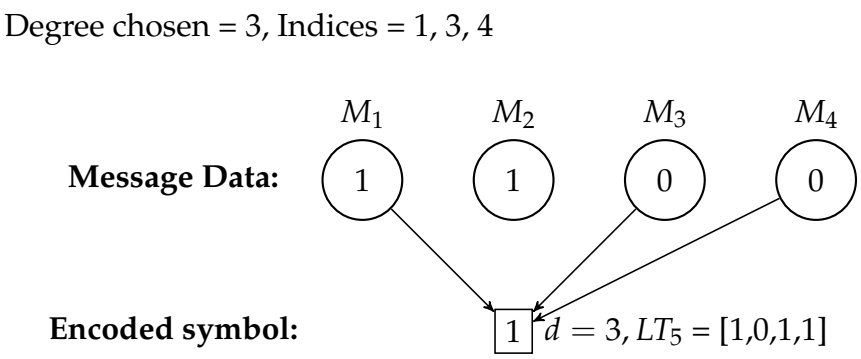

Figure 2.6: The process of encoding the third symbol can be seen. The degree chosen for this symbol is 3, and the indices randomly chosen for that are 1, 3 and 4, and so those 3 data symbols are XOR-ed, and the result is an encoded symbol.

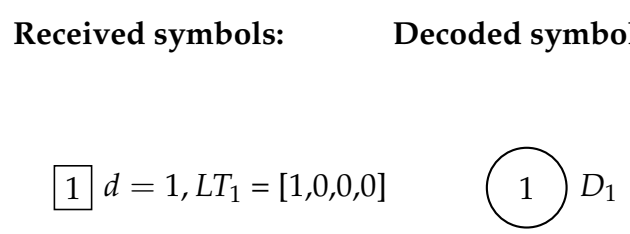

Figure 2.7: Step 1. The first symbol is received. It has a degree of one and is thus immediately decoded. No symbols enter the buffer

.

to decode LT symbols. This is not the case when using BP on the same example, as shown in Figs. 2.7 to 2.14. Here D_x is the x^{th} decoded symbol and assuming no errors occurred, it is equivalent to M_x.

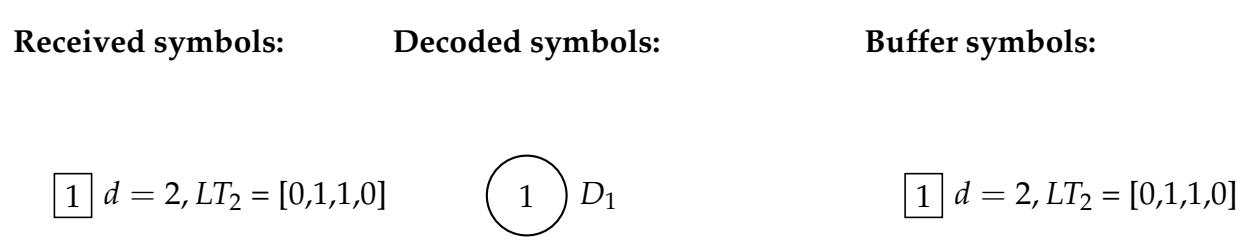

Figure 2.8: Step 2. The second symbol arrives but does not have a degree of one and does not include any of the already decoded symbols, so it is added to the buffer

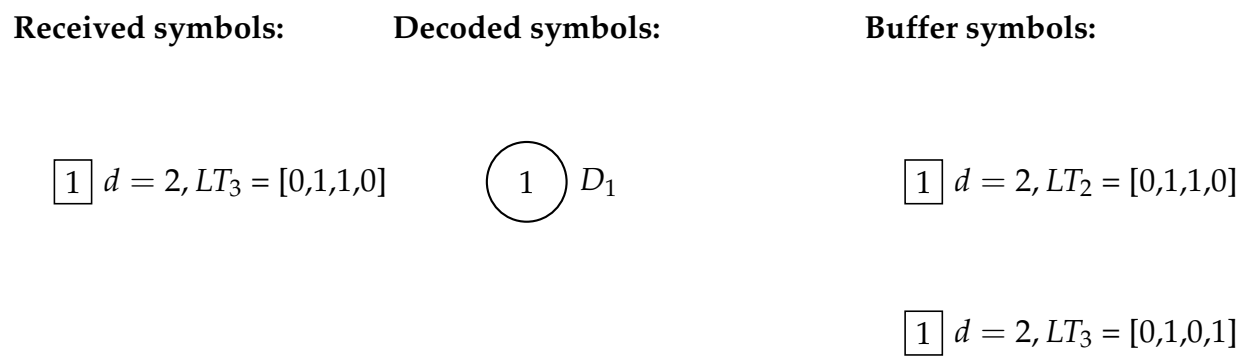

Figure 2.9: Step 3. The third symbol arrives but does not have a degree of one and does not include any of the already decoded symbols, so it is added to the buffer, and now the buffer contains two symbols

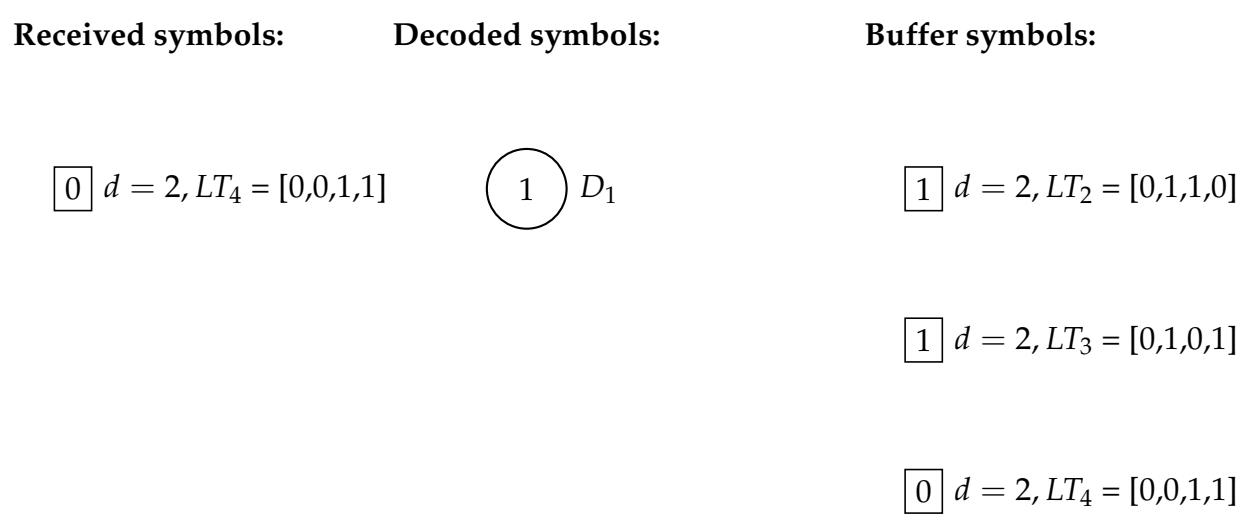

Figure 2.10: Step 4. The fourth symbol arrives but does not have a degree of one and does not include any of the already decoded symbols, so it is added to the buffer, and now the buffer contains three symbols

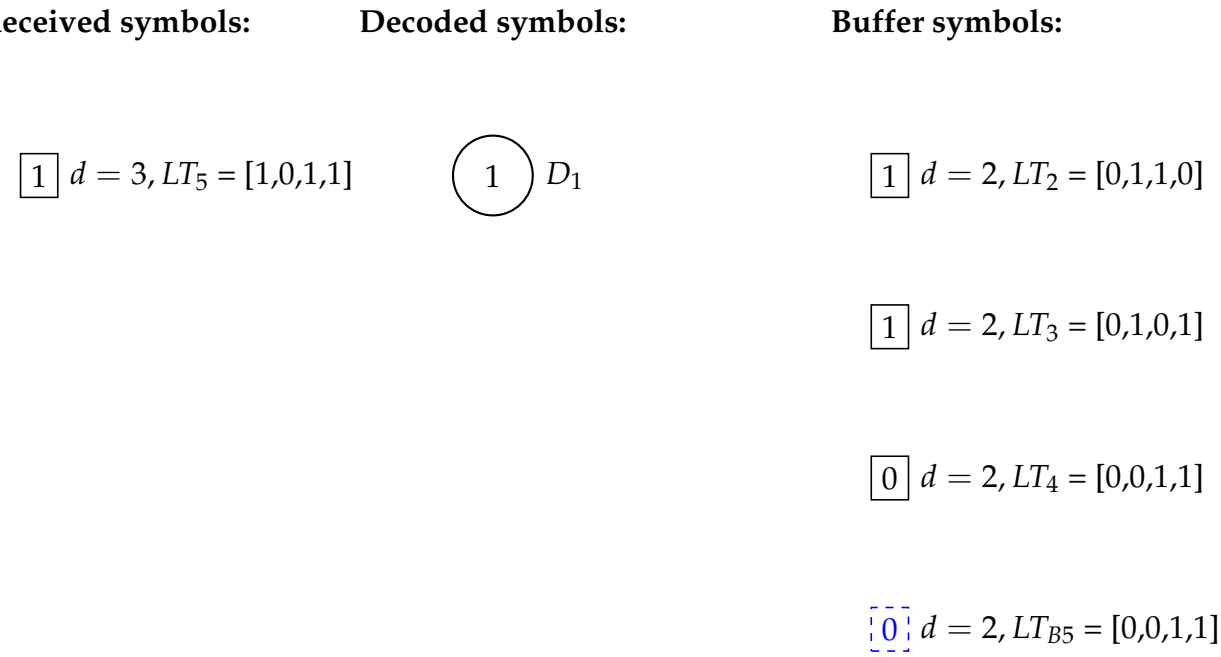

Figure 2.11: Step 5. The fifth symbol arrives but does not have a degree of 1. However, it does include one of the decoded symbols, so that symbol is removed and the degree lowered by 1. This new modified symbol, LT_{B5}, is still not of degree one and does not include any of the already decoded symbols, so it is added to the buffer, and now the buffer contains four symbols

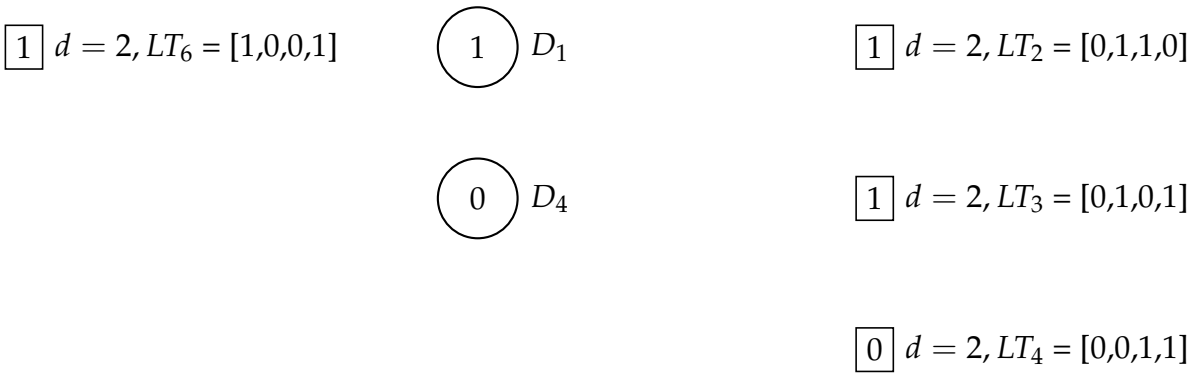

Figure 2.12: Step 6. The sixth symbol arrives. It has a degree of two but includes a symbol that has been decoded. This symbol is removed and what remains is a degree one symbol, a source symbol, D_4, which is added to the decoded symbols.

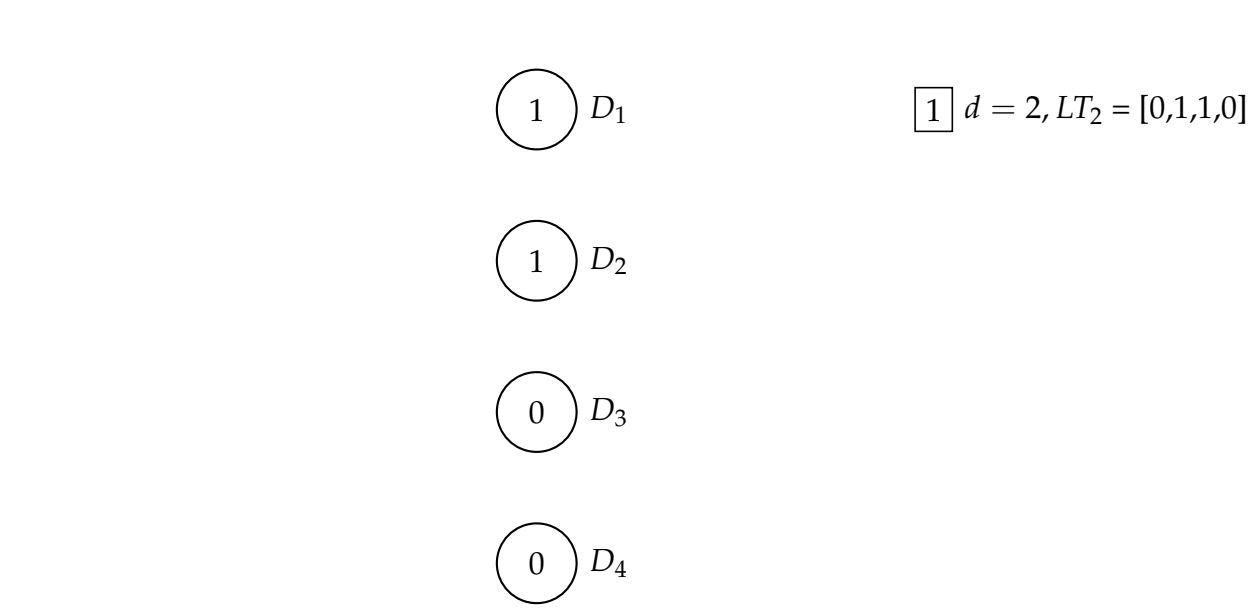

Figure 2.13: Step 7. Since the previous step added a new symbol to the decoded ones, that symbol is removed from the corresponding symbols in the buffer, which happened to be degree 2. This results in two symbols being added to the decoded and one symbol left in the buffer.

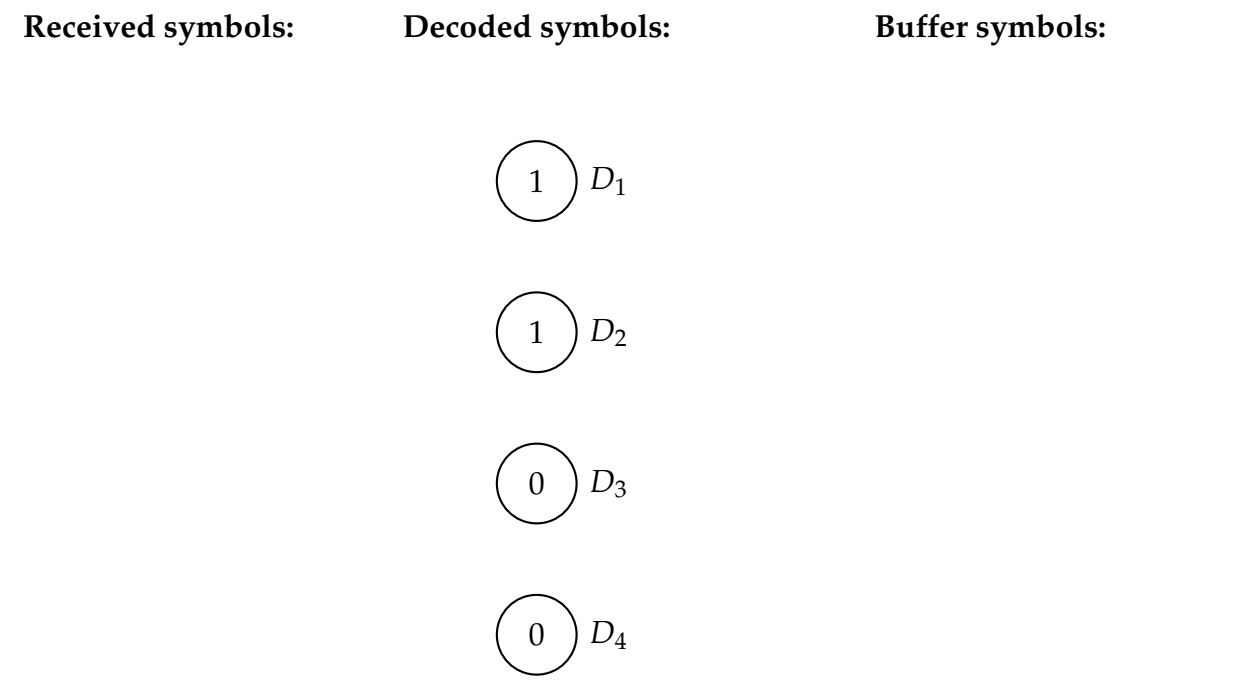

Figure 2.14: Decoding complete. The final symbol in the buffer did not provide any information as after the decoded symbols were removed from it, it had degree zero.

2.3.3 Decoding: Gaussian Elimination

OFG is a GE adjacent algorithm for decoding LT codes that generate a sparse solution matrix to improve decoding efficiency [56] . OFG and other GE based methods work on the presentation of LT codes in the form of Eq. 2.30

Received symbols: G**:** m**:** y**:** **XOR**

$\boxed{1}$ $d = 1, LT_1$ = [1,0,0,0] $\begin{bmatrix} 1 & 0 & 0 & 0 \\ 0 & 0 & 0 & 0 \\ 0 & 0 & 0 & 0 \\ 0 & 0 & 0 & 0 \end{bmatrix} \begin{bmatrix} M_1 \\ M_2 \\ M_3 \\ M_4 \end{bmatrix} = \begin{bmatrix} 1 \\ 0 \\ 0 \\ 0 \end{bmatrix}$ None

Figure 2.15: Step 1: The first symbol is received. The lowest index is 1, and that row of G is empty, so the symbol is directly inserted. No XOR operations are needed.

Received symbols: G**:** m**:** y**:** **XOR**

$\boxed{1}$ $d = 2, LT_2$ = [0,1,1,0] $\begin{bmatrix} 1 & 0 & 0 & 0 \\ 0 & 1 & 1 & 0 \\ 0 & 0 & 0 & 0 \\ 0 & 0 & 0 & 0 \end{bmatrix} \begin{bmatrix} M_1 \\ M_2 \\ M_3 \\ M_4 \end{bmatrix} = \begin{bmatrix} 1 \\ 1 \\ 0 \\ 0 \end{bmatrix}$ None

Figure 2.16: Step 2: The first symbol is received. The lowest index is 2, and that row of G is empty, so the symbol is directly inserted. No XOR operations are needed.

$$G \cdot m = y, \tag{2.30}$$

where G is a $N \times K$ vector of indices corresponding to the encoded symbols received and m is the $N \times 1$ vector of source symbols, and y is a $N \times 1$ vector of encoded symbols. $N \geq K$ in general and $N = K$ in the case of OFG. Before any back substitutions are performed, y corresponds to the encoded symbols received.

The initial assumption is that G is a partial upper triangular matrix where the leftmost 1 in a row is on the diagonal or the row is empty. When a symbol is received, the index of the lowest symbol part of that encoded symbol is checked, which can be denoted as s_i. The row that corresponds to that index, $G[s_i]$, is checked. If the row is empty, the new symbol is added to the row. If the row is non-empty, the symbol corresponding to that row is XOR-ed with the received symbol, which results in a new symbol where $s_i' > s_i$. This process is repeated with $G[s_i']$ until the symbol is placed into G or all the 1s are eliminated. This is the basic OFG, but it can be augmented with a swap heuristic.

The heuristic is that if the new symbol has a lower degree than the row it is compared to, it is swapped with that row, and that row becomes the new symbol, and the process continues as normal. This results in a sparser matrix at the end, which reduces the complexity of the final back substitution. The process of OFG for the example in Fig. 2.3 can be seen in Figs. 2.15 to 2.21. The resulting G matrix is triangular as per the assumption, which results in simpler back substitution. In the case presented, the difference between OFG and IG is not present for the final G and B matrices, respectively. Still, the OFG algorithm spreads the complexity of triangulation throughout the process and has steps to ensure that the resulting matrix is sparse. IG does not have this same goal, so if triangulation fails, the new symbols are not added with the goal of sparsity, and so a full row in B will never be replaced by a lower degree and thus better row later on.

In the case presented in Fig. 2.3, the decoding can only be completed after the sixth symbol arrives because symbols of degree 1 or that can be reduced to degree 1using the decoded symbols are needed. Symbols 4 and 5 are linearly dependent on the previous symbols and so provide no new information.

Received symbols:	G**:**	m**:**	y**:**	**XOR**
$\boxed{1}$ $d = 2, LT_3$ = [0,1,0,1]	$\begin{bmatrix} 1 & 0 & 0 & 0 \\ 0 & 1 & 1 & 0 \\ 0 & 0 & 1 & 1 \\ 0 & 0 & 0 & 0 \end{bmatrix}$	$\begin{bmatrix} M_1 \\ M_2 \\ M_3 \\ M_4 \end{bmatrix}$	$= \begin{bmatrix} 1 \\ 1 \\ 0 \\ 0 \end{bmatrix}$	$LT_3' = G[2] \oplus LT_3$ $y' = 0, d' = 2$ LT_3' = 0,0,1,1

Figure 2.17: Step 3: The third symbol is received. The lowest index is 2, and that row of G is filled, and this symbol has a higher degree. An XOR operation is performed with $G[2]$, and the resulting symbol has the lowest index 3, and that row is empty, so the symbol is inserted. No further XOR operations needed.

Received symbols:	G**:**	m**:**	y**:**	**XOR**
$\boxed{0}$ $d = 2, LT_4$ = [0,0,1,1]	$\begin{bmatrix} 1 & 0 & 0 & 0 \\ 0 & 1 & 1 & 0 \\ 0 & 0 & 1 & 1 \\ 0 & 0 & 0 & 0 \end{bmatrix}$	$\begin{bmatrix} M_1 \\ M_2 \\ M_3 \\ M_4 \end{bmatrix}$	$= \begin{bmatrix} 1 \\ 1 \\ 0 \\ 0 \end{bmatrix}$	$LT_4' = G[3] \oplus LT_4$ $y' = 0, d' = 0$ LT_4' = 0,0,0,0

Figure 2.18: Step 4: The fourth symbol is received. The lowest index is 3, and that row of G is filled, and this symbol has a higher degree. An XOR operation is performed with $G[3]$ and the resulting symbol has degree zero and thus is discarded as it provided no new information

Received symbols:	G**:**	m**:**	y**:**	**XOR**
$\boxed{1}$ $d = 3, LT_5$ = [1,0,1,1]	$\begin{bmatrix} 1 & 0 & 0 & 0 \\ 0 & 1 & 1 & 0 \\ 0 & 0 & 1 & 1 \\ 0 & 0 & 0 & 0 \end{bmatrix}$	$\begin{bmatrix} M_1 \\ M_2 \\ M_3 \\ M_4 \end{bmatrix}$	$= \begin{bmatrix} 1 \\ 1 \\ 0 \\ 0 \end{bmatrix}$	$LT_5' = \mathrm{G}[1] \oplus LT_5$ $y' = 0, d' = 2$ LT_5' = 0,0,1,1

Figure 2.19: Step 5: The fifth symbol is received. The lowest index is 1, and that row of G is filled, and this symbol has a higher degree. An XOR operation is performed with G[1], and the resulting symbol has degree two and thus is taken forward as if it was just received

This shows a feature of rateless codes that makes them good for symbol erasure channels because if symbols 4 and 5 were lost/erased, the original symbols could still be decoded. There have been efforts to implement decoding on an Field Programmable Gate Array (FPGA) for a link that could operate at 1 Gigabits per second (Gbps) [29]. This was done on Raptor codes, but the algorithm used was BP, and because Raptor codes include LT codes, a similar system would be possible for LT codes.

Received symbols:	G**:**	m**:**	y**:**	**XOR**
$\boxed{0}$ $d = 2, LT'_5$ = [0,0,1,1]	$\begin{bmatrix} 1 & 0 & 0 & 0 \\ 0 & 1 & 1 & 0 \\ 0 & 0 & 1 & 1 \\ 0 & 0 & 0 & 0 \end{bmatrix}$	$\begin{bmatrix} M_1 \\ M_2 \\ M_3 \\ M_4 \end{bmatrix}$	$= \begin{bmatrix} 1 \\ 1 \\ 0 \\ 0 \end{bmatrix}$	$LT''_5 = \text{G}[3] \oplus LT'_5$ $y'' = 0, d'' = 0$ $LT''_5 = 0,0,0,0$

Figure 2.20: Step 6: The modified fifth symbol is treated as received. The lowest index is 3, and that row of G is filled, and this symbol has a higher degree. An XOR operation is performed with G[3], and the resulting symbol has degree zero and thus is discarded as it provided no new information

Received symbols:	G**:**	m**:**	y**:**	**XOR**
$\boxed{1}$ $d = 3, LT_6$ = [1,0,0,1]	$\begin{bmatrix} 1 & 0 & 0 & 0 \\ 0 & 1 & 1 & 0 \\ 0 & 0 & 1 & 1 \\ 0 & 0 & 0 & 1 \end{bmatrix}$	$\begin{bmatrix} M_1 \\ M_2 \\ M_3 \\ M_4 \end{bmatrix}$	$= \begin{bmatrix} 1 \\ 1 \\ 0 \\ 0 \end{bmatrix}$	$LT'_6 = \text{G}[1] \oplus LT_6$ $y' = 0, d' = 1$ $LT'_6 = 0,0,0,1$

Figure 2.21: Final Step: The sixth symbol is received. The lowest index is 1, and that row of G is filled, and this symbol has a higher degree. An XOR operation is performed with G[3], and the resulting symbol has the lowest index as 4, and this row is empty, so the symbol is entered. The resulting G matrix is very sparse and triangular. As a result, the back substitution and thus decoding of the symbols is simple

.

CHAPTER 3

Fritchman modelling for the FSO channel

This chapter is based on the following publication:

X. Nghatsane L. Cheng, and M. A. Cox, "Fritchman modeling for correlated turbulence-induced errors in FSO communication," *Applied Optics 60*, 1801–1808 (2021)

The author was responsible for the conceptualisation of the work as well the experimental data collection and analysis. The paper was written with assistance from the co-authors.

WHEN lasers propagate through the air, the transmitted beam undergoes fading because of attenuation and atmospheric turbulence. This has resulted in numerous studies to better model and correct for errors on the FSO channel. Still, to date, this problem is largely unsolved [10, 44]. An aspect of turbulence-induced fading that causes significant mitigation difficulty is deep fading, where the received signal is below a usable threshold. Commonly used probabilistic models for FSO channel fading, such as Log-Normal [44] and the Gamma-Gamma PDF [58, 59] can accurately predict the total amount of deep fading over an extended time frame when used in the right conditions [46]. While it is generally accepted that the FSO channel does have memory (inherent in Taylor's frozen turbulence hypothesis) [34–37], models based only on probability distributions are insufficient for modelling this memory. Therefore research and development of turbulence mitigation strategies is hindered.

Models that account for memory are needed to better aid the design of fading mitigation strategies for use in FSO systems. The overall BER of the two models may be similar or identical, but in the model that does not account for memory, the spread of these errors is distributed differently. The resulting designs of FEC or interleaving would likely end up sub-optimal, as shown in [60, 61]. Specifically, these codes would not be equipped to deal with so-called burst errors typically found in memory channels. They would fail if deployed on real channels that were more prone to bursts than random errors unless they were made extremely strong, to the point of wasting capacity.

Indeed, studies using Markov modelling techniques have been done to model the FSO channel's memory [18–24]. However, they have primarily focused on the transmitted or received signal and thus directly model physical phenomena. This has been discussed in the literature review in 1.1.

Based on this review, a Fritchman-based Markov modelling approach (which is an extension of the Gilbert-Elliot approach in [27]) is proposed for the FSO channel considering the resulting digital signal in a bit-wise fashion [50, 62]. This significantly reduces the resulting channel model

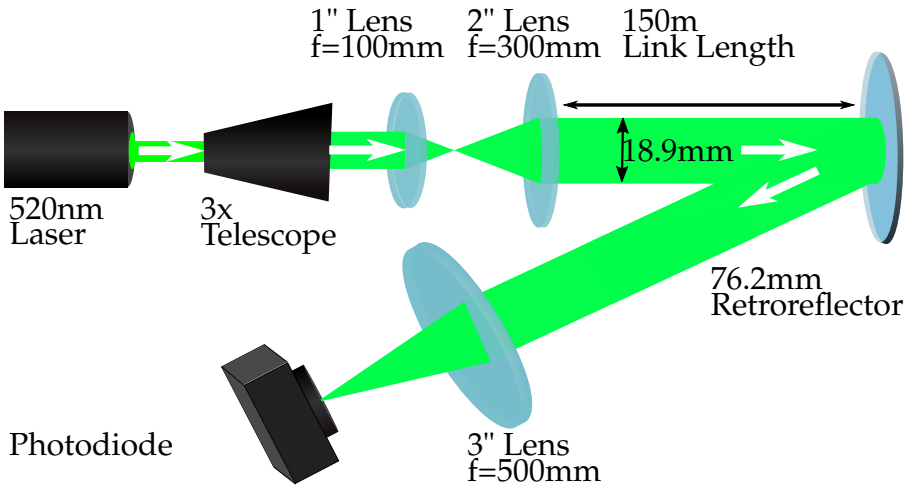

Figure 3.1: Experimental Setup used to transmit and receive the link. The beam is expanded using a telescope to reduce the effects of divergence and is focused on the photodiode for signal acquisition.

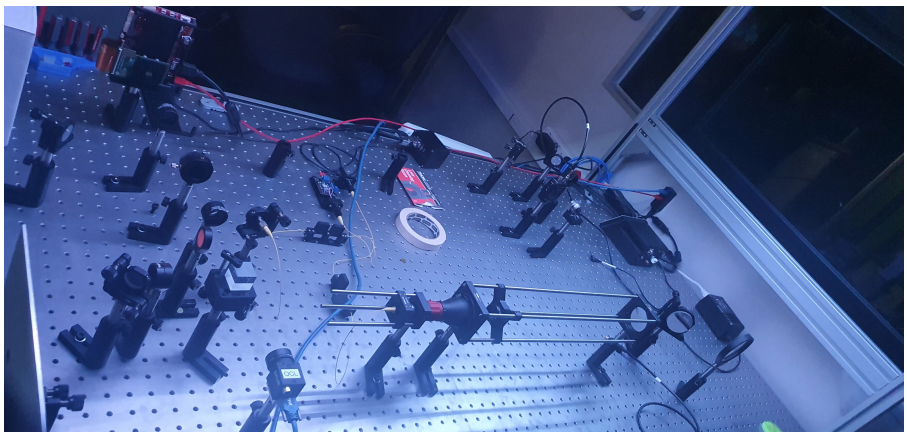

Figure 3.2: A picture of the setup that was used for the link in this study. A stable optics bed was used to isolate the errors to being turbulence-induced to as great an extent as possible.

complexity, allowing for fast, efficient and holistic channel simulation. Several Fritchman models are developed using data obtained from a 300 m link in different turbulence conditions and the approach for developing these models is presented. These models are beneficial for modelling the result of bursty deep fading. Such models enable the use of existing mitigation techniques developed for other challenging memory channels such as power-line communications [63–65]. This will ultimately help improve the performance of FSO links in future.

3.1 Experimental Setup And Methodology

The data used for this experiment was recorded using a setup represented in Fig. 3.1 and shown in the picture of the actual implementation in Figs. 3.2 and 3.3. Though it is expected that feedback based tracking (or adaptive optics) would improve the performance of the link, tracking was not used. An expanded 520 nm modulated laser beam was made to propagate over 300 m (150 m to a retro-reflector and back along a slightly offset path to prevent atmospheric reciprocity) and recorded for offline analysis. The laser was operating at a transmitted power of 3 mW. The link was situated inland at the University of the Witwatersrand in Johannesburg, South Africa, at an altitude of approximately 1.7 km.

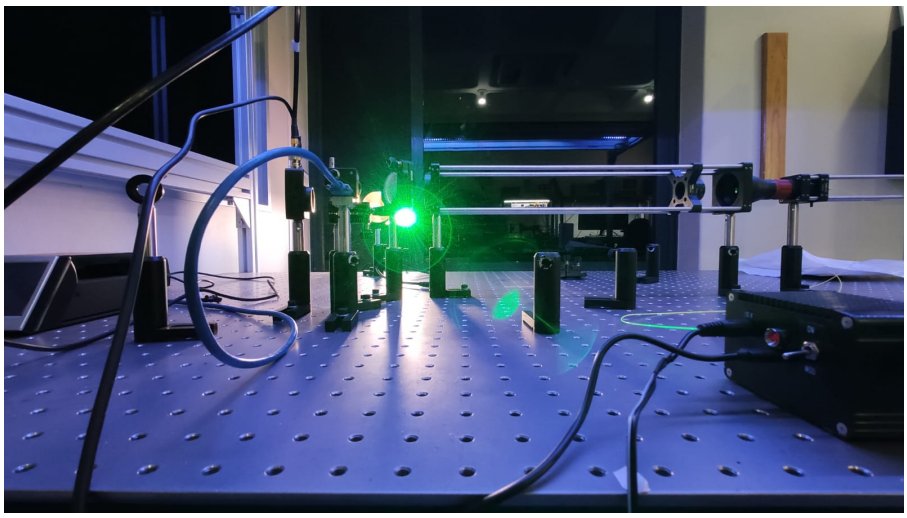

Figure 3.3: An alternative angle of the setup demonstrating the green laser used

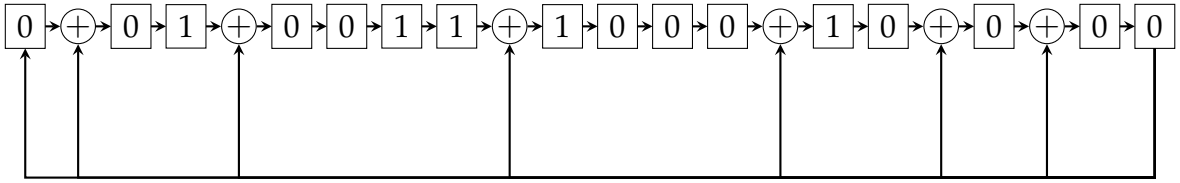

Figure 3.4: The Galois LFSR used for producing the bitstream used in this simulation. Note that the state presented corresponds to the starting configuration determined by the seed of 0x2710. The arrows indicate the direction of shifting at each iteration. This next state from this starting configuration is 0x1388.

The link established was relatively simple, using hardware that was put together to establish an FSO link. The bitstream used was based on a Galois Linear Feedback Shift Register (LFSR) to achieve sufficient randomness in the bitstream to simulate a real signal. A 16 bit LFSR was considered sufficient to achieve the randomness required when the speed of the link and the implementation hardware was considered. To achieve a maximal period, the seed used was 0x2710, 10000 in decimal, and the polynomial used was 0xD008, 53526 in decimal. The resulting LFSR can be seen in Fig. 3.4.

The modulation and LFSR functionality was achieved using a Teensy 4.0. This was achieved by programming a simple script that would turn a given pin on and off based on the bitstream from the LFSR implementation, and this pin was attached to a custom laser driver. This was set up on a stable optics table, as shown in Fig. 3.2. Alignment to the retroreflector required waiting until the evening to see the incident and returning beams. A (model) photodiode was used to receive the laser, which was connected to a USRPN210.

To implement demodulation, MATLAB was first used to record the samples of the signal from the USRP. The signal was modulated using NRZ-OOK at 4 Kb/s and recorded over 24 hour periods. The samples were recorded at a sample rate of 200000 samples/sec. The 24 hour period was chosen to capture the dynamics of the link throughout the day without creating a continuous multi-day sample that would have been extremely large and subsequently detrimental for analysis. This was seen as sufficient to capture the signal without resulting in extremely large files. The relatively simple structure of the link and equipment used meant that a clocking signal was not available for use. The initial approach to demodulating was assuming that the transmitted and received signal worked with the assumption that a clocking signal at double the transmitted signal's frequency would allow for successful demodulation.

In this assumption, a bit lasted 2.5×10^{-5} seconds. With the sample rate above, this corresponded to 50 samples. The sampling clock being at double the transmission frequency meant that only 25 of

these samples would be used for demodulation. While the assumption held for a portion of the signal, physical inspection showed that the signal would vary by a few samples, with some bits having 24 or 23. At first, this deviation didn't result in any errors in demodulation. Over an entire frame, enough of these occurrences resulted in the demodulated bitstream being largely incorrect as enough shifts would have occurred to cause a bit to be skipped and the subsequent bits to all be incorrect. This deviation can be seen in Figure 3.5.

The first attempt to solve this synchronisation error was to recover the clocking signal from the transmitted signal. This technique uses an initial approximate frequency of the signal and then applies logic in the clocking signal whenever a transition occurred in the received signal [66]. The method used for this and the final iteration is summarised in Alg. 1

This technique was used to reconstruct a signal that would be a square wave with a varying frequency that varied around double the transmitted signal's frequency. This first started by using the same sampling frequency as the data signal. With this sampling frequency, the period of one sample was calculated. In the case presented, the sampling frequency was 200 kHz and the time step of a sample was 5×10^{-6} s. With a transmitted frequency of 2Khz, the approximate frequency of the recovery clock was 4Khz which corresponded to a period of 2.5×10^{-4}, which corresponded to 50 samples. In an ideal situation, this meant that the recovery clock could be reconstructed by transitioning between a high and low signal every 25 samples. This represents the initial assumption. As stated above, the situation was not ideal, and the recovery clock was to compensate for the phase shifts in the received signal.

This was achieved by altering the logic of transitioning between states every 25 samples to transition every 25 samples unless the data signal triggered a transition. The logic applied for transition occurring is an XOR of the previous and current data signal state. This meant that a transition would only be detected if the signal was above/below the threshold for the previous sample and the opposite was true for the current sample. This is described in Alg. 2. Whenever the data signal triggered a transition, the normal timer for transitioning was reset to zero, the state of the clock was set to high, and the assumed state of the data signal was inverted.

This was because a transition in the data was treated as representative of a new bit. When the clock signal was in a high state, this had the effect of extending that high state beyond the usual 25 samples, typically to 26 or 27 samples. In the opposite case, where the clock signal was in a low state, this would result in the low state being shorter than 25 samples. The first effect meant that if a phase shift caused a bit to be extended a few samples, the effect on the following bit would be minimised by sampling more of the following bit, and this would prevent the following bit from affecting the next bit as it would still be fully sampled. The second effect meant that if a phase shift caused a bit to be shorter than the ideal number of samples, this would cause samples corresponding to the next bit not to be sampled as expected.

Transitions were only triggered in the recovery signal based on transitioning from a one to a zero or vice versa because a bit affecting the sampling of the following identical bit would not affect the recovered bitstream. In contrast, a bit affecting the following bit that was opposite in state could cause a bit flip resulting in an error in the recovered bitstream. This process is summarised in Alg. 1 and compensated for the instances where the number of samples corresponding to a bit deviated from the assumption of 25.

The second iteration of the demodulation did improve on the first one, but due to being based on the signal itself, a problem occurred that would not have been present in the first iteration. The problem was due to the transitions initially being defined as when the signal crossed from the side of a threshold specified as the signal's mean as described in Alg. 2. The second iteration failed to account for a slight amount of signal attenuation. Two transitions occurred to reconstruct the clocking signal if the data signal was near this threshold and crossed over it and back due to slight attenuation. This would result in a bit that corresponded to as little as one sample being recorded.

To solve this, instead of exclusively using a hard threshold, a simple gradient-based algorithm was employed. Continual measurement of the gradient of the samples was calculated, and when the gradient passed a threshold, a transition was deemed to have occurred as described in Alg. 3. This allowed for the recovery of a clocking signal that was heavily dependent on the transmitted signal

Algorithm 1: Clock Recovery Implementation

Data: $D(s)$ where $D(s)$ is the data signal of f_d Hz with s samples
Result: $C(s)$ where $C(s)$ is the clock recovery signal with s samples
$f_c \leftarrow 2 * f_d$;
$S_t \leftarrow 1/2 * f_c$;
$C_s \leftarrow high$;
$T_c \leftarrow false$;
$S_p \leftarrow 0$;
$H \leftarrow false$;
for $i \leftarrow 1$ **to** s **do**
    $C(i) \leftarrow C_s$;
    $T_c \leftarrow F(T_c, H, i, D)$;
    if T_c **then**
        $C_s \leftarrow$ high;
        $H \leftarrow !H$;
        $S_p \leftarrow 0$;
    else if $S_p \geq S_t$ **then**
        $S_p \leftarrow S_p - S_t$;
        $C_s \leftarrow !C_s$;
    $S_p \leftarrow S_p + 1$;
end
where f_c is the approximate frequency of the clocking signal, S_t is half the period of the clocking signal, C_s is used to track the state of the clocking signal, T_c is used to check if a transition should occur based on the data signal, S_p is used to track the number of samples until a transition based on the frequency should occur, and H is used to track whether the state of the data should trigger a transition based on the previous state. F refers to one of the two methods for checking for the transition

Algorithm 2: Initial implementation of checking for transition

if $XOR(H, D(i) > T_d)$ **then**
    return $T_c \leftarrow true$
return $T_c \leftarrow false$;
where T_d is the specified data signal threshold for a transition.

Algorithm 3: Second Iteration of checking for transition

if $XOR(H, D(i) > T_d)$ **then**
    $G \leftarrow gradient(D(i-l), D(i))$;
    return $T_c \leftarrow G > G_t$
return $T_c \leftarrow false$;
where l is the number of samples to calculate the gradient and G_t is a specified gradient threshold for transitioning.

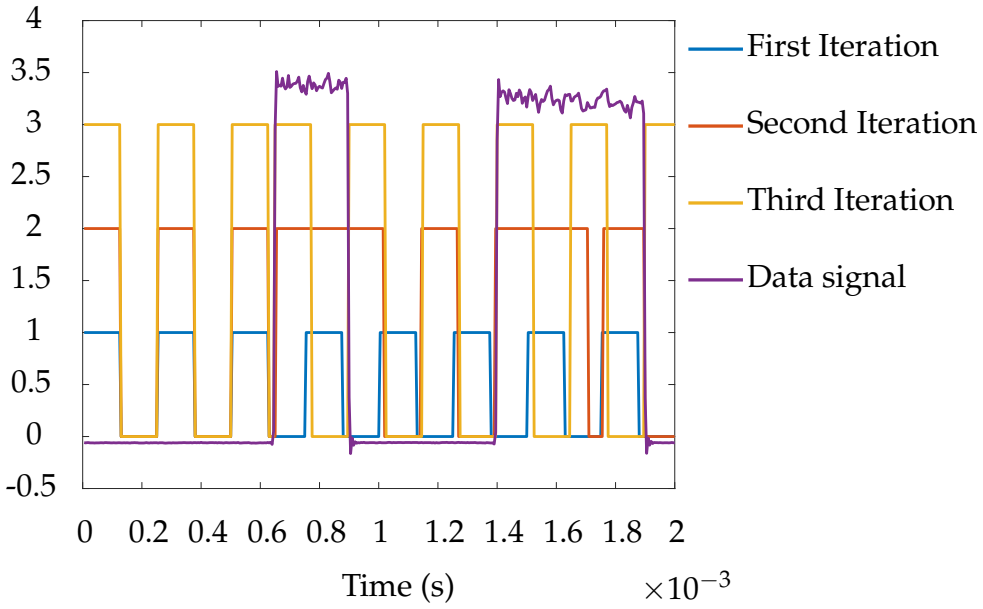

Figure 3.5: This comparison is to show the deficiency of both the initial and second iteration, and the graphs have been scaled for visibility. The first iteration does not align with the data signal and begins to drift. The jitter causes the signal to repeatedly trigger this transition in the second, resulting in one sample covering more than one bit. The third iteration takes advantage of both to better track the signal.

and thus better tracked the intended signal. The gradient-based method worked because, unlike theoretical square waves with an instantaneous transition, square waves from an NRZ-OOK based signal have transition times. These transition times manifest in the form of several samples with an extremely large gradient between them. Figure 3.5 shows the three iterations and the improvement between them. It can be seen that the third iteration better tracks the signal and was deemed to be sufficient to compensate for errors that would have been due to the relatively simple equipment as opposed to the effects of atmospheric turbulence that were the target of the study.

Wind speed, direction and temperature from a weather station on the roof of the transmitting building was also recorded to supplement the optical data with an example shown in Fig. 3.6, which indicates when one of the presented test cases was recorded. Due to the relatively simple setup lacking any form of optical tracking, one form of error that was not compensated for was large scale tracking errors. This probably occurred due to thermal expansion resulting in beam divergence to the point that no samples could be recorded. This is seen in Fig. 3.6 where there is a large gap in the recordings. The rest of the day was sufficient to establish many frames as detailed below, so these errors were not worth compensating for.

The data was split into five minute “frames”, and the average scintillation index for each frame was determined using Eq. 2.1 when the signal was in the on state. Average bit error rate measurements for each frame were also calculated.

Fritchman models were developed based on the received bitstreams for these frames using a Baum-Welch algorithm. The implementation of the algorithm used was the one built into Matlab used for training HMM. The accuracy of the resulting models is measured using the log-likelihood ratio, which also determines when the Baum-Welch algorithm should stop iterating. The fitting tolerance was set to 10^{-12}, and most models were found within 20 iterations. It was found that a three state Fritchman model was adequate to capture the effects of memory in the system. Larger models are indeed more accurate but were deemed insignificantly so.

Larger models increase the computational cost of both training and the use of the model. With the focus of this study in consideration, the additional accuracy does not sufficiently affect the results to warrant the extra computational cost. The number of states in the systems for this experiment is

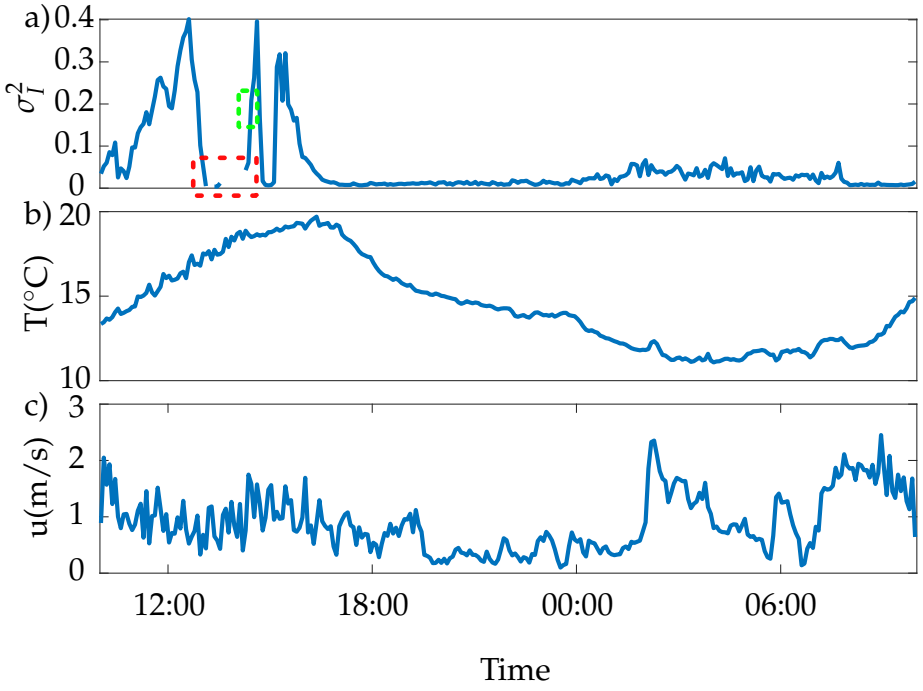

Figure 3.6: The scintillation index, σ_I^2, of the link, perpendicular wind speed, u, and temperature, T on a particular day. Note on (a) in green is the approximate data region used to train the model for $\sigma_I^2 = 0.18$. There is a gap in the measurements highlighted in red, which is due to the complete misalignment of the system, probably due to the thermal expansion of the buildings around midday.

chosen based on these factors. The paradigm of a singular bad state with multiple good states is a standard way to choose the number of states in a Fritchman model and has been demonstrated to be sufficient to capture the memory in the system [64, 67–69]. In addition, a standard Log-Normal distribution was fit to each frame and used to simulate equivalent bitstreams for comparison.

Three of these frames were selected based on their scintillation index for a range of turbulence strengths and are presented here. The scintillation index for each of these test cases is 0.18, 0.35 and 0.52. Unfortunately, the link length makes moderate to strong turbulence conditions unlikely. Nonetheless, the efficacy of the proposed approach is demonstrated, which applies to all turbulence strengths.

3.2 Results and Discussion

The transmission power of the laser, coupled with the link length, resulted in the effect of the turbulence being limited to weak-to-moderate strength. No results for strong turbulence were obtained. In very weak turbulence conditions, the link would be error-free (the baseline BER would be zero) for a long period of time, with random bursts of errors when the turbulence momentarily becomes stronger. Modelling this behaviour is indeed the main contribution of this study.

This section summarises the measurement results and compares the distribution of received errors (as measured) to those that could be expected when simulated using Log-Normal fading in equivalent strength turbulence. It is then shown how a Fritchman modelling approach results in an error distribution closer to what was measured while also maintaining the same BER. This type of model's characteristics is discussed, and then a brief outline of some techniques that might benefit from a model that accounts for the actual bursty error distribution of the FSO channel is provided.

Three cases are presented herein to highlight the accuracy of a Fritchman modelling approach for FSO compared to more common PDF-only signal models. The scintillation indices for each case are

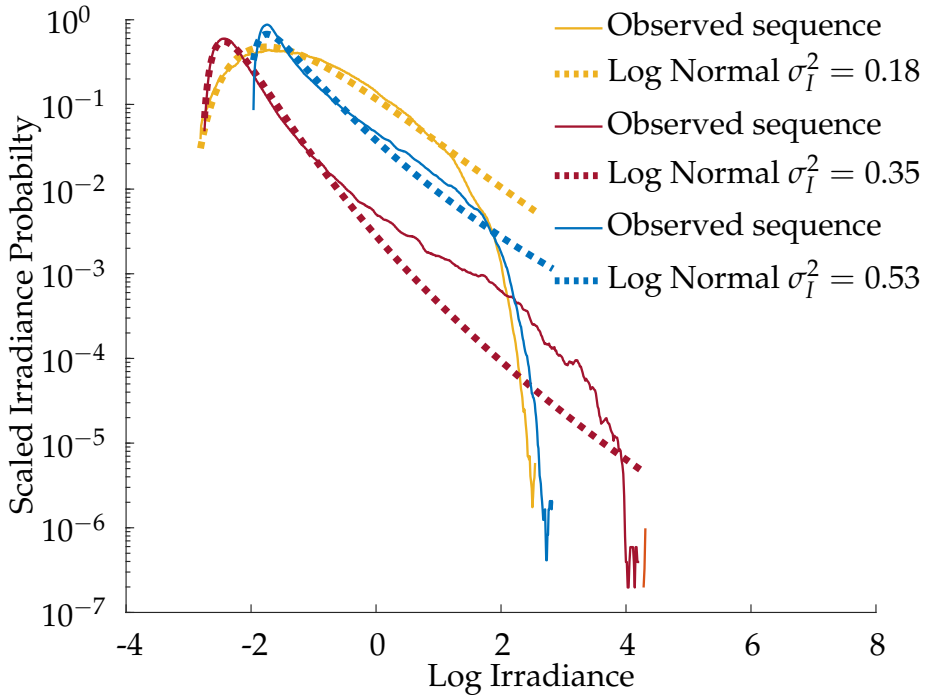

Figure 3.7: Measured fading in comparison to a fitted Log-Normal PDF for each of the cases presented. As expected, the Log-Normal fit is better with weaker turbulence.

$\sigma_I^2 = 0.18$, 0.35 and 0.52 respectively, and the measured PDFs are visible in Fig. 3.7. A Log-Normal model is fitted to each case for comparison, which is also indicated in the figure.

It is clear that as the turbulence becomes stronger, the Log-Normal fit is worse: this is a known limitation of the model, and the use of Gamma-Gamma or more complex fading models would account for this. It was deemed unnecessary to use a more complex model in this work, as the choice of PDF will not significantly impact the distribution of errors. This is because PDF-based models are still IID and therefore have no memory.

σ_I^2 [SI]	0.18	0.35	0.52
T [°C]	19.14	18.64	19.54
u [m/s]	0.65	1.93	1.33
τ [s]	0.019	0.0065	0.0094
BER Observed	4.27×10^{-5}	5.8×10^{-2}	8.9×10^{-2}
BER Fritchman	4.33×10^{-5}	5.78×10^{-2}	9×10^{-2}

Table 3.1: Weather parameters for the different cases presented, according to scintillation index as well as the average bit error rate for the observed sequence and the trained model corresponding to them.

The average weather conditions for each case are given in Tab. 3.1. This data shows the average conditions over the five minute "frames" that are being used to train the model. The BER is also provided, and as expected, the BER gets worse when the turbulence strength increases. In this table, the correlation time, τ, is also given. This has a bearing on the depth of the channels memory. With these standard empirical measures, there is much about the channels memory that cannot be told. Are the errors evenly spread, or are they clumped into bursts?

Unfortunately, no convenient single-number metric exists to describe this "burstiness". For the readers' convenience, the distribution of errors have been plotted in a qualitative way to visualise this burstiness easily and to gain an intuition about the disadvantages of PDF-based models for FSO communication. In Fig. 3.8 (a), a vertical line has been plotted each time a bit is received in error

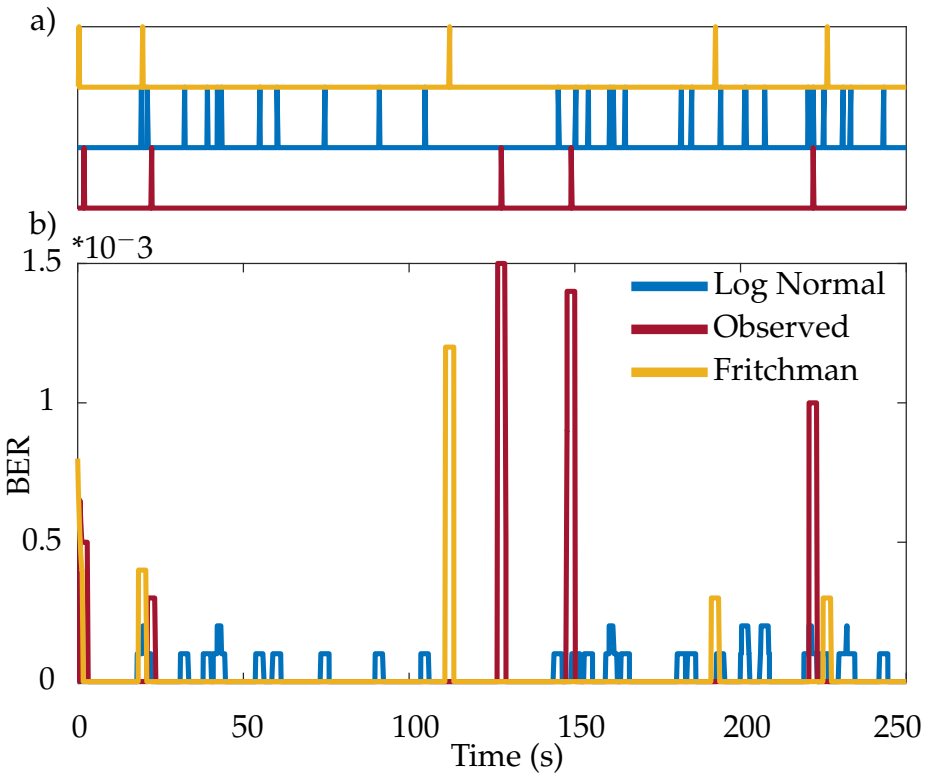

Figure 3.8: (a) A plot of the positions of the errors in a 250-second sample of the bitstream obtained from using the different models and the observed data. Here it can be clearly seen that the Fritchman model more closely resembles the observed sequence when compared to the Log-Normal based sequence. An alternative representation of this data using a moving average to show the number of errors at each point is shown in (b). These two plots correspond to the data for the $\sigma_I^2 = 0.18$ recording, and the BERs of the three sequences are all on the scale of 10^{-5}.

for approximately five minutes of data. On inspection, it is clear that the pattern of errors modelled by random draws from the Log-Normal distribution is quite dissimilar from the observed error distribution, even though they have the same PDF (as shown in Fig. 3.7). In Fig. 3.8 (b) this plot is expanded to a moving average (with a window length of 10k bits) of the number of errors at each point in time. This highlights a similar number of errors in total (i.e. the BER), even though in the observed case, they occur in bursts rather than in a more uniform manner. The specific BER of the sample is not the focus of this graph but instead the discrepancy between the Log-Normal model and the observed sequence.

More scientifically, and as explained in Sec. 2.2, the error-free run plot is a standard way of visualising the channel's memory. While EFRs are not the only possible way to display the characteristics of the bursty channel, they are a standard that can easily scale and show the discrepancies and similarities between models effectively [64, 67].

As shown in Fig. 3.9, it is clear that there is a discrepancy between the observed error-free runs and those predicted by the Log-Normal PDF. The shape of the EFRs denote the nature of the channel in the following ways: in the Log-Normal (and indeed any memoryless PDF-based) model, the error-free runs decrease at a relatively constant rate until the point denoted by the BER. In contrast, the observed distribution drops quickly and then becomes a tail which decreases at a lower rate. Intuitively, if a channel has memory, it is more likely to stay in a specific state for an extended period of time. As error-free runs are the primary concern, the probability of shorter intervals decreases quite rapidly because they indicate changing channel state (i.e. going from no error to an error). Due to the shape of the distributions, the average BER is indeed conserved. Simply put, this discrepancy is generally why conventional error mitigation techniques may not work as well as expected in FSO.

As described in Sec. 2.2, a Fritchman model is a special Markov model commonly used for

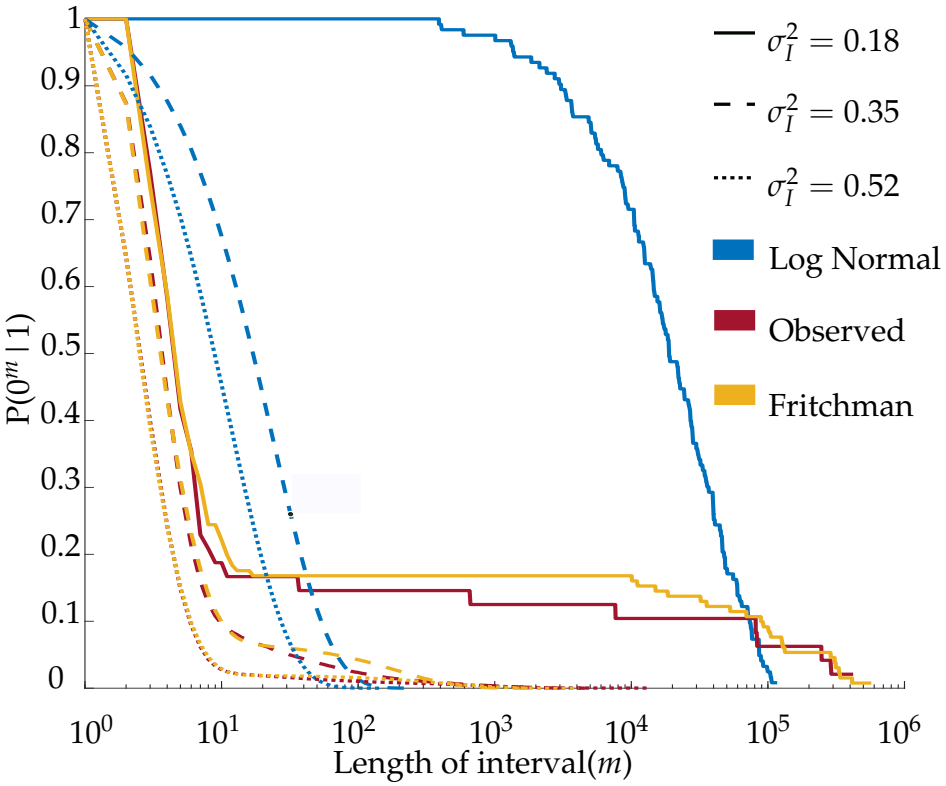

Figure 3.9: The error-free run (EFR) distributions that correspond to the three test cases presented in this work. This plot illustrates the distribution of lengths of good runs, which illustrates the memory present in the channel. At the end of each graph, the tails show that a system will likely persist in a good state once it enters it.

modelling bursty communication channels, but is it suitable for the FSO channel?

The transition probability matrices for the three separate Fritchman models, labelled according to the three different turbulence cases given in Tab. 3.1, are given by Eqs. 3.1, 3.2 and 3.3.

These three matrices show that the models generally behave similarly by having one good state that they tend to persist in (element a_{11} from Eq. 2.15), which captures the nature of the channel to stay in an error-free state for a substantial time. The second good state (a_{22}) also tends to persist but has a higher likelihood of transitioning to the error state than the first good state. These transitions between states, as well as the varying behaviour between the states in the same partition, capture the memory of the system.

$$\mathrm{A}_{0.18} = \begin{bmatrix} 0.9998 & 0 & 0.0002 \\ 0 & 0.7205 & 0.2795 \\ 0.1313 & 0.8687 & 0 \end{bmatrix} \tag{3.1}$$

$$\mathrm{A}_{0.35} = \begin{bmatrix} 0.9950 & 0 & 0.0050 \\ 0 & 0.6716 & 0.3284 \\ 0.0686 & 0.8055 & 0.1259 \end{bmatrix} \tag{3.2}$$

$$\mathrm{A}_{0.52} = \begin{bmatrix} 0.9978 & 0 & 0.0022 \\ 0 & 0.5942 & 0.4048 \\ 0.0194 & 0.6253 & 0.3553 \end{bmatrix}. \tag{3.3}$$

Plots of the resulting error distributions generated from these Fritchman models are also shown in Fig. 3.9. They are an excellent match for the observed sequences compared to the PDF-based model. The number of states in the presented models is sufficient to capture the characteristics of the channel accurately. Additional states could be added to increase further the model's accuracy, which may be required for faster links or stronger turbulence, but is largely situation dependent.

Unfortunately, the models presented are not perfectly applicable to other weather conditions. Some models are fitted to regions of the data with similar scintillation indices, and it is found that they are not universal. As expected, there is a dependence on wind speed and possibly other weather parameters. This is in contrast to PDF-based models for turbulence-induced fading, which are often characterizable by commonly available weather parameters. It is speculated that there may be a methodology to determine the parameters of a Fritchman model given standard measures for turbulence and weather; however, this is the subject of future work. Nevertheless, in the absence of such a methodology, the future development of a database of Fritchman models for a set of common conditions would be beneficial to the community.

That said, in general, some trends can indeed be observed. Lower wind speeds result in longer correlation times, τ. This effect is visible in the EFR plots, with the weakest turbulence case also exhibiting the deepest memory because it had the lowest wind speed. In this case, the result on the communication channel is as follows: there is a low probability of an error occurring (since the turbulence is weak), but when it does occur, there will be quite a long burst of errors. The interrelation between wind speed and turbulence strength is complex and further conclusions cannot be drawn except that, in general, faster wind speed results in shorter tails.

It should be noted that the transmission rate used for this experiment is not sufficiently high to directly map to a practical system on the order of Gbits/s. The transmission rate used affects the decisions regarding the model parameters. At higher speeds, the effect of the memory may be lost at a bit level because individual bits are not "exposed" to the turbulence for as long. This does not, however, mean that the techniques presented herein have no relevance at higher speeds.

While the errors would appear random at a bit level, the effect of the memory in a high-speed system would be present at a codeword (or frame) level. Adapting the techniques presented herein to a codeword level can be accomplished without much difficulty. The training algorithm and Fritchman model can be configured to produce an output of any type, including a codeword of a specified length. The codewords from the simulation would show the effects of memory similarly to the bit level analysis presented here. Future work can focus on adapting these techniques for higher bit rates.

While the focus of this study is not on mitigation techniques, a brief mention of some possibilities and applications of Fritchman modelling serves to highlight the importance of the approach.

Interleaving is a common technique to combat bursty channels, which shuffles a bit-stream based on a mathematical expression that spreads closely grouped bits throughout the bit-stream. At the receiver, the bits are de-interleaved back to their proper positions. In a bursty channel, interleaving is useful when paired with a code more suited to correcting random errors as the errors would be spread throughout the bitstream, essentially appearing as random errors.

An important factor to consider for interleaving is the depth and the algorithms used to interleave the data. The distribution of errors in the channel should inform this. Optimal interleaving methods can only be designed and used when this information (such as the EFR) is present. In the absence of a good model, "educated guesses" at the interleaving depth and algorithm may result in excessive latency or little performance improvement [42, 70, 71]. Whether these are tradeoffs a system designer would choose to make is beyond the scope of this study.

As previously mentioned, error-correcting codes can be designed to better compensate for the errors that are not fully random and are instead correlated. The design of these codes is challenging, and it is therefore important to use existing approaches, which rely on standardised channel models [69, 72, 73]. Burst tolerant codes can be difficult to design and optimise. The techniques presented here allow for rapid iteration when attempting these designs. This could be used in conjunction with existing techniques to optimise burst tolerant codes in the form of rateless codes such as LT codes [55, 74].

3.3 Conclusion

An experiment over a 300 m outdoor optical link has been conducted, and it is shown that Fritchman Markov models are well suited to model the dynamics of FSO channels. The modelling approach

and sample models presented account for the memory in the channel, which results in bursts of errors which are the leading cause of difficulties in FSO error mitigation strategies. Memory-less models currently in widespread use, such as fading PDFs, do not account for this burstiness. The use of Fritchman models over general Markov models is conducive to communications theory as they are already used in other memory channels with associated error mitigation techniques. As such, the models presented in this study and future derived works can be used for optimal development of error-correcting codes, interleaving and protocols for use on FSO channels to extend their range, reliability and capacity. This is shown in the following chapter, where the models developed for this aspect of the research are used to test various FEC configurations, including LT, for use on the channel.

CHAPTER 4

Applying LT codes to the FSO channel using Fritchman models

This chapter is based on the following publication:

X. Nghatsane L. Cheng, and M. A. Cox, "Improving the resilience of free-space optical links using Luby-Transform codes" submitted to the *OSA Continuum*

The author was responsible for the conceptualisation of the work as well the experimental data collection and analysis. The paper was written predominantly by the first author.

The FSO channel can be treated as an erasure channel, and the correction of errors in an erasure channel is notoriously difficult [38–42]. Common methods of FEC more commonly used in other channels are not well suited for erasure channels. In these schemes, every symbol transmitted is important, and so dropped symbols must be re-transmitted. Rateless codes are more suitable for erasure channels as dropped symbols are inherently recoverable, allowing the recovery of source information from a non-specific set of encoded symbols. The first practical implementation of rateless codes were LT codes, and there have been studies on applying these and similar codes for the FSO channel.

This chapter uses four Fritchman models as discussed in the Literature Review in Sec. 1.1 representing various atmospheric conditions to compare uncoded, RS coded, and RS+LT coded configurations. These three configurations are chosen to represent the choices an engineer might be faced with in designing an FSO system that includes FEC. A significant benefit to using LT codes over standard RS coding (which is better suited to memoryless, non-erasure channels) or uncoded channels (for example, a naive, simple system such as "fibre without the fibre") is shown.

4.1 Experimental Setup and Methodology

This aspect of work presented is not intended to suggest an entire system for use, but instead promote the consideration of LT-based systems for future FSO systems. Simulations of accurate models that capture the memory of an FSO channel, as well as demonstrate the use of the models and techniques presented in the previous chapter, are used. To this end, this chapter uses Fritchman models for the channel instead of physical signal models to consider the effect of memory on the system. There is no known method of deriving Fritchman models based on the channel parameters typically used to

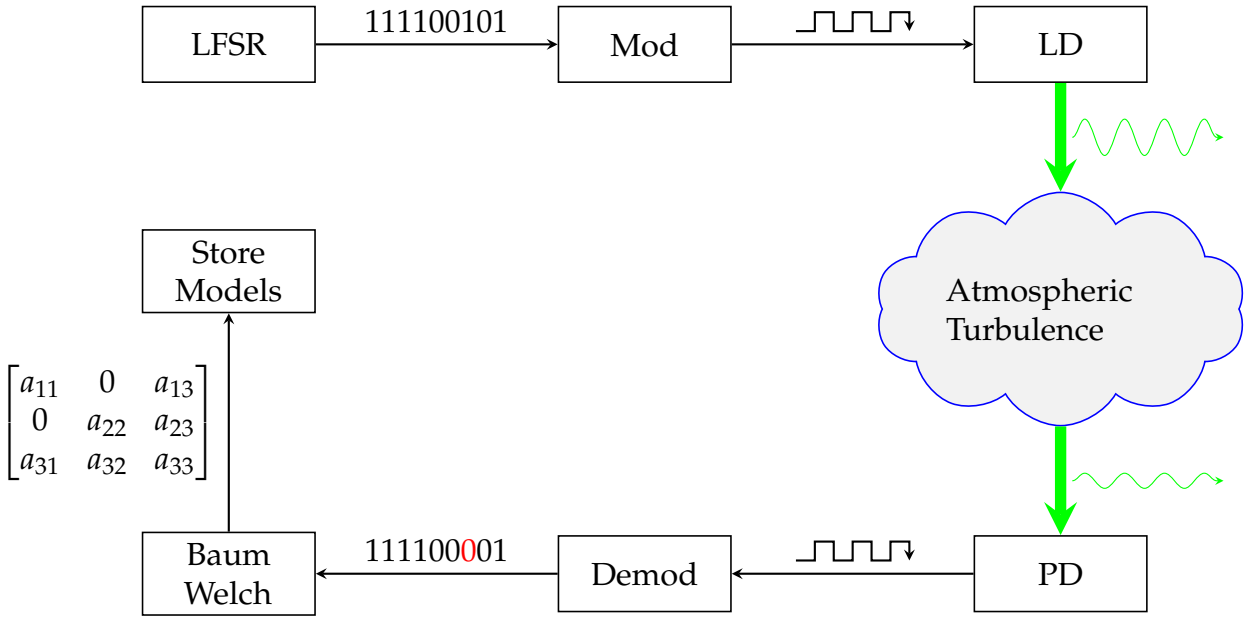

Figure 4.1: A block diagram of the process used to derive the models used in this work. This summarises the techniques used to establish the models in Chap. 3. The Mod in this case is NRZ-OOK modulation, the LD refers to the laser driver, and the PD is the photodiode.

Table 4.1: Simulation configuration variables for the LT and RS codes.

K	100
Q	10
Stop Threshold	50
Reed-Solomon	(255, 239)
CRC32	$x^{32} + x^{26} + x^{23} + x^{22} + x^{16} + x^{12} + x^{11} + x^{10} + x^8 + x^7 + x^5 + x^4 + x^2 + x + 1$

derive a PDF-based signal model. The models used for this paper are derived using the techniques presented in Chap. 3. The same link is used for this aspect of the research, and the techniques used are summarised in Fig. 4.1

This work focuses on the simplest practical implementation of fountain codes, LT codes, as opposed to Raptor codes, which are more complex. This allows us to better demonstrate the effects of the rateless nature of the codes, with less confusion introduced by the inner code of a Raptor code, for instance.

Three system cases are presented: an uncoded scheme, an RS encoded scheme, and an RS with LT (referred to as RS+LT) encoded system. The various parameters associated with these cases are summarised in Tab. 4.1. A high-rate RS code is used for both coded cases to turn the channel into an erasure channel by dropping frames that cannot be decoded. In addition, a standard, high strength Cyclic Redundancy Check (CRC) code is used to drop corrupt frames that were not detected as such by the RS code. A consideration of using a high strength CRC with the RS code is that the number of dropped frames will increase, decreasing the system's throughput. A high rate RS code is used to minimise the redundancy and subsequently decrease in data rate. The setup for the simulation is presented in Figs. 4.2 to 4.4 showing the various ECC configurations.

The number of frames simulated within the system is chosen as a trade-off between improving LT codes with increased K and the decoding complexity that increases with K. In order to find the "decodability", or probability of successfully decoding given a certain number of symbols, of the system, it must be allowed to simulate to high overhead. To prevent the simulation from running

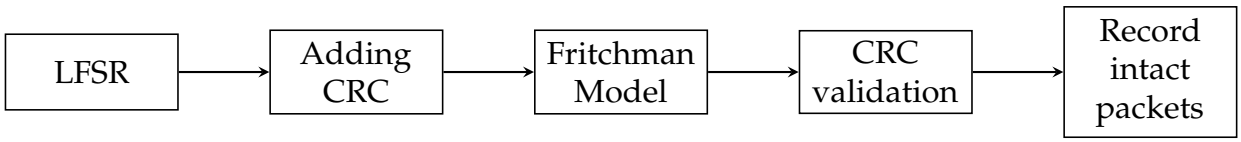

Figure 4.2: A block diagram of the simulation used to test the uncoded system. The CRC validation includes testing the CRC of the received packets after the errors from the Fritchman model are applied and discarding corrupt packets

.

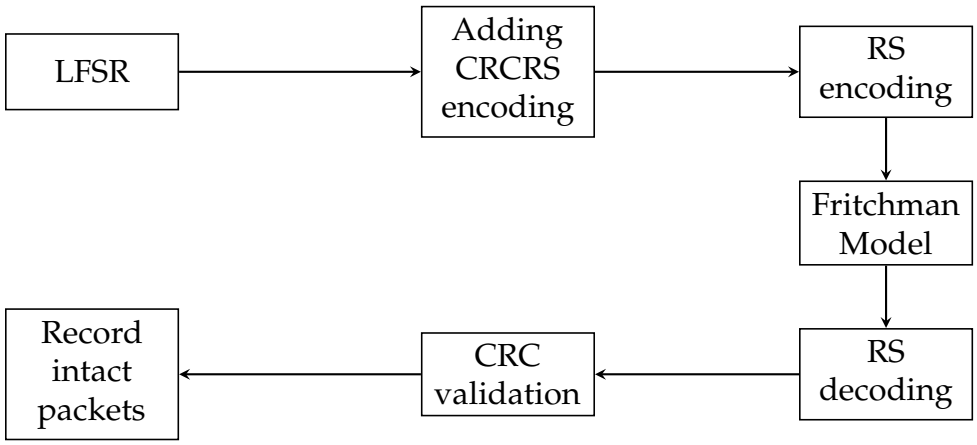

Figure 4.3: A block diagram of the simulation configuration used to test the RS system. The CRC validation is as noted in Fig. ,4.2 and the RS Decoding follows a similar process where packets, where decoding fails, are dropped.

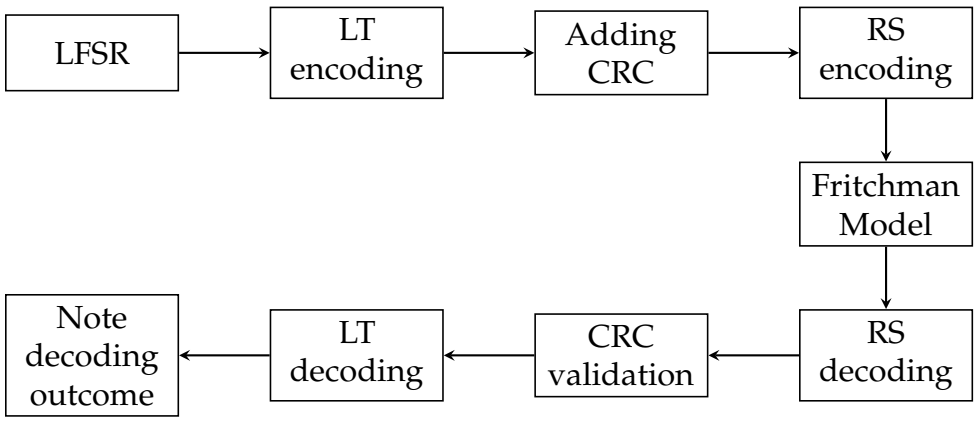

Figure 4.4: A block diagram of the simulation configuration used to test the RS+LT system. The CRC validation and RS Decoding are as noted for the previous configurations.

Table 4.2: Weather parameters and average bit error rate for the different Fritchman models used, according to scintillation index.

Label	σ_I^2 [Scintillation Index (SI)]	T [°C]	u [m/s]	BER
A	0.18	19.14	0.65	4.27×10^{-5}
B	0.45	15.12	1.38	1.3×10^{-3}
C	0.41	15.55	1.22	2.7×10^{-3}
D	0.46	15.77	1.37	2.1×10^{-3}

T is the atmospheric temperature
u is the perpendicular wind speed

endlessly, an overhead threshold is chosen as a stop condition, and the decoding is deemed to have failed when this threshold is reached.

The results presented for the systems being tested will be in the form of decodability and throughput graphs. The decodability of the system relates to the effective rate of the code (which impacts the overhead of the system), the distribution chosen, as well as the behaviour of the channel.

In order to measure the throughput of the system, a fixed number of frames will be sent in each configuration. In the uncoded and RS coded configurations, the number of frames sent is the number of information frames. Throughput is measured as the ratio of the number of frames successfully received to the number transmitted, given by

$$T = \frac{S_R}{K}, \tag{4.1}$$

where S_R is the number of symbols successfully retrieved, and K is the number of source symbols.

For the RS+LT coded configuration, a fixed number of frames will still be used, but this will be the number of information frames with an overhead informed by the decodability graphs. Throughput, in this case, will be the number of frames successfully decoded relative to the number of source packets. Sending a fixed number of frames will demonstrate the throughput and behaviour of the configurations when retransmission is not used. This simulation assumes that the receiver and the transmitter are both aware of the degree and symbols used to generate the encoded symbols.

The decoding BER is not presented because it is largely based on the strength of the CRC and fixed-rate code used, which are not the focus of this study. With the high strength CRC used, the BER is expected to be low as only valid frames would be allowed through the system - at the expense of throughput.

4.2 Results and Discussion

4.2.1 Channel Modelling and Memory Effects

The four models that have been derived using the aforementioned techniques are presented using transition matrices. These matrices are labelled to correspond to the conditions given in Tab. 4.2 and are presented below:

$$\mathrm{A} = \begin{bmatrix} 0.9999 & 0 & 5.43\times10^{-6} \\ 0 & 0.7205 & 0.2795 \\ 0.1313 & 0.8687 & 0 \end{bmatrix} \tag{4.2}$$

$$\mathrm{B} = \begin{bmatrix} 0.9999 & 0 & 0.0001 \\ 0 & 0.6933 & 0.3067 \\ 0.0992 & 0.8273 & 0.0734 \end{bmatrix} \tag{4.3}$$

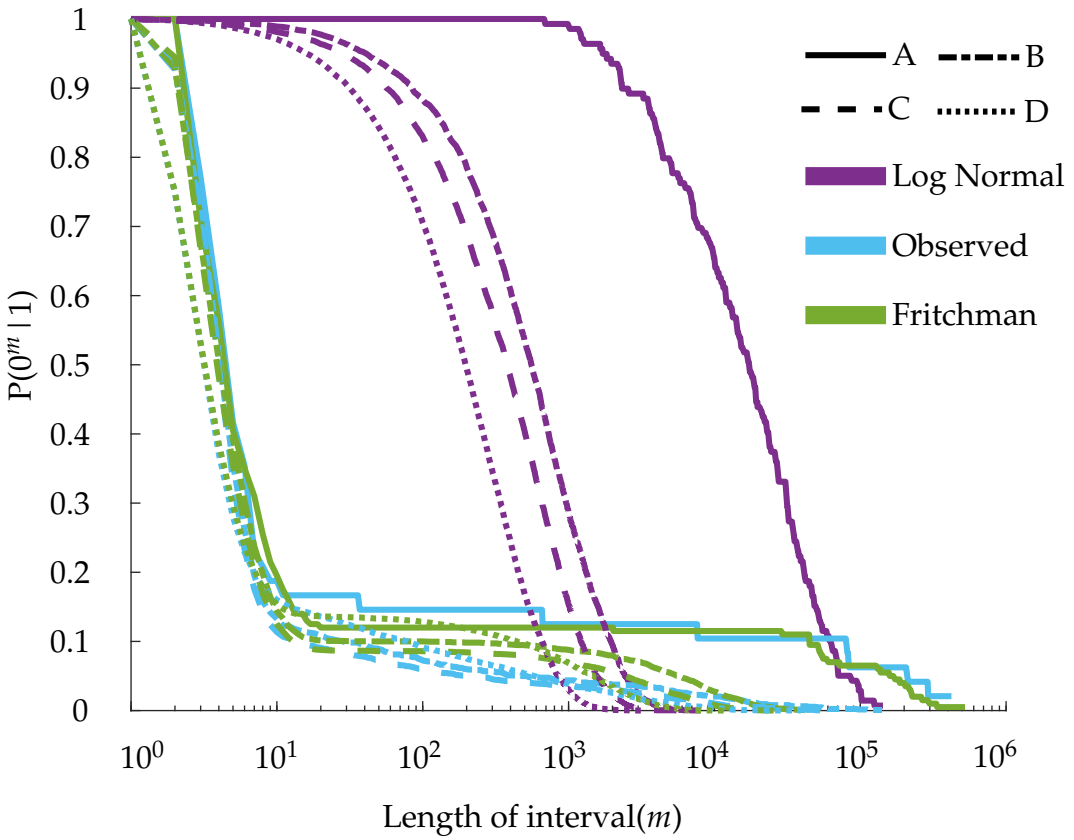

Figure 4.5: The error-free run (EFR) distributions that correspond to the four models that were trained for this work. The memory is evident in the presence of tails in the distribution, indicating that it tends to persist once a good state is entered. The corollary of this is that assuming the same BER as the Log-Normal, the errors must largely be bursty.

$$\mathrm{C} = \begin{bmatrix} 0.9998 & 0 & 0.0002 \\ 0 & 0.6767 & 0.3233 \\ 0.0846 & 0.8567 & 0.0586 \end{bmatrix}. \tag{4.4}$$

$$\mathrm{D} = \begin{bmatrix} 0.9993 & 0 & 0.0007 \\ 0 & 0.6416 & 0.3584 \\ 0.1376 & 0.6111 & 0.2513 \end{bmatrix}. \tag{4.5}$$

The EFRs of the models presented can be seen in Fig. 4.5 and show the same behaviour as a previous study on the same link. The EFR of Fritchman based models more closely matches the channel than the Log-Normal based models. This work focuses on exploring and exploiting the memory in the system. Hence, the cases presented are in similar atmospheric conditions to show that a difference that would not be expected in a Log-Normal based model is present in the trained Fritchman models.

The sharp drop off and length of the tail in the EFRs indicate the significant memory in the channel and highlight the fact that the Fritchman models accurately captured it. Examining the matrices obtained and the graph presented shows a possible correlation with the knee point of the EFRs the model's parameters.

During the initial sharp drop off, the magnitude of the probabilities is in alphabetical order. This initial drop off is due to errors that are largely random and correlates to state S_2 of the models where the probability of transitioning to the error state is relatively high. This can be seen in transition probability a_{23}, which has been noted in orange on the matrices for clarity. This represents the transition from S_2 to the error state S_3, and the magnitudes reflect the same order as the dropoff in the EFRs. This behaviour can likely be attributed to electrical noise in conjunction with turbulence-induced scintillation.

The tails of the EFRs represent the channel being in a very good state for a period of time which corresponds to s_1. The order that the tails begin is D, A, B, C, which is matched by a different transition probability, a_{31} which has been noted in green on the matrices for clarity. This channel state would be caused by the atmospheric turbulence having minimal effects on the beam.

When the tails end, the EFR is showing that the good state has ended. The order in which the good states end is D, C, B, A, which corresponds to transition probability a_{13} which has been noted in red which represents the very good state transitioning to the error. This transition represents a significant change in channel state and could be caused by weather phenomena such as rain or fog or rapid temperature changes.

These observations hold for the observed sequence and are dynamics of the channel that the Log-Normal and other PDF-based models completely miss. As seen in Fig. 4.5 above, the FSO channel has memory which manifests as long tails in the EFR. This results in the errors in the channel being more bursty as opposed to fully random. The consequence is that more packets are completely corrupted due to burst errors than a fully random channel. Conversely, this also means that packets will get through largely intact when the channel is in a good state.

The burstiness can be mitigated by ensuring that no uniquely important packet is sent. At the same time, the persistence of the good state can be taken advantage of by sending as many packets as possible. In addition, models C and D have shown that the channel behaviour can be very different despite some seemingly similar atmospheric conditions. This would result in unforeseen behaviour in the channel, and compensation would need to adapt to this.

Fortunately, an ideal combination of these characteristics is found in fountain codes, of which LT codes are a simple and fundamental implementation.

4.2.2 Forward Error Correction Schemes

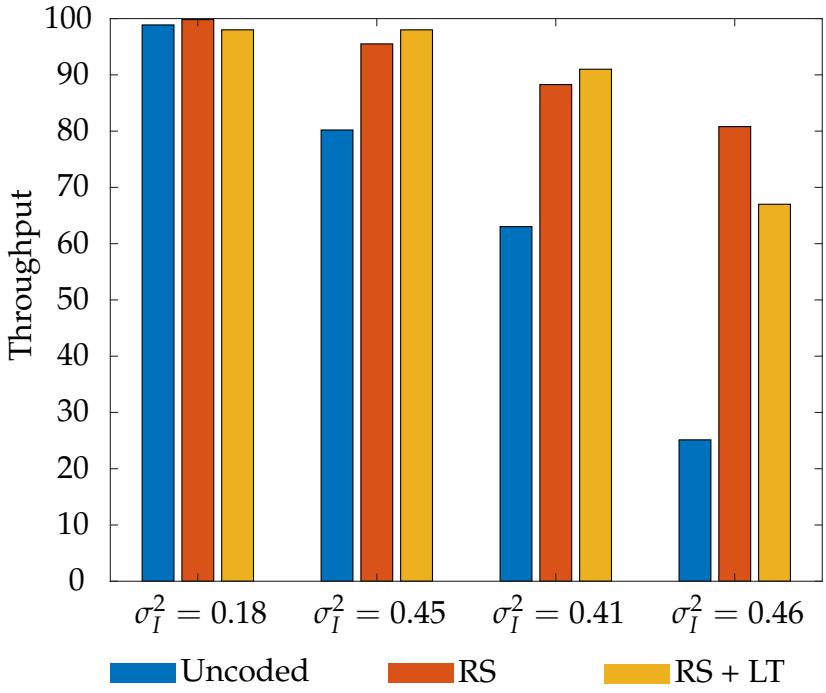

Figure 4.6: Throughput of various models with respect to the configuration used with the LT overhead set to 30%. It is important to note that for the non LT cases, retransmission of the specific dropped packets would be needed, which would also be subject to the same likelihood of dropping.

In Fig. 4.6, an illustrative comparison between the three schemes is made in terms of throughput, where the rate of the LT code is arbitrarily set to 30% based on the decodability graph Fig. 4.7 using

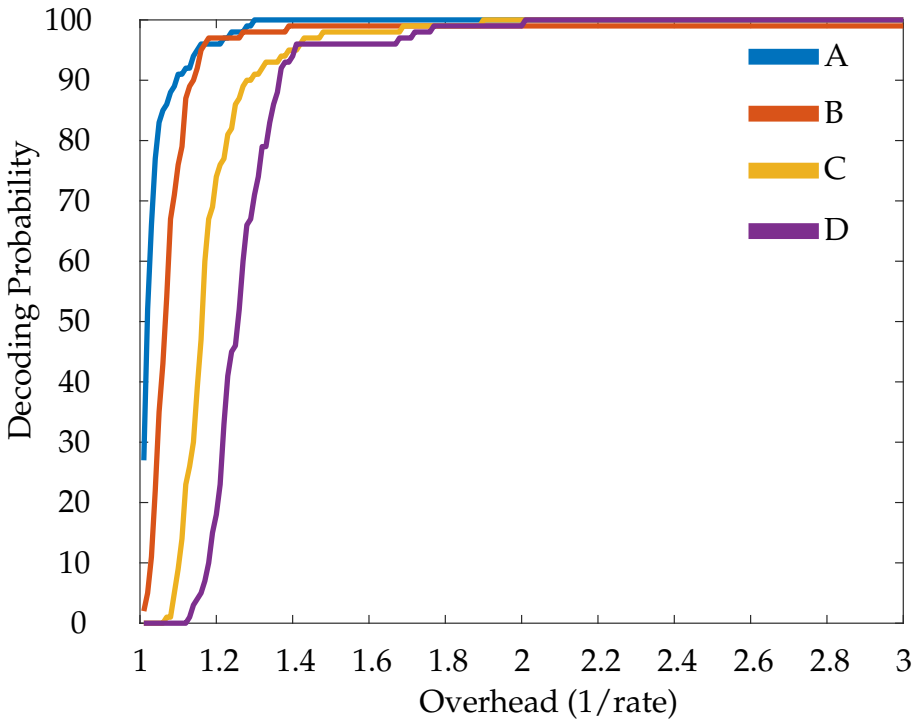

Figure 4.7: Decodability with respect to rate for the models used in the simulation with LT codes applied and OFG decoding.

OFG decoding. It is clear that the introduction of FEC is beneficial to an FSO system, although the extent to which LT codes are beneficial over RS codes is harder to ascertain at a glance.

Figure 4.6 shows that an FSO based system can be improved using rateless codes, but it seems that there is only a marginal improvement in throughput when the LT code is utilised. This observation fails to account for a crucial aspect of an LT based system. In the non-LT cases, retransmission of every lost packet *must* occur, which themselves may also suffer from packet erasure, potentially resulting in an untenable situation in difficult channel conditions (as are relatively common in FSO). While the LT based system indeed suffers packet erasure, those particular packets are not necessarily needed and can be reconstructed by the nature of the fountain code. This means that many of the retransmission costs are avoided because encoded packets can be produced continuously with little concern for those that are lost.

This does, however, come at a cost. The results show that the overhead introduced by the LT coding is 30%; nevertheless, this introduced overhead only lowers the effective data rate of the system by approximately 25%. This overhead could be improved with the use of more optimal distributions, which can be trained using multi-objective algorithms to minimise factors such as the overhead [74, 75].

The trade-off of the additional overhead compared to the throughput is a point of consideration for adopting an LT coded system. The increase in throughput for a given overhead is dependent on the decoding method used, with OFG having higher throughput than BP. For the fixed overhead of 30% used in this simulation, the LT coded scheme generally has higher or equal throughput than the non-LT cases. Throughput can be improved simply by increasing the overhead, as seen in Fig. 4.8.

The functionality of simply increasing the overhead of the system without having to change anything else and achieving increased performance is a key strength of LT codes. This lowers the resultant data rate, so a higher overhead cannot be used at all times. At lower turbulence strengths, the data rate loss might be evaluated as unnecessary considering the system's high throughput. In an adaptive system, the use of LT codes or not and the LT overhead would continuously be tuned based on channel conditions, possibly by using a simple out of band, reliable feedback mechanism such as RF.

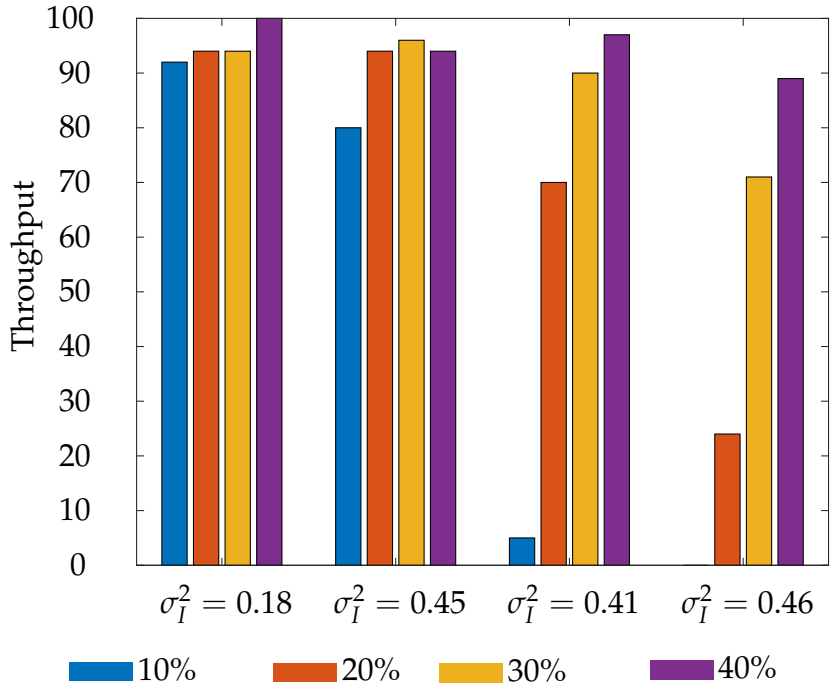

Figure 4.8: Throughput of various models with respect to the configuration used with varying overheads. Note that for model D, no decoding occurred with a 10% overhead

.1

Essentially continuous transmission of encoded packets without regular feedback (and thus retransmissions) has wider benefits. In multi-hop systems, as may be expected in long haul FSO networks, the probability that an individual link loses a packet may be relatively high. To rely on retransmissions for error recovery will likely result in low overall network throughput. If LT codes are used for each link (or at the application layer as is typical but is not the focus of this study), this situation may be averted.

This is not to discount the latency introduced by the LT decoding process. With the use of a method such as OFG as used in this experiment, the additional latency is relatively fixed for a specific configuration of an LT based system. This contrasts the latency of a retransmission based system that scales with link distance and the number of frames dropped.

A final consideration is in very unreliable channel conditions (such as heavy rain or fog). Typical feedback packets may be lost regularly, effectively resulting in a failed link. It is speculated that using fountain codes in these situations may allow an FSO link to continue to operate, albeit at a much lower data rate, which may be preferable to no link at all.

4.3 Conclusion

An experiment has been conducted to further study the memory of the FSO channel by deriving Fritchman Markov-based models. In order to exploit this memory and to improve communication reliability, the effectiveness of fountain codes is demonstrated (in the form of LT codes) using these models for simulation. Empirical Fritchman Markov models accurately capture the channel's memory, allowing for realistic observation of behaviour based on the memory: something not possible when PDF-based models such as Log-Normal and Gamma-Gamma are used.

It is shown that LT codes enable a significant improvement over uncoded erasure channels in terms of throughput (generally, successfully received frames versus transmitted frames) in various channel conditions with the worst case of the uncoded system having 0 throughput. The performance of the RS system can have similar performance in best case scenarios but lacks the simple scalability with regards to overhead of the LT coded system as the specific packets that are dropped would be needed

compared to the LT coded scheme where the specifics of the packets dropped is inconsequential. Importantly, LT codes also avoid the costly and potentially unreliable requirement for re-transmits and feedback, further improving throughput. This allows for the improvement of existing and future FSO installations by unlocking increased range and reliability. Is is also shown that they are unfortunately not a one-size-fits-all solution, and instead, an adaptive scheme that utilises LT codes in the appropriate channel conditions is briefly suggested.

Future work could focus on the development of parameters for the memory models of the channel and the optimisation of the distributions used for LT codes by using multi-objective optimisation techniques. The development of an adaptive system for LT codes would hasten the adoption of LT coded based systems, allowing for improved performance of existing and future FSO links.

CHAPTER 5

Conclusion

The FSO channel is very attractive for use in solving the Last Mile problem due to its high bandwidth and a relative lack of interference. The range of currently existing systems is limited and can be improved with techniques concerning the physical link and techniques in the digital domain. Testing the techniques in the digital domain is done most efficiently with the use of models for channel simulation. Existing digital models are relatively accurate but do not capture the channel's memory, which is crucial to optimal use of a channel. The resulting digital designs are likely sub-optimal, and the development and application of models that capture the memory is an important avenue for research. Results for the development of a model and the use of said model have been presented.

The research question "*How can we harness the memory of the FSO channel to design more optimal ECC?*" has been answered through exploring the two subquestions:

1. *Can the memory of the FSO be modelled using Fritchman Markov modelling within the context of digital communications?*

2. *How can we use the Fritchman model of FSO memory to aid the design of fountain code-based error correction to improve the channel's throughput?*

The answer to the first sub-question is *Yes, the memory of the FSO channel can be captured using a Fritchman Markov based model*. The results of the study submitted and published to the Journal of Applied Optics have shown that Fritchman Markov models are suitable for capturing the memory of the FSO channel. This has been shown in the form of Error Free Runs that show the channel behaviour of the Fritchman model matches that of the real channel better than traditional PDF-based models.

This has been utilised to demonstrate the potential use of rateless codes for FSO in the form of LT codes. It is noted that the models do not fully correspond to the current metrics used to separate channel states. Future work would be developing further measures that correlate to the memory of the channel. This would allow for a simpler comparison of the models, allowing for drawing more conclusions about the effect of memory. While the proposed modelling method does capture the memory of the channel, an aspect that may slow adoption is that the link must be established to train the model. To aid the adoption of this model, future research can focus on finding methods to derive the models based on weather parameters similar to existing memoryless PDF-based models. This model development has answered the first research question and forms a basis for future work optimising and improving the model.

The second sub-question has also been answered, and the answer is *We can use the Fritchman Markov based model using simulations of existing and proposed schemes. This will aid the design of fountain code based ECC to improve the throughput of the channel by allowing meaningful observations and conclusions, that consider the channel's memory, to be made*. The results of the study have been submitted for publication

to the Journal of Optical Communications and Networking. The answer has been shown through the application of various error correction schemes with respect to their throughput. The schemes have been demonstrated to have effects with channel memory without testing on a real-world link.

To further the study and use of Fritchman Markov based models, observations have been drawn based on the EFRs of additional trained models. In addition, to encourage the use of the models developed for the design of digital techniques, the models were used to apply FEC to the channel. LT codes were used to demonstrate the suitability of rateless codes for the channel because they are the first practical implementation of fountain codes. This allowed for deriving conclusions based on the rateless nature of the code as opposed to other aspects of the code. Raptor codes and implementations and improvements such as RaptorQ and Raptor 10 codes are typically better performing than LT codes. While there have been various applications of Raptor codes on FSO, these studies have not used models that capture the memory of the channel. It is recommended that future work focuses on using Raptor codes on the model that has been proposed to design systems that are more optimal for use on the channel. The second research question has been answered with the successful application of LT codes on the aforementioned model. Using the models in their current state or with the suggested optimisations will allow for the design of optimal digital techniques for use on the FSO channel.

Answering the two sub-questions allows an answer to be drawn for the original research question: *Using Fritchman based Markov models, we can train channel models that capture the channel's memory and are suitable for use in designing ECC.*

The research question presented has been addressed, and the impact of the research presented here is that future design and modelling can be based on techniques that better capture the channel. This will allow for a more efficient design of ECC that utilises channel memory and thus increased channel capacity. The research serves as a critical step towards improving digital techniques on the channel while also providing avenues for future work. This will allow for increasing the range and capacity of FSO links, increasing their suitability for solving the Last Mile Problem.

5.1 Future Work

The techniques that have been presented are largely general purpose and can be used with varying channel conditions. The results presented are for low turbulence conditions on a link with relatively low speed. More practical systems would be higher speed and longer range resulting in higher turbulence. The techniques presented would have to be adapted for these conditions. Future work would have to include the training of models on more realistic links and the application of ECC to those models. One of the adaptations that could be made is modelling on a symbol level on higher link speeds instead of the bit level presented here. Fortunately, the techniques presented do not inherently only work at the bit level as the Fritchman model can be trained to emit anything, including errors for multi-byte symbols.

This will allow for the utilisation of Fritchman models for higher bandwidth links, where a single bit does not last long enough to experience the low-frequency effects of turbulence, unlike the low-speed link used in this research. Once the techniques have been successfully adapted for higher speed links, the next crucial step would be to investigate deriving Fritchman models based on channel parameters instead of an established link. This would allow completely supplanting the use of PDF-based models as despite not capturing the memory, they do have the benefit of not requiring a link to be established, allowing for more people to test designs, albeit with the inherent limiting factor of not account for channel memory.

The work presented to apply LT codes to the channel was not intended to be implemented as presented on a real channel as continuous transmission would be utilised on a real channel. While this seems similar to existing retransmission-based systems in which more symbols must be sent, a crucial difference is that the transmission is not dependent on any specific symbol, as detailed above. Consequently, a real-world system that implements Fountain codes would utilise Raptor codes with the continuous transmission noted above. Design of this system with elements of adaptation to minimise wasted throughput due to overhead would be the main step recommended going forward.

References

[1] J. Wang, S. Li, M. Luo, J. Liu, L. Zhu, C. Li, D. Xie, Q. Yang, S. Yu, J. Sun, X. Zhang, W. Shieh, and A. E. Willner, "N-dimentional multiplexing link with 1.036-Pbit/s transmission capacity and 112.6-bit/s/Hz spectral efficiency using OFDM-8QAM signals over 368 WDM pol-muxed 26 OAM modes," in *European Conference on Optical Communication, ECOC*, Institute of Electrical and Electronics Engineers Inc., Nov. 2014.

[2] Z. Qu and I. B. Djordjevic, "500 Gb/s free-space optical transmission over strong atmospheric turbulence channels," *Optics Letters*, vol. 41, no. 14, p. 3285, Jul. 2016.

[3] A. Trichili, M. A. Cox, B. S. Ooi, and M.-S. Alouini, "Roadmap to free space optics," *Journal of the Optical Society of America B*, vol. 37, no. 11, A184, Nov. 2020.

[4] M. M. Abadi, M. A. Cox, R. E. Alsaigh, S. Viola, A. Forbes, and M. P. J. Lavery, "A space division multiplexed free-space-optical communication system that can auto-locate and fully self align with a remote transceiver," *Scientific Reports*, vol. 9, no. 1, pp. 1–8, 2019.

[5] K. David and H. Berndt, "6G Vision and Requirements: Is There Any Need for Beyond 5G?" *IEEE Vehicular Technology Magazine*, vol. 13, no. 3, pp. 72–80, 2018.

[6] S. Dang, O. Amin, B. Shihada, and M.-S. Alouini, "What should 6G be?" *Nature Electronics*, vol. 3, no. 7, pp. 20–29, Jan. 2020.

[7] M. P. J. Lavery, M. M. Abadi, R. Bauer, G. Brambilla, L. Cheng, M. A. Cox, A. Dudley, A. D. Ellis, N. K. Fontaine, A. E. Kelly, C. Marquardt, S. Matlhane, B. Ndagano, F. Petruccione, R. Slavík, F. Romanato, C. Rosales-Guzmán, F. S. Roux, K. Roux, J. Wang, and A. Forbes, "Tackling Africa's digital divide," *Nature Photonics*, vol. 12, no. 5, pp. 249–252, 2018.

[8] M. A. Cox, N. Mphuthi, I. Nape, N. P. Mashaba, L. Cheng, and A. Forbes, "Structured Light in Turbulence," *IEEE Journal of Selected Topics in Quantum Electronics*, vol. 27, no. June, pp. 0–21, Mar. 2020.

[9] A. Trichili, K.-H. Park, M. Zghal, B. S. Ooi, and M.-S. Alouini, "Communicating Using Spatial Mode Multiplexing: Potentials, Challenges and Perspectives," *IEEE Communications Surveys & Tutorials*, p. 1, 2019.

[10] A. E. Willner, Y. Ren, G. Xie, Y. Yan, L. Li, Z. Zhao, J. Wang, M. Tur, A. F. Molisch, and S. Ashrafi, "Recent advances in high-capacity free-space optical and radio-frequency communications using orbital angular momentum multiplexing," *Philosophical Transactions of the Royal Society of London A: Mathematical, Physical and Engineering Sciences*, vol. 375, no. 2087, 2017.

[11] S. Huang, G. R. Mehrpoor, and M. Safari, "Spatial-Mode Diversity and Multiplexing for FSO Communication With Direct Detection," *IEEE Transactions on Communications*, vol. 66, no. 5, pp. 2079–2092, May 2018.

[12] M. A. Cox, L. Cheng, C. Rosales-Guzmán, and A. Forbes, "Modal Diversity for Robust Free-Space Optical Communications," *Physical Review Applied*, vol. 10, no. 2, p. 24 020, Aug. 2018.

[13] D. D. I. Energia and I. D. Informazione, "Tesi Di Dottorato " Free Space Optics Links Affected By Optical Turbulence : Channel Modeling , Measurements and Coding Techniques for Error Mitigation "," 2013.

[14] L. C. Andrews and R. L. Phillips, *Laser Beam Propogation through Random Media*, 5. SPIE—The International Society for Optical Engineering, 2012, vol. 91.

[15] A. Abdulhussein, A. Oka, T. Nguyen, and L. Lampe, "Rateless coding for hybrid free-space optical and radio-frequency communication," *IEEE Transactions on Wireless Communications*, vol. 9, no. 3, pp. 907–913, 2010.

[16] A. Andò, R. Pernice, L. Curcio, S. Stivala, S. Mangione, P. Gallo, M. Campanella, G. Garbo, and A. C. Busacca, "Fading mitigation coding techniques for space to ground free space optical communications," *2014 Euro Med Telco Conference - From Network Infrastructures to Network Fabric: Revolution at the Edges, EMTC 2014*, pp. 1–5, 2014.

[17] J. M. Ooi, "Channels with Memory," in *Coding for Channels with Feedback*, Boston, MA: Springer US, 1998, pp. 61–97.

[18] H. Kazemi, M. Uysal, and F. Touati, "Outage analysis of hybrid FSO/RF systems based on finite-state Markov chain modeling," *2014 3rd International Workshop in Optical Wireless Communications, IWOW 2014*, pp. 11–15, 2014.

[19] A. Touati, S. J. Hussain, F. Touati, and A. Bouallegue, "Effect of Atmospheric Turbulence on Hybrid FSO/RF Link Availability under Qatar Harsh Climate," *World Academy of Science, Engineering and Technology International Journal of Electrical and Computer Engineering*, vol. 9, no. 8, pp. 87–105, 2015.

[20] A. Khatoon, W. G. Cowley, and N. Letzepis, "FSO/RF correlation measurement and hybrid system hidden Markov model," *2013 Australian Communications Theory Workshop, AusCTW 2013*, pp. 93–98, 2013.

[21] R. Bosu and S. Prince, "Discrete Markov chain model for transition analysis of optical scintillation in reflection-assisted free space optical links," *Optics Communications*, vol. 475, no. May, p. 126 261, 2020.

[22] A. Mostafa, S. Hranilovic, V. V. Mai, A. T. Pham, H. Kazemi, M. Uysal, F. Touati, H. Moradi, M. Falahpour, H. H. Refai, P. G. LoPresti, M. Atiquzzaman, A. Mostafa, S. Hranilovic, C. T. Nguyen, H. D. Le, V. V. Mai, H. Moradi, M. Falahpour, H. H. Refai, P. G. LoPresti, and M. Atiquzzaman, "Channel measurement and Markov modeling of an urban free-space optical link," *Journal of Optical Communications and Networking*, vol. 4, no. 10, pp. 836–846, 2012.

[23] Z. Hajjarian, J. Fadlullah, and M. Kavehrad, "Use of Markov Chain in Atmospheric Channel Modeling of Free Space Laser," Ph.D. dissertation, 2008, pp. 1–7.

[24] X. Zhu and J. M. Kahn, "Markov chain model in maximum-likelihood sequence detection for free-space optical communication through atmospheric turbulence channels," *IEEE Transactions on Communications*, vol. 51, no. 3, pp. 509–516, 2003.

[25] C. T. Nguyen, H. D. Le, and V. V. Mai, "A cross-layer analysis of TCP/link adaptation technologies over free-space optical links with Markov error model," *Photonic Network Communications*, vol. 36, no. 3, pp. 279–288, 2018.

[26] H. D. Le, V. V. Mai, C. T. Nguyen, and A. T. Pham, "Design and Analysis of Sliding Window ARQ Protocols With Rate Adaptation for Burst Transmission Over FSO Turbulence Channels," *Journal of Optical Communications and Networking*, vol. 11, no. 5, pp. 151–163, 2019.

[27] H. Henniger, "Transmission performance analysis of free-space optical communications using Gilbert-Erasure channel," *IEEE Transactions on Communications*, vol. 60, no. 1, pp. 55–61, 2012.

[28] A. Andò, S. Mangione, L. Curcio, S. Stivala, G. Garbo, R. Pernice, and A. C. Busacca, "Recovery capabilities of rateless codes on simulated turbulent terrestrial free space optics channel model," *International Journal of Antennas and Propagation*, vol. 2013, 2013.

[29] W. Zhang, S. Hranilovic, and C. Shi, "Soft-switching hybrid FSO/RF links using short-length raptor codes: Design and implementation," *IEEE Journal on Selected Areas in Communications*, vol. 27, no. 9, pp. 1698–1708, 2009.

[30] M. Lu, L. Liu, and S. Hranilovic, "Raptor-coded free-space optical communications experiment," *Journal of Optical Communications and Networking*, vol. 8, no. 6, pp. 398–407, 2016.

[31] L. Liu, M. Safari, and S. Hranilovic, "Systematic raptor codes for atmospheric optical channels," *2013 13th Canadian Workshop on Information Theory, CWIT 2013*, pp. 190–194, 2013.

[32] G. Prakash, A. Nayak, M. Kulkarni, and S. Acharya, "On the improved performance of luby transform codes over selective repeat ARQ in turbulent free space optical links," *Proceedings - 16th IEEE International Conference on Computational Science and Engineering, CSE 2013*, pp. 1195–1200, 2013.

[33] G. Prakash, M. Kulkarni, U. Sripati, and M. N. Kalyanpur, "Performance analysis of Free Space Optical links encoded using Luby Transform codes," *Proceedings - 2012 International Conference on Communication, Information and Computing Technology, ICCICT 2012*, pp. 1–6, 2012.

[34] Z. Kolka, V. Biolkova, O. Wilfert, and D. Biolek, "Simulation model of correlated FSO channels," *Proceedings of 14th Conference on Microwave Techniques, COMITE 2015*, pp. 22–25, 2015.

[35] H. Henniger and A. Gonzalez, "Transmission scheme and error protection for simplex long-distance atmospheric FSO systems," *The Mediterranean Journal of Electronics and Communications*, vol. 2, pp. 118–126, Jul. 2006.

[36] S. Z. Denic, I. Djordjevic, J. Anguita, B. Vasic, and M. A. Neifeld, "Information theoretic limits for free-space optical channels with and without memory," *Journal of Lightwave Technology*, vol. 26, no. 19, pp. 3376–3384, 2008.

[37] J. A. Anguita, M. A. Neifeld, B. Hildner, and B. Vasic, "Rateless coding on experimental temporally correlated fso channels," *Journal of Lightwave Technology*, vol. 28, no. 7, pp. 990–1002, 2010.

[38] S. Lin and D. Costello, *Error Control Coding*. 2004.

[39] B. D. Trumpis and P. L. McAdam, "Performance of convolutional codes on burst noise channels," in *NTC '77; National Telecommunications Conference, Volume 3*, vol. 3, Jan. 1977, p. 36.

[40] G. Forney, "Burst-Correcting Codes for the Classic Bursty Channel," *IEEE Transactions on Communication Technology*, vol. 19, no. 5, pp. 772–781, 1971.

[41] R. G. Gallager, *Information Theory and Reliable Communication*. USA: John Wiley and Sons, Inc., 1968.

[42] A. I. Drukarev, K. P. Yiu, Kai Yiu, and K. P. Yiu, "Performance of Error-Correcting Codes on Channels with Memory," *IEEE Transactions on Communications*, vol. 34, no. 6, pp. 513–521, 1986.

[43] M. A. Cox, "Improving the Resilience of Free-Space Optical Links using Structured Modes of Light," Ph.D. dissertation, University of the Witwatersrand, Johannesburg, 2019, pp. 0–2.

[44] L. C. Andrews, R. L. Phillips, and C. Y. Young, "Laser Beam Scintillation with Applications," *Laser Beam Scintillation with Applications*, 2009.

[45] L. Andrews and R. Phillips, "Laser Beam Propagation Through Random Media," in, SPIE Optical Engineering Press, 2005, ch. 11, pp. 441–472.

[46] M. Beason, L. Andrews, and S. Gladysz, "Statistical comparison of probability models of intensity fluctuation," *Environmental Effects on Light Propagation and Adaptive Systems II*, no. October, p. 12, 2019.

[47] L. Yang, B. Zhu, J. Cheng, and J. F. Holzman, "Free-Space Optical Communications Using on-off Keying and Source Information Transformation," *Journal of Lightwave Technology*, vol. 34, no. 11, pp. 2601–2609, 2016.

[48] E. O. Elliott, "Estimates of Error Rates for Codes on Burst-Noise Channels," *Bell System Technical Journal*, vol. 42, no. 5, pp. 1977–1997, 1963.

[49] M. Mushkin and I. Bar-David, "Capacity and Coding for the Gilbert-Elliot Channels," vol. 35, no. 6, pp. 1277–1290, 1989.

[50] B. D. Fritchman, "A Binary Channel Characterization Using Partitioned Markov Chains," *IEEE Transactions on Information Theory*, vol. 13, no. 2, pp. 221–227, 1967.

[51] W. H. Tranter, K. S. Shanmugan, T. S. Rappaport, and K. L. Kosbar, *Principles of Communication Systems Simulation with Wireless Applications*. Prentice Hall, 2003, vol. 1, p. 800.

[52] M. Oudelha and R. N. Ainon, "HMM parameters estimation using hybrid Baum-Welch Genetic Algorithm," *Proceedings 2010 International Symposium on Information Technology - Engineering Technology, ITSim'10*, vol. 2, no. l, pp. 542–545, 2010.

[53] P. M. Baggenstoss, "A modified Baum-Welch algorithm for hidden Markov models with multiple observation spaces," *IEEE Transactions on Speech and Audio Processing*, vol. 9, no. 4, pp. 411–416, 2001.

[54] S. Thai, "Markov Characterization of the HF Channel," *IEEE T*, vol. C, pp. 24–32, 1969.

[55] M. Luby, "LT codes," in *The 43rd Annual IEEE Symposium on Foundations of Computer Science, 2002. Proceedings.*, Nov. 2002, pp. 271–280.

[56] V. Bioglio, M. Grangetto, R. Gaeta, and M. Sereno, "On the fly Gaussian Elimination for LT codes," *IEEE Communications Letters*, vol. 13, no. 12, pp. 953–955, 2009.

[57] S. Kim, K. Ko, and S. Y. Chung, "Incremental Gaussian elimination decoding of raptor codes over BEC," *IEEE Communications Letters*, vol. 12, no. 4, pp. 307–309, 2008.

[58] M. A. Al-Habash, "Mathematical model for the irradiance probability density function of a laser beam propagating through turbulent media," *Optical Engineering*, vol. 40, no. 8, p. 1554, Aug. 2001.

[59] W. Gappmair and M. Flohberger, "Error performance of coded FSO links in turbulent atmosphere modeled by gamma-gamma distributions," *IEEE Transactions on Wireless Communications*, vol. 8, no. 5, pp. 2209–2213, 2009.

[60] Y. Q. Shi, X. M. Zhang, Z. C. Ni, and N. Ansari, "Interleaving for combating bursts of errors," *IEEE Circuits and Systems Magazine*, vol. 4, no. 1, pp. 29–42, 2004.

[61] K. E. Olson and P. K. Enge, "Forward Error Correction for an Atmospheric Noise Channel," *IEEE Transactions on Communications*, vol. 40, no. 5, pp. 863–872, 1992.

[62] C. Pimentel, "Modeling burst channels using partitioned fritchman's Markov models," *IEEE Transactions on Vehicular Technology*, vol. 47, no. 3, pp. 885–899, 1998.

[63] A. D. Familua and L. Cheng, "Modeling of in-house CENELEC A-band PLC channel using Fritchman model and Baum-Welch algorithm," *ISPLC 2013 - 2013 IEEE 17th International Symposium on Power Line Communications and Its Applications, Proceedings*, pp. 173–178, 2013.

[64] ——, "First and Second-Order Semi-Hidden Fritchman Markov models for a multi-carrier based indoor narrowband power line communication system," *Physical Communication*, vol. 29, pp. 55–66, 2018.

[65] A. D. Familua, "A Block Diagonal Markov Model for Indoor Software-Defined Power Line Communication," *IEEE PES/IAS PowerAfrica Conference: Power Economics and Energy Innovation in Africa, PowerAfrica 2019*, no. July, pp. 1–6, 2019.

[66] S. I. Ahmed and T. A. Kwasniewski, "Overview of oversampling clock and data recovery circuits," in *Canadian Conference on Electrical and Computer Engineering, 2005.*, 2005, pp. 1876–1881.

[67] D. G. Holmes, L. Cheng, M. Shimaponda-Nawa, A. D. Familua, and A. M. Abu-Mahfouz, "Modelling noise and pulse width modulation interference in indoor visible light communication channels," *AEU - International Journal of Electronics and Communications*, vol. 106, pp. 40–47, 2019.

[68] A. D. Familua and L. Cheng, "A semi-hidden Fritchman Markov modeling of indoor CENELEC A narrowband power line noise based on signal level measurements," *AEU - International Journal of Electronics and Communications*, vol. 74, pp. 21–30, 2017.

[69] M. D. Knowles and A. I. Drukarev, "Bit Error Rate Estimation for Channels with Memory," *IEEE Transactions on Communications*, vol. 36, no. 6, pp. 767–769, 1988.

[70] L. Kanal and A. Sastry, "Models for Channels with Memory and Their Applications to Error Control," *Proceedings of the IEEE*, vol. 66, no. 7, pp. 724–744, 1978.

[71] T. Stephen and P. S. Schmied, "Interleaving and Error-Burst Distribution," *IEEE Transactions on Communications*, vol. 71, no. 5, pp. 1811–1815, 1974.

[72] H. Lai and S. Kallel, "An Efficient Convolutional Coding/Decoding Strategy for Channels with Memory," *IEEE Transactions on Communications*, vol. 43, no. 11, pp. 2678–2686, 1995.

[73] A. Van Heerden and H. C. Ferreira, "Evaluating non-binary error correcting codes on bursty channels with a partitioned Markov model," *Proceedings of the 1993 IEEE South African Symposium on Communications and Signal Processing, COMSIG 1993*, pp. 114–117, 1993.

[74] C.-m. Chen, Y.-p. Chen, T.-c. C. Shen, and J. K. Zao, "Optimizing degree distributions in LT codes by using the multiobjective evolutionary algorithm based on decomposition," *2010 IEEE World Congress on Computational Intelligence, WCCI 2010 - 2010 IEEE Congress on Evolutionary Computation, CEC 2010*, 2010.

[75] J. K. Zao, M. Hornansky, and P. L. Diao, "Design of optimal short-length LT codes using evolution strategies," *2012 IEEE Congress on Evolutionary Computation, CEC 2012*, pp. 10–15, 2012.

Appendix

Fritchman modelling for correlated turbulence-induced errors in FSO communication

XONGILE NGHATSANE[1], LING CHENG[1], AND MITCHELL A. COX[1,*]

[1] School of Electrical and Information Engineering, University of the Witwatersrand, Johannesburg, South Africa
[*] Corresponding author: mitchell.cox@wits.ac.za

Compiled January 25, 2021

Free Space Optics based communication links are an attractive potential solution for solving the last mile challenge but suffer from turbulence-induced fading. This fading causes errors in the received signal. While models exist to predict how the turbulence affects the signal, these models often do not account for the channel's memory. Typical fading models accurately predict the average effect of the channel on a signal but not the distribution of the errors and the individual length of events such as deep fades. To better model the channel, this paper presents an alternative approach to modelling the channel: Fritchman Markov modelling. The models produced accurately match the behaviour of the channel and can be used to develop robust and efficient error mitigation strategies in future.

http://dx.doi.org/10.1364/ao.XX.XXXXXX

1. INTRODUCTION

With the ever-increasing digital nature of society, telecommunications form a vital part of developed nations. Optical fibre forms the backbone of the modern Internet, and multiple communication methods are used for short-distance or "last mile" connections. Radio is sometimes used, but Free Space Optical communication (FSO) is an attractive alternative because of interference and bandwidth limitations in the heavily used radio frequency spectrum. State of the art experimental FSO systems that make use of multiple degrees of freedom of light such as wavelength, polarisation and space (via orthogonal spatial modes) have been demonstrated at data rates on the order of petabits per second over a lab bench [1], to hundreds of gigabits per second in simulated turbulence [2]. Modern, commercial FSO technology can sustain gigabits per second over several kilometres, making FSO a viable technology for future brown fields installations where fibre is too difficult or too expensive to install [3, 4]. For these reasons, it is expected that FSO will be a significant part of the future 6G era [5, 6], but FSO has also been suggested as a possible technology to help bridge the digital divide [7].

When lasers propagate through the air, the transmitted beam undergoes fading because of attenuation and atmospheric turbulence. This has resulted in numerous studies to better model and correct for errors on the FSO channel. Still, to-date this problem is largely unsolved. TeWillner2017,Andrews2009. An aspect of turbulence-induced fading that causes significant mitigation difficulty is deep fading, where the received signal is below a usable threshold. Commonly used probabilistic models for FSO channel fading, such as Log-Normal [8] and the Gamma-Gamma Probability Distribution Functions (PDF) [9, 10] can accurately predict the total amount of deep fading over an extended time frame when used in the right conditions [11]. While it is generally accepted that the FSO channel does have memory (inherent in Taylor's frozen turbulence hypothesis) [12–15], models based only on probability distributions are insufficient for modelling this memory and therefore research and development of turbulence mitigation strategies is hindered.

Models that account for memory are needed to better aid design of fading mitigation strategies for use in FSO systems. The overall Bit Error Rate (BER) of two models may be similar or identical, but in the model that does not account for memory, the spread of these errors is distributed differently. The resulting designs of Forward Error Correcting Codes (FEC) or interleaving would likely end up sub-optimal, as shown in [16, 17]. Specifically, these codes would not be equipped to deal with so-called burst errors typically found in memory channels. They would fail if they were deployed on real channels that were more prone to bursts than random errors, unless they were made extremely strong, to the point of wasting capacity.

Indeed, studies using Markov modelling techniques have been done to model the FSO channel's memory. However, they have been primarily focused on the transmitted or received signal, and thus model physical phenomena directly. Here we provide a brief review of the literature to provide context to our contribution.

Markov chains have been used extensively in hybrid RF/FSO system modelling, which are systems in which RF and FSO systems are used in conjunction to take advantage of both technologies. RF and FSO each suffer from different atmospheric conditions and so a combination of both can be utilised for op-

timal reliability. Markov chains have been used to model the link selection that would be required for soft switching if one of the links suffered an outage [18]. Expressions for the outage probability given weather parameters were provided, thus aiding future design of hybrid systems. A demonstration link in Qatar used Markov modelling for a Hybrid FSO/RF link using Raptor codes to facilitate soft switching [19]. Their Markov chain was also used to model the fading and derive a mathematical expression for the outage probability. In a similar vein, Hidden Markov Models (HMM) have been used to simulate the variation in fading and turbulence due to weather in an FSO/RF hybrid channel. This study was focused on modelling the fade correlation and different propagation states of the hybrid system [20].

Markov chains have also been used to develop models for analysing a pure FSO channel's fading behaviour. These chains have been developed using turbulence state information and verified using a turbulence chamber [21]. An eight and 64-state Markov model of the received signal in a 1.8 km urban FSO link are presented in [22]. Comparisons of the measured data were shown to fit existing distributions for FSO. The proposed Markov model fit the measured data while also capturing the non-stationary nature of the channel. Ray tracing has also been used in conjunction with Markov chains to model the FSO channel [23]. Markov modelling has been used to optimise a Maximum-Likelihood Sequence Detection (MLSD) algorithm [24], where a single step Markov chain is used to simplify the algorithm used significantly. Lastly, an Auto-Regressive Moving-Average (ARMA) based time series model has been presented to capture the memory of angle-of-arrival fluctuations which result in focal-spot beam wander and hence fading [25].

Markov models have also proven useful in modelling overall network performance rather than signal-only effects. They have been used to develop models for the channel state of an FSO channel, focusing on cross layer performance, the effects on the commonly-used Transmission Control Protocol (TCP) and technologies such as Automatic Repeat Requests (ARQ) and Adaptive Modulation Coding [26, 27]. A similar study focused on the loss of Ethernet frames in an FSO based system [28]. Here, the Gilbert-Erasure channel is used to model frame loss. The applicability of the model is shown in relation to the training data but not to a simulation based on "conventional" PDF models.

Here we propose a Fritchman-based Markov modelling approach (which is an extension of the Gilbert-Elliot approach in [28]) for the FSO channel considering the resulting digital signal in a bit-wise fashion [29, 30]. This significantly reduces the resulting channel model complexity, allowing for fast, efficient and holistic channel simulation. We present several Fritchman models developed using data obtained from a 300 m link in different turbulence conditions and describe the approach in detail. These models are beneficial for modelling the result of bursty deep fading. Such enables the use of existing mitigation techniques developed for other challenging memory channels such as power-line communications [31–33]. This will ultimately help improve the performance of FSO links in future.

2. BACKGROUND

A. Atmospheric Turbulence

In FSO communications, a dominant source of fading that must be compensated for is atmospheric turbulence. Aberrations due to turbulence are caused by randomly varying cells of air which have different temperature and thus different refractive index which move around due to physical processes such as wind and convection. These cells have various sizes. The larger cells cause large-scale turbulence effects such as beam wander, whereas the smaller cells within the larger cells predominantly cause wavefront distortion known as scintillation [8, 34]. The combination of these effects leads to random fluctuations in the received wavefront and therefore the received intensity, known as turbulence induced signal fading.

The Scintillation Index, SI, is an intuitive measure of turbulence strength and is defined as the normalised variance of the irradiance fluctuations given by

$$\sigma_I^2 = \frac{\langle I^2 \rangle}{\langle I \rangle^2} - 1, \tag{1}$$

where I is the received optical intensity and $\langle \cdot \rangle$ represents the ensemble average [8]. The wind speed naturally has an impact on the turbulence characteristics and can be used to calculate an important measure of turbulence called the correlation time, which naturally describes how long the turbulence conditions can be assumed to be correlated, given by

$$\tau = \frac{\sqrt{\lambda L}}{u}, \tag{2}$$

where u is the perpendicular (to the direction of laser propagation) wind velocity, λ is the wavelength of the laser and L is the propagation distance [8]. For an FSO system that is being used over several kilometres, the typical correlation time is on the order of milliseconds, barring extreme wind speeds. For a system established over 3 km with a 520 nm laser and a perpendicular wind speed of 10 m/s, the correlation time is 3.9 ms, for example.

As mentioned in the introduction, notable models for turbulence induced intensity fluctuations are based on Gamma-Gamma and Log-Normal distributions. While the Gamma-Gamma model is generally more accurate under a wider range of turbulence conditions from weak to strong, the simpler Log-Normal model, which is accurate for weak turbulence conditions in shorter FSO links, is used in this work.

The Log-Normal distribution is based on the so-called Rytov variance, σ_R^2, which is another measure of irradiance variance. In weak turbulence where $\sigma_R^2 \ll 1$, the Rytov variance is approximately equal to the scintillation index, which is conducive to experimental measurement. The Rytov variance for a plane wave (or collimated Gaussian beam) is given by

$$\sigma_R^2 = 1.23 C_n^2 k^{7/6} L^{11/6}, \tag{3}$$

where C_n^2 is the refractive index structure constant and $k = 2\pi/\lambda$ is the wave number [8]. The log intensity variation is given by

$$l = \ln \left| \frac{A(r)}{A_0(r)} \right|^2 \tag{4}$$

where $A_0(r)$ is the amplitude of the received signal in a turbulence free channel, while $A(r)$ is the amplitude of the signal in a turbulent channel [8]. Through manipulation of the above parameters the PDF for the log normal distribution is found as given by

$$\mathrm{P}(I) = \frac{1}{\sqrt{2\pi\sigma_R^2}} \frac{1}{I} \exp\left\{ -\frac{(\ln(I/I_0) - E[l])^2}{2\sigma_R^2} \right\} \tag{5}$$

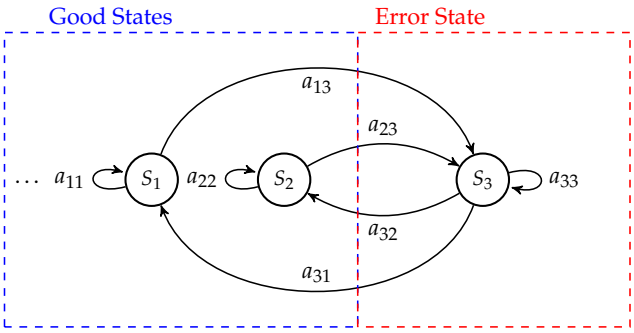

Fig. 1. Three state Fritchman model that presents the state transition matrix shown in Eq. 7. Note that there are no transitions between states S_1 and S_2. The ellipsis on the figure represents the possibility to extend the number of good states if needed to better model the system in question.

for $I \geq 0$, where $E[l]$ is the expectation of the log intensity variation[8]. The PDF produces a distribution of the intensity normalised by $E[l]$.

Using the PDF given by Eq. 5, samples of the received irradiance can be taken. With increased turbulence strength, the likelihood of a deep fade and/or error increases. The fades will be randomly distributed because the samples are independent and identically distributed, IID.

In a typical FSO system that uses NRZ-OOK modulation, the choice of the optimal threshold for I_u is typically driven by existing techniques and insight [35]. Factors such as the noise inherent to the equipment should also be taken into consideration. With equipment that is more sensitive and has less noise, the threshold can be set lower as the noise is less likely to distort the signal to a degree that it causes errors.

B. Fritchman Markov Models for Errors

Fritchman models are Markov models that were formed as an extension of the Gilbert-Elliot model that was initially developed for so-called binary symmetric channels [29]. Fritchman models are N-state partitioned Markov models that have proven suitable for modelling bursty communication channels. The states are partitioned into two groups with N and $N-k$ states in each, representing "good" and "error" channel states.

This is an important feature for modelling a communication channel as these states and the distribution of their occurrences are important to a systems designer. Conveniently, the model can be used without having to know the cause of the states, which can represent turbulence induced phenomena such as the beam wandering completely off the receiver for a time, causing a burst of errors. An example three state Fritchman model with two good states and one bad state is shown in Fig. 1.

The models presented in this paper are first order models and can be described using an $N \times N$ state transition matrix. The entries in the state transition matrix, A, represent the probabilities of transitioning to one state given a current state, expressed as

$$\mathrm{a}_{ij} = \mathrm{P}(s_t = S_j | s_{t-1} = S_i). \tag{6}$$

The structure of a Fritchman model is quite particular. It is standard practice to use one error state and $N-1$ good states to describe bursty communication channels. Errors can only be emitted by the error state. Fritchman models are Semi-Hidden Markov models because the state of the system can be discerned when there is an error, but not when there is no error. The states are assumed to only transition to themselves or states in the other partition, as can be seen in Fig. 1 which has a state transition matrix given by

$$A = \begin{bmatrix} a_{11} & 0 & a_{13} \\ 0 & a_{22} & a_{23} \\ a_{31} & a_{12} & a_{33} \end{bmatrix}. \tag{7}$$

Note that there are zeros in the matrix, indicating that the states cannot transition to states within their partition. In addition to the state transition matrix, the Fritchman model is also described by an emission matrix. Assuming the model is being used to produce an add-modulo-two error sequence, the emission matrix will be a $2 \times N$ matrix that gives the probability of each state emitting either an error or not. Since the good states do not output errors, the emission matrix for the model shown in Fig 1 is given by

$$B = \begin{array}{c} \begin{matrix} S_1 & S_2 & S_3 \end{matrix} \\ \begin{bmatrix} 1 & 1 & 0 \\ 0 & 0 & 1 \end{bmatrix} \end{array} \begin{array}{l} Good \\ Error \end{array}, \tag{8}$$

which has been annotated for convenience. Note that the probabilities are either one or zero, indicating that the states only have one possible output corresponding to the partition they are in.

The last element required to describe the model is the initial state probability vector. This provides the probability of being in a specific state when the model is started, given by

$$\Pi = \begin{bmatrix} \pi_1 & \pi_2 & \pi_3 \end{bmatrix}. \tag{9}$$

The Fritchman model is thus fully described using these three parameters: $F = (A, B, \Pi)$.

The model parameters can be found using the so-called Baum-Welch algorithm, which is an iterative algorithm that uses an initial estimate for the parameters of the Markov model as well as a sequence from the system that is being modelled [36–38].

The algorithm finds the possible sequence of states that could have produced the given output sequence. Using these traced sequences, the state transition matrix is modified to produce a sequence that closely matches the predicted sequence, measured using mean squared error.

To drive this algorithm, an initial set of $F = (A, B, \Pi)$ must be provided. This initial set includes the assumption of the number of states in the system as well as constraints that ensure that specific states can only emit the correct output and that some states cannot transition to each other as is the requirement for Fritchman modelling.

Since our goal is to model the presence and degree of memory in an FSO system, we require a way to measure and visualise it. A useful and intuitive method to show the presence of memory is called an Error Free Run (EFR) distributions.

An error free run is defined as the interval between two consecutive errors in an error sequence (a sequence of zeros and ones, where the ones represent received errors) as defined by

$$\mathrm{P}(0^m|1) = 1 - \mathrm{P}_g(m-1)]\mathrm{P}(0^1|1), \tag{10}$$

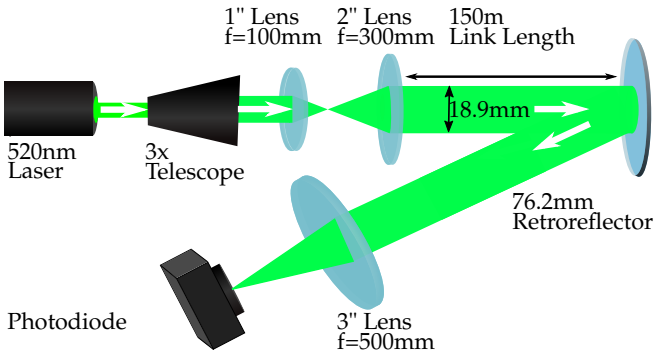

Fig. 2. Experimental Setup used to transmit and receive the link. The beam is expanded using a telescope to reduce the effects of divergence and is focused on to the photodiode for signal acquisition.

where

$$\mathrm{P}(0^1|1) = \frac{N_g}{N_e}, \tag{11}$$

and

$$\mathrm{P}_g(m-1) = \frac{N_g(1) + N_g(2) + N_g(3) + \ldots + N_g(m-1)}{N_g}. \tag{12}$$

Here, m is the length of the interval between successive errors and $\mathrm{P}(0^m|1)$ is the probability of m error free outputs given the occurrence of an error. N_g is the total number of gaps, N_e is the total number of errors and $N_g(m)$ is the number of gaps of length m[39]. Here, a gap is defined as the region between two successive errors.

The EFR of a sequence from a channel with no memory would have high probabilities at the beginning but due to having no memory, there would be a sharp drop off in probability as the interval length grew. The sharpness of this drop would be limited by the BER of the sequence. In contrast, the EFR of a channel with memory would naturally also drop. Still, it would have a significantly longer tail, possibly with additional features depending on the nature of the system.

3. EXPERIMENTAL SETUP AND METHODOLOGY

The data used for this experiment was recorded using the setup shown in Fig. 2. Though it is expected that feedback based tracking (or adaptive optics) would improve the performance of the link, tracking was not used. An expanded 520 nm modulated laser beam was made to propagate over 300 m (150 m to a retro-reflector and back along a slightly offset path to prevent atmospheric reciprocity) and recorded for offline analysis. The laser was operating at a transmit power of 3 mW. The link was situated inland at the University of the Witwatersrand in Johannesburg, South Africa, at an altitude of approximately 1.7 km.

The signal was modulated using Non-Return to Zero On-Off Keying (NRZ-OOK) at 4 Kb/s and recorded over 24 hour periods. Wind speed, direction and temperature from a weather station on the roof of the transmitting building was also recorded to supplement the optical data with an example shown in Fig. 3, which also indicates when one of the presented test cases comes from.

The data was split into five minute "frames", and the average scintillation index for each frame was determined using Eq. 1

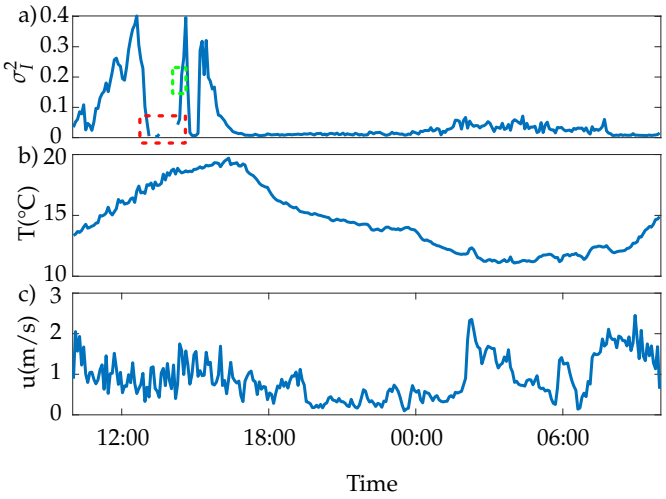

Fig. 3. The scintillation index, σ_I^2, of the link, perpendicular wind speed, u, and temperature, T on a particular day. Note on (a) in green is the approximate region of data used to train the model for $\sigma_I^2 = 0.18$. There is a gap in the measurements, highlighted in red, which is due to complete misalignment of the system probably due to thermal expansion of the buildings around midday.

when the signal was in the on state. Average bit error rate measurements for each frame were also calculated.

Fritchman models were developed based on the received bit streams for these frames using a Baum-Welch algorithm. The accuracy of the resulting models is measured using the log-likelihood ratio, which also determines when the Baum-Welch algorithm should stop iterating. The fitting tolerance was set to 10^{-12} and most models were found within 20 iterations. It was found that a three state Fritchman model was adequate to capture the effects of memory in the system. Larger models are indeed more accurate but were deemed insignificantly so.

Larger models increase the computational cost of both training and the use of the model. With the focus of this study in consideration, the additional accuracy does not sufficiently affect the results to warrant the extra computational cost. The number of states in the systems for this experiment is chosen based on these factors. The paradigm of a singular bad state with multiple good states is a standard way to choose the number of states in a Fritchman model and has been demonstrated to be sufficient to capture the memory in the system [32, 40–42]. In addition, a standard Log-Normal distribution was fit to each frame and used to simulate equivalent bit streams for comparison.

Three of these frames were selected based on their scintillation index, for a range of turbulence strengths, and are presented here. The scintillation index for each of these test cases is 0.18, 0.35 and 0.52. Unfortunately, the link length makes moderate to strong turbulence conditions unlikely. Nonetheless, we are able to demonstrate the efficacy of our approach, which is applicable to all turbulence strengths.

4. RESULTS AND DISCUSSION

The transmission power of the laser, coupled with the link length, resulted in the effect of the turbulence being limited to weak-to-moderate strength. No results for strong turbulence were obtained. In very weak turbulence conditions the link would be

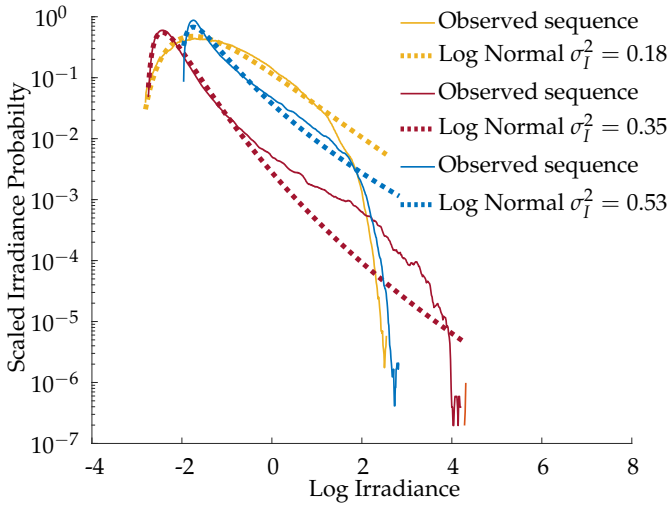

Fig. 4. Measured fading in comparison to a fitted Log-Normal PDF for each of the cases presented. As expected, the Log-Normal fit is better with weaker turbulence.

error free (the baseline BER would be zero) for a long period of time, with random bursts of errors when the turbulence momentarily becomes stronger. Modelling this behaviour is indeed the main contribution of this paper.

In this section we begin by summarising the measurement results and comparing the distribution of received errors (as measured) to those that could be expected when simulated using Log-Normal fading in equivalent strength turbulence. We then proceed to show how a Fritchman modelling approach results in an error distribution that is closer to what was measured, while also maintaining the same BER. We discuss the characteristics of this type of model, and then provide a brief outline of some techniques that might benefit from a model that accounts for the actual bursty error distribution of the FSO channel.

Three cases are presented here to highlight the accuracy of a Fritchman modelling approach for FSO in comparison to more common PDF-only signal models. The scintillation indices for each case are $\sigma_I^2 = 0.18$, 0.35 and 0.52 respectively, and the measured PDFs are visible in Fig. 4. We fit a Log-Normal model to each case for comparison, and this is also indicated on the figure.

It is clear that as the turbulence becomes stronger, the Log-Normal fit is worse: this is a known limitation of the model and the use of Gamma-Gamma or more complex fading models would account for this. It was deemed unnecessary to use a more complex model in this work, as the choice of PDF will not have a significant impact on the distribution of errors. This is because PDF-based models are still Independent and Identically Distributed (IID) and therefore have no memory.

The average weather conditions for each case are given in Tab. 1. This data shows the average conditions over the five minute "frames" that are being used to train the model. The BER is also provided and as expected, when the turbulence strength increases, the BER gets worse. In this table, the correlation time, τ, is also given. This has a bearing on the depth of the channels memory. With these standard empirical measures we cannot tell much about the channels memory. Are the errors evenly spread or are they clumped into bursts?

Unfortunately, no convenient single-number metric exists to describe this "burstiness". For the readers convenience we

σ_I^2 [SI]	0.18	0.35	0.52
T [°C]	19.14	18.64	19.54
u [m/s]	0.65	1.93	1.33
τ [s]	0.019	0.0065	0.0094
BER Observed	4.27×10^{-5}	5.8×10^{-2}	8.9×10^{-2}
BER Fritchman	4.33×10^{-5}	5.78×10^{-2}	9×10^{-2}

Table 1. Weather parameters for the different cases presented, according to scintillation index as well as the average bit error rate for the observed sequence and the trained model corresponding to them.

have plotted the distribution of errors in a qualitative way to easily visualise this burstiness, and to gain an intuition about the disadvantages of PDF-based models for FSO communication. In Fig. 5 (a), a vertical line has been plotted each time a bit is received in error for approximately five minutes of data. On inspection, it is clear that the pattern of errors modelled by random draws from the Log-Normal distribution is quite dissimilar from the the observed error distribution, even though they have the same PDF (as shown in Fig. 4). In Fig. 5 (b) this plot is expanded to a moving average (with a window length of 10k bits) of the number of errors at each point in time. This highlights the fact that there are a similar number of errors in total (i.e. the BER), even though in the observed case they occur in bursts rather than in a more uniform manner. The specific BER of the sample is not the focus point of this graph but instead the discrepancy between the Log Normal model and the observed sequence.

More scientifically, and as explained in Sec. 2B, the error-free run plot is a standard way of visualising the channel's memory. While EFRs are not the only possible way to display the characteristics of the bursty channel, they are a standard that can easily scale and show the discrepancies and similarities between models effectively [32, 40].

As shown in Fig. 6, it is clear that there is a discrepancy between the observed error-free runs and those predicted by the Log-Normal PDF. The shape of the EFRs denote the nature of the channel in the following ways: in the Log-Normal (and indeed any memoryless PDF-based) model, the error free runs decrease at a relatively constant rate until the point denoted by the BER. In contrast, the observed distribution drops quickly and then becomes a tail which decreases at a lower rate. Intuitively, if a channel has memory it is more likely to stay in a specific state for an extended period of time. As we are concerned with error free runs, the probability of shorter intervals decreases quite rapidly because they indicate changing channel state (i.e. going from no error to an error). Due to the shape of the distributions, the average BER is indeed conserved. Simply put, this discrepancy is generally the reason why conventional error mitigation techniques may not work as well as expected in FSO.

As described in Sec. 2B, a Fritchman model is a special type of Markov model which is commonly used for modelling bursty communication channels, but is it suitable for the FSO channel?

The transition probability matrices for the three separate Fritchman models, labelled according to the three different turbulence cases given in Tab. 1, are given by Eqs. 13, 14 and 15.

These three matrices show that the models generally behave similarly by having one good state that they tend to persist in (element a_{11} from Eq. 7), which captures the nature of the

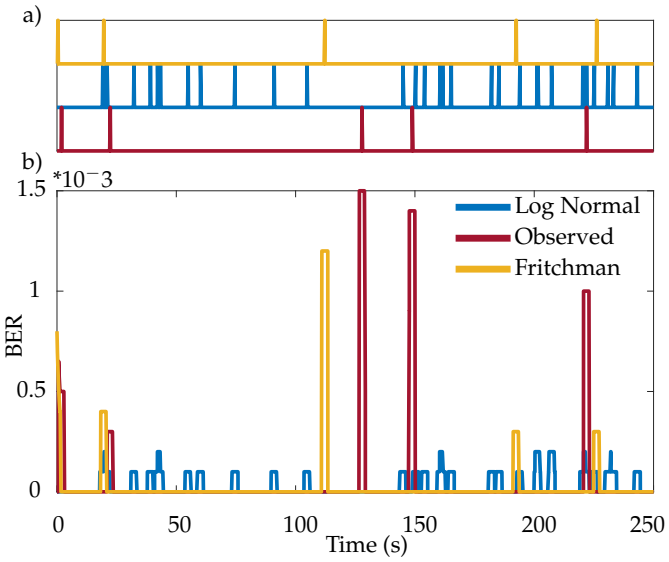

Fig. 5. (a) A plot of the positions of the errors in a 250 second sample of the bit stream obtained from using the different models and the observed data. Here it can be clearly seen that the Fritchman model more closely resembles the observed sequence when compared to the Log-Normal based sequence. An alternative representation of this data using a moving average to show the number of errors at each point is shown in (b). These two plots correspond to the data for the $\sigma_I^2 = 0.18$ recording and the BERs of the three sequences are all on the scale of 10^{-5}.

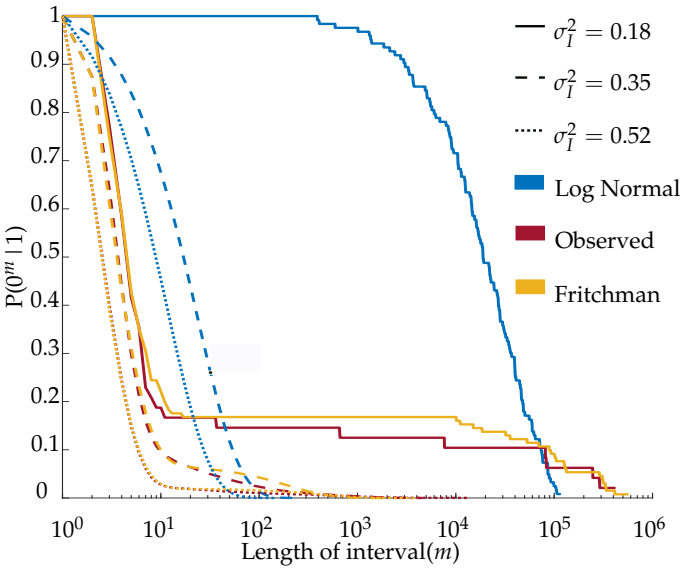

Fig. 6. The error free run (EFR) distributions that correspond to the three test cases presented in this work. This plot illustrates the distribution of lengths of good runs which illustrates the memory present in the channel. The tails at the end of each graph show likely it is for a system to persist in a good state once it enters it.

channel to stay in an error-free state for a substantial time. The second good state (a_{22}) also tends to persist, but has a higher likelihood of transitioning to the error state than the first good state. These transitions between states, as well as the varying behaviour between the states in the same partition, capture the memory of the system.

$$A_{0.18} = \begin{bmatrix} 0.9998 & 0 & 0.0002 \\ 0 & 0.7205 & 0.2795 \\ 0.1313 & 0.8687 & 0 \end{bmatrix} \quad \textbf{(13)}$$

$$A_{0.35} = \begin{bmatrix} 0.9950 & 0 & 0.0050 \\ 0 & 0.6716 & 0.3284 \\ 0.0686 & 0.8055 & 0.1259 \end{bmatrix} \quad \textbf{(14)}$$

$$A_{0.52} = \begin{bmatrix} 0.9978 & 0 & 0.0022 \\ 0 & 0.5942 & 0.4048 \\ 0.0194 & 0.6253 & 0.3553 \end{bmatrix}. \quad \textbf{(15)}$$

Plots of the resulting error distributions generated from these Fritchman models are also shown in Fig. 6. They are an excellent match for the observed sequences compared to the PDF-based model. The number of states in the presented models are sufficient to accurately capture the channels characteristics. Additional states could be added to further increase the accuracy of the model, which may be required for faster links or stronger turbulence, but is largely situation dependent.

Unfortunately, the models presented are not perfectly applicable to other weather conditions. We fitted a number of models to regions of the data with similar scintillation indices and found that they are not universal. As expected, there is a dependence on wind speed and possibly other weather parameters. This is in contrast to PDF-based models for turbulence-induced fading which are often characterizable by commonly available weather parameters. We speculate that there may be a methodology to determine the parameters of a Fritchman model given standard measures for turbulence and weather, however, this is the subject of future work. Nevertheless, in the absence of such a methodology, the future development of a database of Fritchman models for a set of common conditions would be very useful to the community.

That said, in general some trends can indeed be observed. Lower wind speeds result in longer correlation times, τ. This effect is visible in the EFR plots, with the weakest turbulence case also exhibiting the deepest memory because it had the lowest wind speed. The result on the communication channel in this case is as follows: there is a low probability of an error occurring (since the turbulence is weak), but when it does occur, there will be quite a long burst of errors. The interrelation between wind speed and turbulence strength it complex and we cannot draw further conclusions except that in general, faster wind speed results in shorter tails.

It should be noted that the transmission rate used for this experiment is not sufficiently high to directly map to a practical system on the order of Gbits/s. The transmission rate used affects the decisions regarding the model parameters. At higher speeds, the effect of the memory may be lost at a bit level because individual bits are not "exposed" to the turbulence for as long. This does not, however, mean that the techniques presented here have no relevance at higher speeds.

While the errors would appear random at a bit level, the effect of the memory in a high speed system would be present at a

codeword (or frame) level. Adapting the techniques presented here to a codeword level can be accomplished without much difficulty. The training algorithm and Fritchman model can be configured to produce an output of any type, including a codeword of specified length. The codewords from the simulation would show the effects of memory similarly to the bit level analysis presented here. Future work can focus on adapting these techniques for higher bit rates.

While the focus of this paper is not on mitigation techniques, a brief mention of some possibilities and applications of Fritchman modelling serves to highlight the importance of the approach.

A common technique to combat bursty channels is interleaving, which shuffles a bit-stream based on a mathematical expression which spreads closely grouped bits throughout the bit-stream. At the receiver, the bits are de-interleaved back to their proper positions. In a bursty channel, interleaving is useful when paired with a code more suited to correcting random errors as the errors would be spread throughout the bitstream, essentially appearing as random errors.

An important factor to consider for interleaving is the depth and the algorithms used to interleave the data. This should be informed by the distribution of errors in the channel. Optimal interleaving methods can only be designed and used when this information (such as the EFR) is present. In the absence of a good model, "educated guesses" at the interleaving depth and algorithm may result in excessive latency or little performance improvement [43–45]. Whether these are tradeoffs a system designer would choose to make is beyond the scope of this paper.

As previously mentioned, error correcting codes can be designed to better compensate for the errors that are not fully random and are instead correlated. The design of these codes is challenging and it is therefore important to use existing approaches, which rely on standardised channel models [42, 46, 47]. Burst tolerant codes can be difficult to design and optimise. The techniques presented here allow for rapid iteration when attempting these designs. This could be used in conjunction with existing techniques for the optimisation of burst tolerant codes in the form of rateless codes such as Luby-Transform (LT) codes [48, 49].

5. CONCLUSION

An experiment over a 300 m outdoor optical link has been conducted and we show that Fritchman Markov models are well suited to model the dynamics of FSO channels. The modelling approach and sample models presented account for the memory in the channel which results in bursts of errors which are the leading cause of difficulties in FSO error mitigation strategies. Memory-less models that are currently in widespread use such as fading PDFs do not account for this burstyness. The use of Fritchman models over general Markov models is conducive to communications theory as they are already used in other memory channels with associated error mitigation techniques. As such, the models presented in this study, as well is in future derived works can be used for optimal development of error correcting codes, interleaving and protocols for use on FSO channels to extend their range, reliability and capacity.

FUNDING

M.A.C would like to acknowledge South African National Research Foundation grant 121908. X.N would like to acknowledge South African National Research Foundation for their financial assistance.

Disclosures. The authors declare no conflicts of interest.

REFERENCES

1. J. Wang, S. Li, M. Luo, J. Liu, L. Zhu, C. Li, D. Xie, Q. Yang, S. Yu, J. Sun, X. Zhang, W. Shieh, and A. E. Willner, "N-dimentional multiplexing link with 1.036-Pbit/s transmission capacity and 112.6-bit/s/Hz spectral efficiency using OFDM-8QAM signals over 368 WDM pol-muxed 26 OAM modes," in *European Conference on Optical Communication, ECOC,* (Institute of Electrical and Electronics Engineers Inc., 2014).
2. Z. Qu and I. B. Djordjevic, "500 Gb/s free-space optical transmission over strong atmospheric turbulence channels," Opt. Lett. **41**, 3285 (2016).
3. A. Trichili, M. A. Cox, B. S. Ooi, and M.-S. Alouini, "Roadmap to free space optics," J. Opt. Soc. Am. B **37**, A184 (2020).
4. M. M. Abadi, M. A. Cox, R. E. Alsaigh, S. Viola, A. Forbes, and M. P. Lavery, "A space division multiplexed free-space-optical communication system that can auto-locate and fully self align with a remote transceiver," Sci. Reports **9**, 1–8 (2019).
5. K. David and H. Berndt, "6G vision and requirements: Is there any need for beyond 5G?" IEEE Veh. Technol. Mag. **13**, 72–80 (2018).
6. S. Dang, O. Amin, B. Shihada, and M.-S. Alouini, "What should 6G be?" Nat. Electron. **3**, 20–29 (2020).
7. M. P. J. Lavery, M. M. Abadi, R. Bauer, G. Brambilla, L. Cheng, M. A. Cox, A. Dudley, A. D. Ellis, N. K. Fontaine, A. E. Kelly, C. Marquardt, S. Matlhane, B. Ndagano, F. Petruccione, R. Slavík, F. Romanato, C. Rosales-Guzmán, F. S. Roux, K. Roux, J. Wang, and A. Forbes, "Tackling Africa's digital divide," Nat. Photonics **12**, 249–252 (2018).
8. L. C. Andrews, R. L. Phillips, and C. Y. Young, "Laser Beam Scintillation with Applications," Laser Beam Scintillation with Appl. (2009).
9. M. A. Al-Habash, "Mathematical model for the irradiance probability density function of a laser beam propagating through turbulent media," Opt. Eng. **40**, 1554 (2001).
10. W. Gappmair and M. Flohberger, "Error performance of coded FSO links in turbulent atmosphere modeled by gamma-gamma distributions," IEEE Transactions on Wirel. Commun. **8**, 2209–2213 (2009).
11. M. Beason, L. Andrews, and S. Gladysz, "Statistical comparison of probability models of intensity fluctuation," in *Environmental Effects on Light Propagation and Adaptive Systems II,* (2019), p. 12.
12. Z. Kolka, V. Biolkova, O. Wilfert, and D. Biolek, "Simulation model of correlated FSO channels," Proc. 14th Conf. on Microw. Tech. COMITE 2015 pp. 22–25 (2015).
13. H. Henniger and A. Gonzalez, "Transmission scheme and error protection for simplex long-distance atmospheric FSO systems," The Mediterr. J. Electron. Commun. **2**, 118–126 (2006).
14. S. Z. Denic, I. Djordjevic, J. Anguita, B. Vasic, and M. A. Neifeld, "Information theoretic limits for free-space optical channels with and without memory," J. Light. Technol. **26**, 3376–3384 (2008).
15. J. A. Anguita, M. A. Neifeld, B. Hildner, and B. Vasic, "Rateless coding on experimental temporally correlated fso channels," J. Light. Technol. **28**, 990–1002 (2010).
16. Y. Q. Shi, X. M. Zhang, Z. C. Ni, and N. Ansari, "Interleaving for combating bursts of errors," IEEE Circuits Syst. Mag. **4**, 29–42 (2004).
17. K. E. Olson and P. K. Enge, "Forward Error Correction for an Atmospheric Noise Channel," IEEE Transactions on Commun. **40**, 863–872 (1992).
18. H. Kazemi, M. Uysal, and F. Touati, "Outage analysis of hybrid FSO/RF systems based on finite-state Markov chain modeling," 2014 3rd Int. Work. Opt. Wirel. Commun. IWOW 2014 pp. 11–15 (2014).
19. A. Touati, S. J. Hussain, F. Touati, and A. Bouallegue, "Effect of Atmospheric Turbulence on Hybrid FSO/RF Link Availability under Qatar Harsh Climate," World Acad. Sci. Eng. Technol. Int. J. Electr. Comput. Eng. **9**, 87–105 (2015).

20. A. Khatoon, W. G. Cowley, and N. Letzepis, "FSO/RF correlation measurement and hybrid system hidden Markov model," 2013 Aust. Commun. Theory Work. AusCTW 2013 pp. 93–98 (2013).
21. R. Bosu and S. Prince, "Discrete Markov chain model for transition analysis of optical scintillation in reflection-assisted free space optical links," Opt. Commun. **475**, 126261 (2020).
22. A. Mostafa and S. Hranilovic, "Channel measurement and Markov modeling of an urban free-space optical link," J. Opt. Commun. Netw. **4**, 836–846 (2012).
23. Z. Hajjarian, J. Fadlullah, and M. Kavehrad, "Use of markov chain in atmospheric channel modeling of free space laser communications," in *MILCOM 2008 - 2008 IEEE Military Communications Conference,* (2008), pp. 1–7.
24. X. Zhu and J. M. Kahn, "Markov chain model in maximum-likelihood sequence detection for free-space optical communication through atmospheric turbulence channels," IEEE Transactions on Commun. **51**, 509–516 (2003).
25. M. A. Cox, N. Mphuthi, I. Nape, N. Mashaba, L. Cheng, and A. Forbes, "Structured light in turbulence," IEEE J. Sel. Top. Quantum Electron. **27**, 1–1 (2020).
26. C. T. Nguyen, H. D. Le, and V. V. Mai, "A cross-layer analysis of TCP/link adaptation technologies over free-space optical links with Markov error model," Photonic Netw. Commun. **36**, 279–288 (2018).
27. H. D. Le, V. V. Mai, C. T. Nguyen, and A. T. Pham, "Design and Analysis of Sliding Window ARQ Protocols With Rate Adaptation for Burst Transmission Over FSO Turbulence Channels," J. Opt. Commun. Netw. **11**, 151–163 (2019).
28. H. Henniger, "Transmission performance analysis of free-space optical communications using Gilbert-Erasure channel," IEEE Transactions on Commun. **60**, 55–61 (2012).
29. B. D. Fritchman, "A Binary Channel Characterization Using Partitioned Markov Chains," IEEE Transactions on Inf. Theory **13**, 221–227 (1967).
30. C. Pimentel, "Modeling burst channels using partitioned fritchman's Markov models," IEEE Transactions on Veh. Technol. **47**, 885–899 (1998).
31. A. D. Familua and L. Cheng, "Modeling of in-house CENELEC A-band PLC channel using Fritchman model and Baum-Welch algorithm," ISPLC 2013 - 2013 IEEE 17th Int. Symp. on Power Line Commun. Its Appl. Proc. pp. 173–178 (2013).
32. A. D. Familua and L. Cheng, "First and Second-Order Semi-Hidden Fritchman Markov models for a multi-carrier based indoor narrowband power line communication system," Phys. Commun. **29**, 55–66 (2018).
33. A. D. Familua, "A Block Diagonal Markov Model for Indoor Software-Defined Power Line Communication," IEEE PES/IAS PowerAfrica Conf. Power Econ. Energy Innov. Afr. PowerAfrica 2019 pp. 1–6 (2019).
34. L. Andrews and R. Phillips, *Laser Beam Propagation Through Random Media* (SPIE Optical Engineering Press, 2005), chap. 11, pp. 441–472.
35. L. Yang, B. Zhu, J. Cheng, and J. F. Holzman, "Free-Space Optical Communications Using on-off Keying and Source Information Transformation," J. Light. Technol. **34**, 2601–2609 (2016).
36. W. H. Tranter, K. S. Shanmugan, T. S. Rappaport, and K. L. Kosbar, *Principles of Communication Systems Simulation with Wireless Applications*, vol. 1 (Prentice Hall, 2003).
37. M. Oudelha and R. N. Ainon, "HMM parameters estimation using hybrid Baum-Welch Genetic Algorithm," Proc. 2010 Int. Symp. on Inf. Technol. - Eng. Technol. ITSim'10 **2**, 542–545 (2010).
38. P. M. Baggenstoss, "A modified Baum-Welch algorithm for hidden Markov models with multiple observation spaces," IEEE Transactions on Speech Audio Process. **9**, 411–416 (2001).
39. S. Thai, "Markov Characterization of the HF Channel," IEEE T **C**, 24–32 (1969).
40. D. G. Holmes, L. Cheng, M. Shimaponda-Nawa, A. D. Familua, and A. M. Abu-Mahfouz, "Modelling noise and pulse width modulation interference in indoor visible light communication channels," AEU - Int. J. Electron. Commun. **106**, 40–47 (2019).
41. A. D. Familua and L. Cheng, "A semi-hidden Fritchman Markov modeling of indoor CENELEC A narrowband power line noise based on signal level measurements," AEU - Int. J. Electron. Commun. **74**, 21–30 (2017).
42. M. D. Knowles and A. I. Drukarev, "Bit Error Rate Estimation for Channels with Memory," IEEE Transactions on Commun. **36**, 767–769 (1988).
43. L. Kanal and A. Sastry, "Models for Channels with Memory and Their Applications to Error Control," Proc. IEEE **66**, 724–744 (1978).
44. T. Stephen and P. S. Schmied, "Interleaving and Error-Burst Distribution," IEEE Transactions on Commun. **71**, 1811–1815 (1974).
45. A. I. Drukarev and K. P. Yiu, "Performance of Error-Correcting Codes on Channels with Memory," IEEE Transactions on Commun. **34**, 513–521 (1986).
46. H. Lai and S. Kallel, "An Efficient Convolutional Coding/Decoding Strategy for Channels with Memory," IEEE Transactions on Commun. **43**, 2678–2686 (1995).
47. A. Van Heerden and H. C. Ferreira, "Evaluating non-binary error correcting codes on bursty channels with a partitioned Markov model," Proc. 1993 IEEE South Afr. Symp. on Commun. Signal Process. COMSIG 1993 pp. 114–117 (1993).
48. M. Luby, "Lt codes," in *The 43rd Annual IEEE Symposium on Foundations of Computer Science, 2002. Proceedings.*, (2002), pp. 271–280.
49. C.-m. M. Chen, Y.-p. P. Chen, T.-c. C. Shen, J. K. Zao, S. S. S. Member, Y.-p. P. Chen, T.-c. C. Shen, J. K. Zao, and S. S. S. Member, "Optimizing degree distributions in LT codes by using the multiobjective evolutionary algorithm based on decomposition," 2010 IEEE World Congr. on Comput. Intell. WCCI 2010 - 2010 IEEE Congr. on Evol. Comput. CEC 2010 (2010).